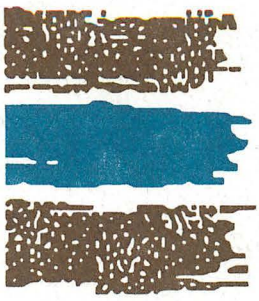

EDWARDS UNDERGROUND
WATER DISTRICT

REPORT 95-02

REGIONAL DISTRIBUTION OF PERMEABILITY IN THE EDWARDS AQUIFER

REGIONAL DISTRIBUTION OF PERMEABILITY IN THE EDWARDS AQUIFER

Final Report

by

Susan D. Hovorka, Robert E. Mace, and Edward W. Collins

assisted by

E. M. Boghici, N. D. Johns, Jun Liao, and N. L. Baghai

Prepared for
Edwards Underground Water District
under Contract No. 93-17-FO

Alan R. Dutton, Principal Investigator

Bureau of Economic Geology
Noel Tyler, Director
The University of Texas at Austin
Austin, Texas 78713-8924

January 1995

CONTENTS

Figures

Tables

Plates (in pocket)

EXECUTIVE SUMMARY

Three integrated data sets that provide information about the distribution of permeability in the Edwards aquifer were compiled and interpreted during this study. These are (1) structural and thickness maps of the Edwards aquifer, (2) permeability data determined from well tests, and (3) the contribution of the rock matrix to permeability based on sample analysis and wireline log interpretation. This basic information is needed for improvement of hydrologic models of the Edwards aquifer. Hydrologic models can be used to guide management decisions, for example by predicting the response of water level and spring discharge to variations in the amount and location of recharge and pumping, or by determining probable flow directions for contaminants from a spill. The three data sets have been digitized and prepared as map coverages in an ARC/INFO geographic information system (GIS) to be available to future users in a commonly used electronic data base. Original and interpreted data are presented in this report to meet the needs of future users. Additional products of this study are geologic and hydrologic interpretations that improve understanding of how water flows through the Edwards aquifer.

Structural and thickness maps of the Edwards aquifer show in detail the elevation of the top of the aquifer, the thickness of the aquifer, and the location and geometry of faults that offset the aquifer. Structural maps build on previous maps of the aquifer and Edwards outcrop belt but include new data, in particular from the Edwards Underground Water District well logging program. Thickness maps show that the thickness of the aquifer ranges from less than 500 ft in the northern part of the aquifer to more than 900 ft near the southern and western limits of the aquifer.

The top of the Edwards aquifer lies at near-surface elevations of 700 to 1,200 ft above sea level in the shallowest (unconfined) part of the aquifer. Toward the south and east, the top of the aquifer is encountered at greater depths, as much as 3,400 ft below sea level in the southernmost extension of the aquifer in Frio County. Much of this change in elevation occurs along a system of faults known as the Balcones Fault Zone. Recent surface mapping of structure along the Balcones Fault Zone was used to interpret similar structural features in the subsurface. The Balcones Fault Zone is

composed of multiple fault blocks. A few faults offset the entire thickness of the aquifer and juxtapose the aquifer against less permeable units, creating a barrier to flow. Most faults have smaller displacements and do not completely offset the aquifer. In addition, the effect of faults as barriers to flow is limited because faults are arranged in an overlapping, subparallel pattern known as en echelon, leaving areas of continuous strata known as relay ramps between them.

The probable effects on transmissivity of faults having different amounts of displacement were studied in outcrop. A typical fault of the Balcones Fault Zone is surrounded by a zone of highly fractured and brecciated strata. Faults with large offset have wider highly fractured zones than those with small offsets. Abundant fractures are well connected and could produce a zone of high permeability parallel to the fault plane. Relay ramps between en echelon faults contain abundant intersecting fractures, which might increase the transmissivity of these areas of potential flow between fault blocks. Even the middle of blocks bounded by large faults typically contains small faults and fractures, showing that fractures are present throughout the aquifer.

Many fractures have been enlarged by solution, producing fracture porosities as high as 0.3 percent near the largest faults. Measurements of fracture in outcrops document that solution increases the width of fractures as well as increasing the roughness of fracture surfaces. Digitizing photomosaics of outcrops shows that large and small caves account for 1 to 3 percent of the volume of the aquifer. Caves form preferentially in dolomitic rocks and breccia and in calcitized evaporite beds, as well as along faults and fractures. Large caves form preferentially in areas where fractures intersect more soluble beds.

Water-well test data were compiled from public data files and published reports and used to calculate specific capacity for each well. An equation relating the decline in water level when the well was pumped (specific capacity) to transmissivity was developed specifically for the Edwards aquifer. This calibrated equation was used to determine permeability from the abundant specific capacity tests available throughout the aquifer.

Geostatistical analysis shows that aquifer permeability has an element of spatial continuity with a large amount of small-scale randomness. This means that whereas two wells drilled close

together can have very different aquifer properties, permeability is nonetheless distributed in a regional pattern. The area of highest transmissivity is in the southern part of the confined aquifer near the fresh/saline interface. The average transmissivity in the unconfined aquifer in Comal and Hays Counties is lower than the average in the confined aquifer. This reduction in transmissivity is only partly an effect of a thinner saturated section in the unconfined aquifer because a reduction is also seen in hydraulic conductivity, which is independent of thickness. How far this area of low transmissivity in the unconfined aquifer extends into Bexar and Medina Counties cannot be determined because well-test data are sparse. The vertical distribution of permeability was calculated for research wells where multiple intervals were tested and shows variation of 10 to 100 times within each well.

The permeability and porosity of various unfractured Edwards rock types were measured using core plugs. Permeability was calculated from porosity derived from wireline logs using equations developed for specific rock types. The average permeability calculated from specific-capacity tests, which includes flow through fractures, caves, and matrix, is 125 times greater than the average permeability of the matrix alone. The distribution of matrix permeability, however, overlaps the low end of the distribution of total permeability, showing that some of the poorer wells could be producing mostly from the matrix. The comparison of values of permeability in matrix and conduits (fractures and caves) can be used to interpret and model transport of contaminants through the aquifer.

Zones of high matrix permeability were related to sections where dolomite has been preferentially dissolved. Dolomite originally formed preferentially in several intervals within the Edwards Group and decreased from a maximum at San Marcos to a minimum in the Uvalde area. The amount of dolomite that has been dissolved depends on the position within the aquifer.

Matrix permeability has a geographical distribution similar to that of total permeability, the highest values being found deep in the aquifer near the fresh/saline interface and the lowest values in outcrop. This distribution suggests that more dolomite has dissolved near the fresh/saline interface where over geologic time two waters are being mixed. Increased dolomite dissolution has

increased the permeability of the matrix, the width of solution-enlarged fractures, and the abundance of caves. Vertical variations in permeability show that high permeability is associated with dolomitized intervals. The effect of fractures and faults on permeability is superposed on the stratigraphically controlled variation.

Comparison of the three data sets documents how the total permeability in the Edwards aquifer is made up of fracture, karst, and matrix contributions. Both small-scale and regional variation in the total permeability can be related to variations in the contribution of each component.

ABSTRACT

The Edwards aquifer of South Texas is a dual-porosity/dual-permeability system. To describe the permeability structure of the aquifer quantitatively, the distribution of various factors controlling permeability was quantified, and geographic and geologic relationships were analyzed. The major contributors to permeability are (1) structurally controlled fractures and faults, (2) highly porous carbonate matrix, and (3) vertically and horizontally extensive cave systems.

Structural mapping of the Edwards Formation in outcrop and in the subsurface was used to define the location and amount of offset along faults and to define areas of potentially higher fracture intensity. Composite displacements of 1,400 to 1,850 ft (430 to 560 m) across the aquifer occur along a series of en echelon normal faults with throws of 100 to 850 ft (30 to 260 m). The areas between the en echelon faults, known as relay ramps, create and maintain the connection of the aquifer unit through faulted regions. Smaller faults and smaller relay ramps within the large fault-bounded blocks impact the permeability distribution primarily because of associated fractures.

Specific capacity test results from throughout the aquifer were used to calculate transmissivity using a relationship between specific capacity and transmissivity developed for the Edwards aquifer. Transmissivities vary eight orders of magnitude from 0.1 to 10,000,000 ft^2/day (0.01 to 1,000,000 m^2/day). Statistical analysis shows that transmissivity systematically varies in different areas of the aquifer but that variability within any area is high, reflecting the heterogeneous contribution of fractures, matrix, and karst to transmissivity.

The distribution of caves and their relationship to stratigraphy and structure was examined using photomosaics of outcrops. Karst processes enlarge fractures by solution and increase their aperture and roughness. Preferential dissolution of dolomitic tidal flat and dolomitized subtidal facies creates stratigraphically controlled conduits and high, touching-vug permeability.

Intense diagenesis of the Edwards rocks is the principle control on the relationships between porosity and matrix permeability. Matrix porosity–permeability transforms were developed for (1) particle-dominated aquifer units, (2) the fine-grained Salmon Peak Formation, (3) particle-dominated units in outcrop, and (4) the saline portion of the Edwards, south and east of the aquifer.

INTRODUCTION

The purpose of this study is to define the three-dimensional distribution of hydraulic conductivity in the Edwards aquifer. The Edwards aquifer is an economically important, geologically complex, prolific but heavily used ground-water resource. Because of the complex interrelation of hydraulic conductivity, aquifer stratigraphy, karst and fracture porosity, and aquifer storage, accurate predictions of water levels and aquifer discharge to springs need to be based on a numerical model of ground-water flow in the aquifer. In order to develop a new generation of models of the Edwards aquifer, additional detailed hydrologic data are needed. Hovorka and others (1993) generated a regional, three-dimensional porosity data set to evaluate aquifer storage. This report presents data on the three-dimensional distribution of hydraulic conductivity in the Edwards aquifer. Interpretive maps have been stored in an ARC/INFO Geographical Information System (GIS) to provide a quality-controlled data set that can be consulted to (1) determine the hydrologic and structural information available in an area, (2) incorporate additional data, and (3) serve as a basis for additional work, including hydrologic model development.

Geologic Setting

The Edwards aquifer extends over an area of about 3,000 square miles (7,800 km^2) in Hays, Comal, Bexar, Medina, Uvalde, and Kinney Counties (Fig. 1). The limits of the southern part of the Edwards aquifer are: the fresh/saline-water interface commonly known as the bad water line on the south and east (Schultz, 1994), the edge of the Edwards Group outcrop on the north, and the mapped ground-water divides near Brackettville, Kinney County, and Kyle, Hays County. This regional permeability study area extends a convenient distance beyond the limits of the aquifer (Fig. 1). The Edwards aquifer lies in and is associated with the Balcones Fault Zone. Edwards rocks crop out across the northern part of the study area, but the top of

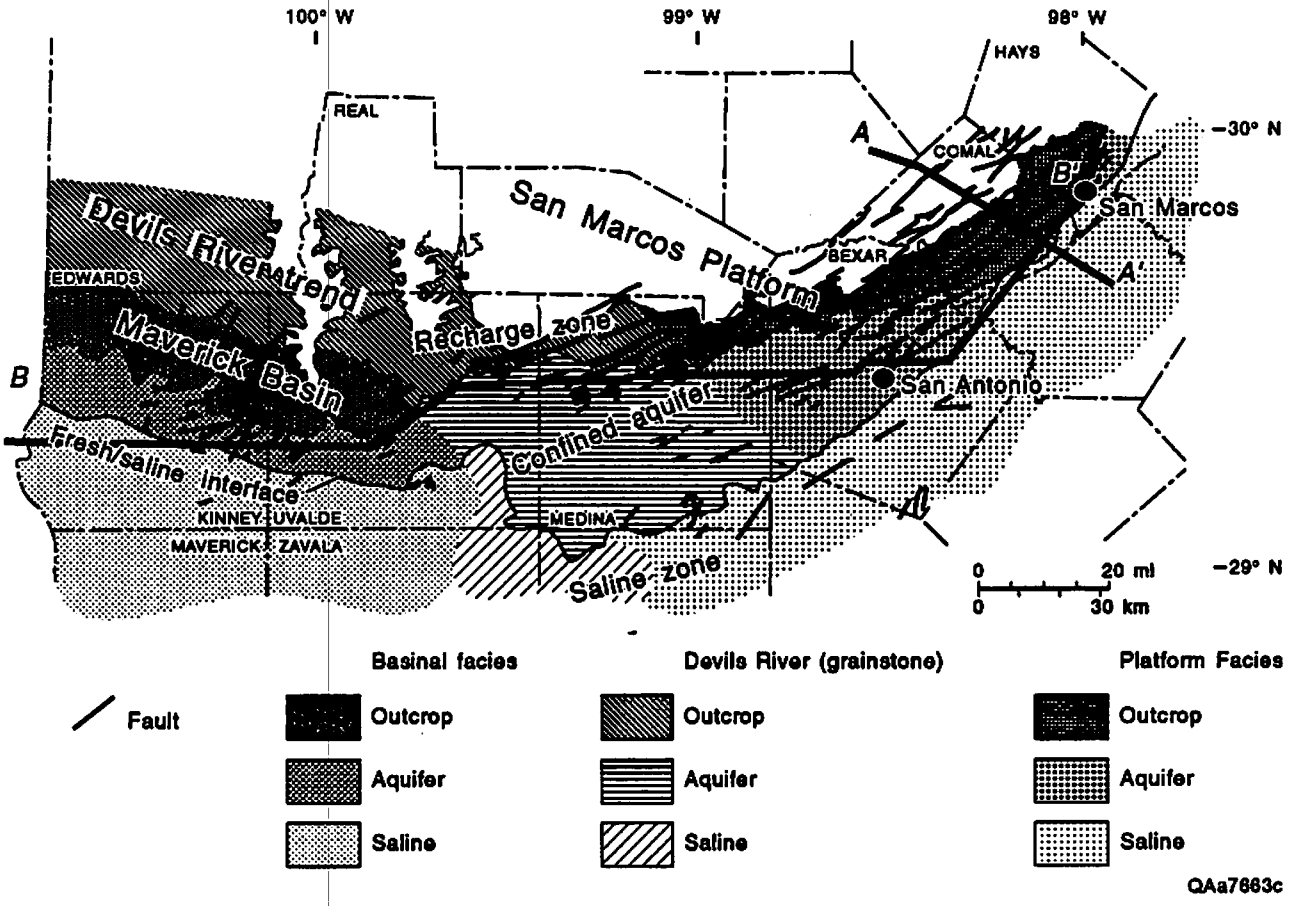

Figure 1. Structural, hydrologic, and facies setting of the Edwards aquifer. Major faults of the Balcones Fault Zone are extracted from the four sheets of the 1:250000-scale geologic Atlas of Texas (Brown and others, 1974; Proctor and others; 1974; Waechter and others, 1977). The Edwards Group outcrop forms the recharge zone of the aquifer. The Edwards Group is down dropped toward the south, where it is overlain by the Del Rio Formation and younger low-permeability rocks. In this setting the aquifer is mostly confined. The fresh/saline-water interface (Schultz, 1992; 1993; 1994) defines the downdip extent of the freshwater aquifer. Three major depositional facies belts that trend oblique to the aquifer are (1) Maverick Basin, (2) Devils River trend, and (3) San Marcos Platform. Cross section A–A′ in Figure 5; B–B′ in Figure 8.

the aquifer lies at depths as great as 3,000 ft (900 m) below the surface in the southern part of the study area. The Edwards outcrop is the recharge zone of the aquifer, and the aquifer is unconfined in this area because the top of the aquifer is in contact with the atmosphere. The aquifer is confined where the Edwards Group is overlain and essentially sealed by younger, low-permeability rocks.

The Edwards Group in different parts of the study area is divided into six formations (Fig. 2). Each formation is made up of a characteristic suite of interbedded lithologies with distinctive hydrologic and petrophysical properties. The present rock character depends on the environment in which the sediments were deposited, the modifications that occurred during compaction and stabilization as sediments were lithified, and alteration when the rocks were uplifted as a result of faulting. The Person and Kainer Formations (Rose, 1972) are found on the San Marcos Platform (Hays, Comal, and Bexar Counties). These formations have been subdivided into informal units on the basis of regionally correlated cycle patterns, which can be used to show lateral changes in facies (Fig. 2). The relationship between these cycle-based units and the lithologically defined units of Rose (1972) and Maclay and Small (1986) is shown in Figure 2. The Devils River Formation (Rose, 1972), deposited on the platform margin, forms the aquifer in most of Medina County and eastern and northern Uvalde County (Fig. 2). The West Nueces, McKnight, and Salmon Peak Formations, deposited in the Maverick Basin (Smith, 1964; Miller, 1983), form the aquifer in southern and western Uvalde and Kinney Counties. The Georgetown Formation (Fig. 2), which overlies and is partly equivalent to the Edwards Group (Moore, 1964), was included within the Edwards in order to avoid stratigraphic complexity not relevant to this study. The Del Rio Formation, overlying the Georgetown Formation, is a calcareous shale distinctively recognizable in outcrop, cuttings, core, and geophysical logs. It is the major confining unit separating the Edwards from overlying units; therefore, the base of the Del Rio Formation is used as the top of the study interval. The top of the Glen Rose Formation, which underlies the Edwards aquifer, defines the base of the study interval.

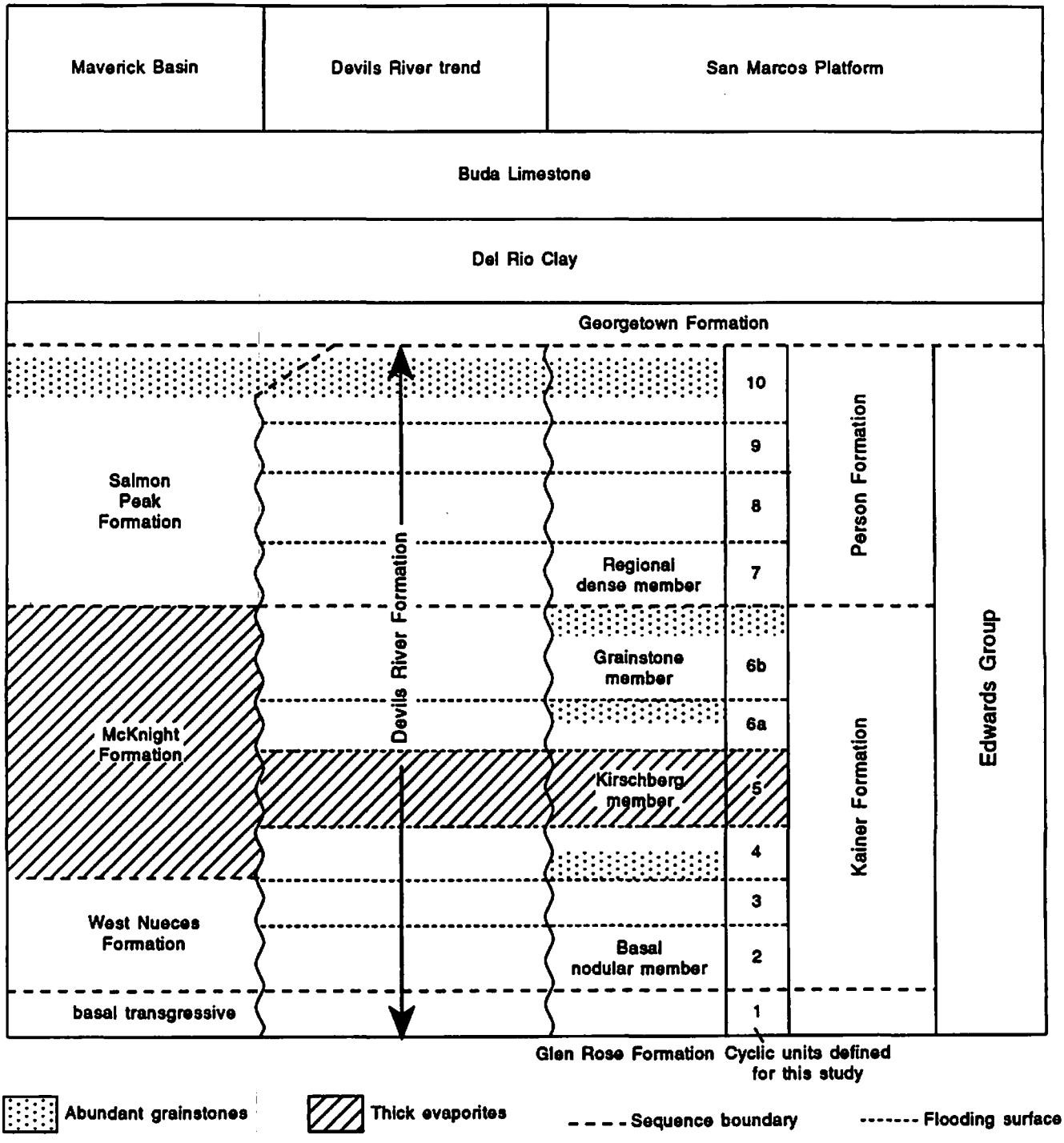

Figure 2. Stratigraphic units within the Edwards Group. Formation names assigned to the Maverick Basin, the Devils River trend, and the San Marcos Platform from Rose (1972). Cyclic units are from Hovorka and others (1993).

Hydraulic Conductivity—A Definition

Hydraulic conductivity is a hydrologic and rock property that affects the ease of water movement. In the classic set of experiments at a water-filtering plant in Dijon, France, Darcy (1856) showed that (1) the rate of discharge of water through a sand-bed filter is directly and linearly proportional to the force, or hydraulic-head gradient, applied to the water and (2) the proportionality constant varies with sand texture. Hydraulic conductivity (K) is defined, therefore, as the proportionality constant or the slope of the line relating discharge (q, volumetric flow rate per unit cross-sectional area [L/t]) and the hydraulic-head gradient (grad h [L/L/]

$$q = -K \cdot \text{grad}\, h\,, \tag{1}$$

where the negative sign indicates that flow is in the direction of decreasing hydraulic head. Hydraulic conductivity has units of length/time (L/t). Darcy's law is valid for nonturbulent ground-water flow. In high-velocity, turbulent flow, the relationship between discharge and gradient no longer is linear.

Hydraulic conductivity, K, is related to intrinsic permeability, k, by

$$K = \frac{\rho g}{\mu} k\,, \tag{2}$$

where ρ is the fluid density (M/L^3), g is the gravitational acceleration constant (L/t^2), and μ is the dynamic viscosity (M/Lt) (Freeze and Cherry, 1979). Intrinsic permeability has dimensions of length squared (L^2) and is solely a rock property, affected by porosity, pore-size distribution, geometry of pore-to-pore connections, and the tortuosity of pore-scale flow paths. Petroleum engineers commonly report intrinsic permeability in units of darcys, where one darcy is approximately equal to 10^{-8} cm^2. Intrinsic permeability can be converted to hydraulic conductivity, assuming typical values of fluid density and viscosity; for fresh water in the Edwards aquifer, K (ft/day) = 2.74 k (darcys).

The rate of ground-water flow in the Edwards aquifer, therefore, is controlled by the distribution of hydraulic conductivity in the aquifer and the hydraulic-head gradient between recharge and discharge areas. Darcy's law generally applies throughout the porous Edwards aquifer except perhaps in the immediate vicinity of high-capacity water wells (Ward, 1964; Eagon and Johe, 1972).

Previous Work

The structure, stratigraphy, and hydrology of the Edwards aquifer have been extensively documented by previous studies. This study builds on the results obtained by these studies. Data and interpretation from these studies were compiled and integrated with the additional data and analysis generated during this study.

Structure

Previous maps of the Edwards aquifer in the subsurface were published by Klemt and others (1979) and Maclay and Small (1986). The Edwards outcrop was mapped at 1:250,000 scale by Brown and others (1974), Proctor and others (1974), and Waechter and others (1977). More detailed mapping includes Grimshaw (1976), Grimshaw and Woodruff (1986), Baumgardner and Collins (1991), Collins and others (1991a, b), Raney and Collins (1991), Collins (1992a, b, c, d; 1993a, b, c, d, e, f, g, h; 1994a, b, c, d, e), Stein (1993), and the USDA Soil Conservation Service (1993). Some of the mapping of the members of the Edwards Group currently under way at the U.S. Geological Survey (USGS) were examined but have not yet been published (Ted Small, USGS, personal communication, 1994); preliminary results of the USGS study were examined but could not be incorporated in this report.

Stratigraphy and Geomorphology

Rose (1972) and Smith (1964) compiled comprehensive works on stratigraphy and facies describing the Edwards Group. Abbott (1973) and Maclay and Small (1986) described the lithologies within the aquifer. Ellis (1986a, b) compared the diagenesis in the aquifer with that in the saline Edwards. Langford (1942), Kastning (1983, 1986), and Veni (1987, 1988) described cave formation in the Edwards. Woodruff and Abbott (1986) described the geomorphic evolution of the aquifer region.

Hydraulic Properties

Garza (1968) calculated that transmissivities of the Edwards aquifer in the vicinity of San Antonio are in the range of 1 to 2 million ft^2/d (90,000 to 200,000 m^2/d). Marquardt and Elder (1979) listed specific capacity test data for selected wells in Bexar County. Klemt and others (1979) noted that transmissivity of the Edwards aquifer ranges from less than 133 ft^2/d (12 m^2/d) near the outcrop to over 2.6 million ft^2/d (240,000 m^2/d) in Bexar and Comal Counties. Klemt and others (1979) analyzed pump-test and specific capacity results with analytic solutions that assume radial flow in an extensive, homogeneous, porous medium. Klemt and others (1979) argued on the basis of a paper by Eagon and Johe (1972) that although the Edwards has fractures and conduits, for long-term tests, the overall behavior of the Edwards aquifer would satisfy these assumptions. Klemt and others (1979) measured transmissivity and coefficient of storage using three wells in the unconfined portion of the aquifer. Transmissivity ranged from 1,700 to 52,000 ft^2/d (160 to 4,800 m^2/d), and hydraulic conductivity ranged from 8 to 107 ft/d (2.4 to 33 m/d). Klemt and others (1979) also generated a transmissivity map for the Edwards aquifer from specific capacity and step drawdown tests. Maclay and others (1980) presented data and information on specific capacity, well yields, and aquifer tests. Maclay and others (1980) conducted an aquifer test adjacent to the Guadalupe River and the fresh/saline-water interface near New Braunfels using a discharge well and two observation wells. Maclay

and others (1980) also conducted an aquifer test at Mission Station in downtown San Antonio using several observation wells. Maclay and Small (1976, 1983) divided the Edwards into eight hydrostratigraphic subdivisions on the basis of geophysical log and core data and determined that highly permeable beds occur at stratigraphically controlled intervals. Slade and others (1985) studied a portion of the Edwards aquifer near Austin (north of the ground-water divide at Kyle) and estimated transmissivities ranging between 3 and 47,000 ft^2/d (0.3 to 4,400 m^2/d). Slade and others (1985) interpreted specific capacity tests using the methods decribed by Bentall (1963, p. 338–340). However, when Slade and others (1985) placed these transmissivities into a numerical ground-water flow model, the match to hydraulic head was poor. Model-adjusted estimates of transmissivity ranged from 100 to 1.15 million ft^2/d (9.3 to 107,000 m^2/d). Hydraulic conductivity ranged between 0.4 and 4,180 ft/d (0.12 to 1,300 m/d). Maclay and Small (1986) generated a map of relative transmissivity values for the Edwards aquifer on the basis of specific capacities with an ordinal rating from 0 to 10. Maclay and Small (1986) divided the Edwards aquifer into 21 subareas and assigned an ordinal rating to each subarea, higher ratings indicating higher transmissivities. Maclay and Small (1988) suggested that an ordinal rating of 1 is about 200,000 ft^2/d (19,000 m^2/d) and an ordinal rating of 10 is about 2 million ft^2/d (190,000 m^2/d). Guyton and Associates (1986) conducted numerous hydraulic tests on monitor wells constructed near the fresh/saline-water interface—flow tests at 50-ft (15-m) penetration intervals and packer tests at different intervals. Other hydraulic tests on monitor wells were conducted by Poteet and others (1992) along two fresh/saline-water interface transects and by Waugh (1993) in southern Medina County. Ogden and others (1986) summarized aquifer tests in the Edwards and Glen Rose Formations in the vicinity of San Marcos performed by Rothermel (1984) and Quick (1985). Transmissivity ranged between 2.5 and 40,000 ft^2/d (0.2 and 3,700 m^2/d), and wells located near faults, fractures, and lineaments had higher specific capacity and transmissivity values. Maclay and Land (1988) based transmissivity estimates for a numerical flow model mostly on information published by Maclay and Small (1984) and Maclay and others (1980): 8,600 to 1.7 million ft^2/d (800 to 160,000 m^2/d) for the

unconfined zone, 1.7 million to 8.6 million ft^2/d (160,000 to 800,000 m^2/d) for the confined portion, and 86 to 8,600 ft^2/d (8 to 800 m^2/d) for the slightly saline zone.

Storativity

Maclay and Rettman (1973) estimated the regional specific yield of the Edwards aquifer in the San Antonio area to be 0.025 on the basis of annual differences between recharge and discharge and water-level fluctuations in wells near the outcrop. Maclay and Small (1976) determined that the unconfined storage coefficient ranged between 0.05 and 0.20 depending on rock types. Klemt and others (1979) showed that the average coefficient of storage is 0.06 in the outcrop and 0.0005 in the confined part of the aquifer. Klemt and others (1979) thought that 0.0004 and 0.0007 from two tests were unreasonably low estimates of storage coefficient and perhaps were affected by fractures. Sieh (1975) determined that the storage coefficient in the Edwards most likely ranges between 0.0004 and 0.0008 and averages 0.0003. Maclay and Small (1984) estimated the storage coefficient for the confined portion of the aquifer to range from 0.00001 to 0.0001. Slade and others (1985) stated that the storage coefficient probably ranges from 0.00003 to 0.00006 and specific yield probably ranges from 0.008 to 0.064 for the Edwards aquifer in the Austin area. Maclay and Small (1986) calculated a confined storage coefficient of 0.00016 from an equation by Jacob (1950). Maclay and Land (1988) used a finite-difference model to determine that the storage coefficient of the unconfined portion of the aquifer was 0.05. Hovorka and others (1993) used barometric pressure fluctuations to find an average storage coefficient of 0.00026 for the confined part of the aquifer.

Hydrologic Simulations

Klemt and others (1979) generated a finite-difference model to investigate the influence of projected water demands on aquifer storage and spring flow, to determine the effectiveness of artificial recharge, and to discover whether ground-water management could protect spring

flow at Comal and San Marcos springs. Mahin and Campana (1983) and Campana and Mahin (1985) developed a discrete-state compartment, or mixing cell, model of the Edwards aquifer and used tritium concentrations in recharge water, ground water, and spring water to calibrate and validate the model. Wanakule and others (1986) applied an optimization technique using a ground-water simulator to determine optimal pumping rates for the Edwards aquifer. Maclay and Land (1988) used a finite-difference model modified to include barrier faults to investigate the effect of geologic structure and ground-water flow and values of transmissivity, anisotropy, and storage coefficient. Calibrated results suggest that transmissivity in the confined portion of the aquifer between San Antonio and Comal Springs is high and that storage coefficient for the unconfined portion of the aquifer is about 0.05. Maclay and Land also identified two areas of regional flow that converge at Comal Springs. Thorkildsen and McElhaney (1992) improved the finite-difference model developed by Klemt and others (1979) to evaluate management plans by incorporating new data and calibrating the model to historical recharge and pumpage rates. Wanakule and Anaya (1993) developed a lumped parameter model to simulate monthly water levels and spring flows for the Edwards aquifer. This model is a more simplified representation of the aquifer than a finite-difference model in that parameters are lumped into drainage basins. Kuniansky (1994) and Kuniansky and Holligan (in press) assembled a finite-element model of the Edwards and Trinity aquifers. Models are also under development at The University of Texas at Austin to investigate spring flow augmentation at San Marcos and Comal springs (J. M. Sharp, Jr., The University of Texas at Austin, personal communication, 1994).

METHODS

To develop a complete understanding of the spatial distribution of permeability in the Edwards aquifer, researchers on this study first collected a spectrum of different types of permeability data and then compared and interrelated these various data sets. Most of the information is appended to this report in an ARC/INFO GIS computer format. The intention is that future users can extract hydrogeologic data needed at whatever scale desired.

This study was organized into four tasks: (1) prepare improved, detailed structural maps of the Edwards Group in the outcrop and in the subsurface; (2) quantify the transmissivity of the aquifer using field-scale tests of hydrologic properties; (3) define calibrated relationships between porosity determined from wireline logs and matrix permeability measured on core sample plugs taken from outcrops and from subsurface cores; and (4) quantify the influence of faults on permeability, diagenesis, and secondary porosity.

Structural Data Set

A structure map of the aquifer region was constructed to determine the geologic framework of the strata that comprise the Edwards aquifer. This map illustrates faults, the Edwards Group outcrop, and the subsurface structure of the top of the aquifer (base of Del Rio Formation). The part of the map covering the Edwards outcrop was compiled from a variety of sources. Outcrop geology between New Braunfels and San Antonio was compiled from recent 1:24,000-scale maps by Baumgardner and Collins (1991), Collins and others (1991a, b), Raney and Collins (1991), and Collins (1992a, b, c, d; 1993a, b, c, d, e, f, g, h; 1994a, b, c, d, e). A recent 1:50,000-scale map of the Edwards outcrop in Bexar County (Stein, 1993) was also used for checking existing maps and for compiling the surface geology of the San Antonio area. The surface geology at San Marcos was modified from 1:250,000-scale mapping by Proctor and others (1974) and 1:24,000-scale mapping by Grimshaw (1976) and Grimshaw and Woodruff (1986). Outcrop geology of the Edwards Group west of San Antonio was compiled from 1:250,000-scale maps by Brown and others (1974) and Waechter and others (1977). The distribution of igneous plugs is based on their mapped geometry in outcrop and might not describe their geometry in the subsurface.

The subsurface structure on the top of the Edwards aquifer (base of the Del Rio Formation) was interpreted using data from about 1,100 wells (Pl. 1). The major source of data is stratigraphic interpretation of well logs collected from the files of the Edwards Underground Water District (EUWD) and the surface casing division of the Texas Water Development Board

(TWDB). In addition, published well log and stratigraphic data (Rose, 1972; Small, 1984; Schultz, 1992, 1993, 1994) and unpublished well data (TWDB/EUWD files, 1993) were compiled. Well locations were extracted from the log headers and from lease maps prepared by the TWDB surface casing division. Elevations entered on log headers were used if available; otherwise ground elevation at the well was estimated using 1:24,000-scale topographic maps. Discrepancies in location and elevation were resolved using location descriptions on the logs, and the uncertainties were noted in the data base. The largest location discrepancies were found where lease maps were used for well location, probably because of old map projections used for those base maps. Existing regional structure maps of the aquifer by Klemt and others (1979) and Maclay and Small (1986) were reviewed. Major structural discontinuities were identified using 100-ft (30.5-m) contour intervals. Subsurface interpretations and compilations of the outcrop geology were made on 1:100,000-scale base maps. These maps were digitized using the DIGIT module of the CPS-PC[1] using universal transverse mercator (UTM) projection reference coordinates and formatted for input into ARC/INFO GIS[2] and SGM StrataModel©.

Isopach Maps

One basic element needed for several parts of this study was an updated set of contoured isopach maps showing the thickness of rock units. These maps were used to create computer models of the volume of the aquifer for matrix permeability mapping. They also were used to correct specific capacity for partial penetration of wells and to determine hydraulic conductivity from transmissivity. The offset along faults can be compared to the total aquifer thickness to calculate the effect on transmissivity owing to decreased effective thickness of the aquifer across the fault. In addition, isopach maps can be used as input to future hydrologic models. In this study, three-dimensional computer models of the aquifer were created on the basis of structural elevation maps for the top or bottom of the aquifer. In the Edwards outcrop,

[1]Contour Plotting System (CPS), Radian Corporation, Austin, TX.
[2]Environmental Systems Research Institute, Inc. (ESRI), ARC/INFO Geographic Information System (GIS), Redlands, CA.

the top of the Glen Rose Formation was used as the structural reference horizon. For the subsurface, the base of the Del Rio Formation was used as the structural reference horizon. Then a series of additional, subparallel structural surfaces were generated by subtracting thicknesses of the stratigraphic subdivisions from the structural reference horizon. This method is preferable to that of creating separate structure maps for each horizon, especially in structurally complex areas, because it eliminates uncontrolled thickness variation that can be introduced by contouring and gridding procedures.

Isopach maps of the total thickness of the Edwards Group and the thickness of the upper Edwards interval (Hovorka and others, 1993) were revised to incorporate additional geophysical log and core data examined in this study, local revisions in stratigraphic interpretations, and published stratigraphic data (Rose, 1972; Small, 1984). The criteria used for identification of stratigraphic markers were (1) distinctive, regionally recognizable log patterns (Table 1), (2) conservation of unit thickness, (3) interpretation of structure, (4) stratigraphic concepts developed during core, outcrop, and log examination, and (5) previous log interpretation. No logs were collected for some published data, so these data were evaluated for consistency with stratigraphic data collected for this study.

Formation thickness at well locations in the confined part of the Edwards aquifer was found from the Edwards isopach, or thickness, map generated for this study. This isopach map was digitized in ARC/INFO GIS and loaded into CPS. CPS generates a continuous surface by which a value such as Edwards thickness can be found for any x or y coordinate in the domain. Well locations were fed into CPS, and thicknesses were gridded and interpolated. For the outcrop area, the thickness of the saturated part of the formation was of interest. This was determined manually using maps of the top of the Glen Rose (bottom of the Edwards) and knowledge of land-surface elevation and depth to water at the well.

Table 1. Criteria for definition of stratigraphic units used in this study.

Stratigraphic unit	Lithologic and facies character	Log response
Del Rio Formation	Shale, sharp, unconformable (?) contact with the underlying Georgetown Formation.	High gamma log response, low resistivity. Local and regional variability in the break between the Del Rio and the Georgetown Formation, probably depending on the amount of glauconite and shale in the Georgetown. Contact placed at the base of the blocky shale where resistivity begins to increase and gamma decrease.
Georgetown Formation	Low porosity, locally argillaceous and glauconitic, subtidal facies.	High resistivity and commonly high gamma at base, not separated from Edwards.
Person Formation	Cyclic platformal carbonates, high lateral variability; regional flooding surface defines the base of the slightly argillaceous subtidal regional dense member (RDM).	Low gamma, variable but generally high porosity log response. RDM base selected at base of a slightly higher gamma, low SP, low porosity unit, conserving thickness as much as possible. This is the most uncertain log pick in the aquifer because of structural and karstic complexity and similarity of the RDM lithology to other cycle bases.
Kainer Formation	Cyclic platformal carbonates, high lateral variability; maximum flooding surface defines the base of the slightly argillaceous subtidal basal nodular member (regional facies equivalent to the Walnut Formation).	Low gamma, variable but generally high porosity log response. Base Kainer selected at near the base of a slightly higher gamma, low SP, low porosity unit, conserving regional thickness trends as much as possible. Complexity results from log responses to salinity and facies changes commonly seen at this stratigraphic boundary. The upper Glen Rose tidal flats may be slightly time transgressive off the crest of the San Marcos Platform, and the maximum flooding surface (highest gamma response, dark recycled grains) may occur on top of or a few tens of feet above the top of the Glen Rose tidal flats. The base of the bleached aquifer rock may conform to or occur slightly above or below the maximum flooding surface.
Glen Rose Formation	Cyclic platformal carbonates, thinner cycles with higher argillaceous content in tidal flats in upper cycles.	Spiky gamma and porosity log response corresponding to thin cycles, some high porosity, typically decreased resistivity corresponding to higher salinity.
Devils River Formation	Cyclic platformal carbonates, high lateral variability. Hovorka and others (1993) in contrast to Rose (1972) recognized high-frequency cyclicity within the Devils River Formation.	Same log patterns used are in the Kainer and Person Formations; however, RDM difficult to identify where subtidal facies interbedded with grainstones. Upper Devils River becomes more homogeneous in log response toward the Maverick Basin edge.
Salmon Peak*	Thick beds of burrowed, fine-grained miliolid wackestones and packstones, local thin grainstones increase in thickness, grain size, and frequency toward the top.	Moderate to high porosity with little log character, variable response at the base because of collapse.
McKnight	In subsurface two evaporitic units separated by argillaceous carbonate. In the aquifer, evaporite has largely been dissolved.	Complex because of collapse and saline fluids; some argillaceous units with high gamma identified.
West Nueces	Subtidal wackestones, grainstones toward the top.	Low porosity, low to moderate gamma character.

*Nomenclature variable. See Smith (1964), Miller (1983), and Rose (1972) for alternative stratigraphic nomenclature.

Specific Capacity, Transmissivity, and Hydraulic Conductivity Data Set

Specific capacity, transmissivity, and hydraulic conductivity were measured in the Edwards aquifer using various hydraulic tests, including production, penetration, step-drawdown, and packer tests. This section includes an exhaustive compilation of hydraulic test data and describes how specific capacity was related to transmissivity and how results were analyzed.

Data Collection

Data were compiled from Texas Natural Resource Conservation Commission (TNRCC), EUWD, and TWDB files and from reports by Myers (1969), Klemt and others (1979), Marquardt and Elder (1979), Maclay and others (1980), Guyton and Associates (1986), Alexander (1990), Poteet and others (1992), and Waugh (1993).

Specific Capacity

Specific capacities for the Edwards aquifer were mostly found in TNRCC central records and EUWD and TWDB files. Specific capacities were also compiled from the previously cited reports. Well name, pumping rate, drawdown, time of pumping, well diameter, casing diameter, well depth, and open interval length were recorded. Only specific capacities with these data were noted because much of this information was needed for analytical calculations. In many cases, the time over which the specific capacity test was conducted was not noted. Limiting tests to those having all the above information ensured that only the best specific capacity data were used. In some cases, test data indicated lack of drawdown. For example, well AY68-35-1 was pumped at 8,337 gpm (31,600 L/min) with no drawdown recorded. This well clearly has a very high transmissivity. Leaving such tests out of the data base would bias results toward lower specific capacities and transmissivities. To include these tests, therefore, only tests with

pumping rates greater than 50 gpm were recorded, and a minimum drawdown of 1 ft (0.3 m) was assumed, which is thought generally to be the accuracy of water-level measurements by contractors for these tests. For such data the calculated specific capacity is a minimum estimate.

If available, the latitude and longitude of the well were noted. If there were no coordinates for a well, the well location given in driller's records was plotted on a 1:100,000-scale topographic map. These well locations were digitized using ARC/INFO GIS and plotted (Pl. 2). All information was entered into a data base.

Step-Drawdown Tests. Step-drawdown tests are essentially specific capacity tests at different pumping rates. The many unanalyzed step-drawdown tests recorded in the TWDB files were compiled and interpreted in this study. Step-drawdown tests are used to determine the yield of a well, optimal depth to set a pump, and formation parameters, such as the well-loss constant, which is used to calculate the efficiency of the well at any given discharge rate (Domenico and Schwartz, 1990). These tests can also be used to find transmissivity if time-drawdown data are collected (Bisroy and Summers, 1980; Driscoll, 1986). However, time-drawdown data generally have not been recorded during step-drawdown tests in the Edwards aquifer.

Transmissivity and Hydraulic Conductivity

In addition to specific capacity, transmissivity and hydraulic conductivity data were compiled from the previously cited reports and TWDB files. Where possible, test data were reanalyzed to verify transmissivity and storativity estimates.

Vertical Variation Data. Guyton and Associates (1986) and Poteet and others (1992) reported results from tests in which transmissivity and/or specific capacity was determined at different depths. Waugh (1993) presented data on flow tests and drill-stem tests at different depths. Guyton and Associates (1986) conducted tests in San Antonio, Poteet and others (1992) ran tests in San Marcos and New Braunfels, and Waugh (1993) collected test data from a well in

southern Medina County. These tests include what Guyton and Associates (1986) called "50-foot flow tests," in which a flow test was conducted after each 50-ft (15-m) drilling advance. Successive tests were used to determine hydrologic properties over 50-, 100-, 150-, and 200-ft (15-, 30-, 46-, and 61-m) intervals. Guyton and Associates (1986) also conducted packer tests. Poteet and others (1992) conducted packer tests similar to the 50-ft flow tests and additional tests in successively overlapping intervals. Poteet and others (1992) presented plots of the transmissivity against tested interval to demonstrate the variability of transmissivity with depth.

Calculation of Transmissivity from Specific Capacity

Specific capacity is a measure of the productivity of a well (Freeze and Cherry, 1979) and indicates how abundantly a well might yield water. Specific capacity is commonly used to compare production between wells and to choose pump capacity. Because a specific capacity test involves only pumping a well at a constant rate and measuring the resulting drawdown in the water level, it is a cost effective way of measuring a well's productivity. In mathematical terms, specific capacity, SC_W, is defined as the pumping rate, Q, per unit hydraulic head decline in the well, Δh_W:

$$SC_w = \frac{Q}{\Delta h_w}, \tag{3}$$

and it has the same dimensional units as transmissivity (length squared per time). For steady state conditions, specific capacity is a function of well radius, degree of penetration, and transmissivity. For transient conditions, specific capacity is also a function of time (McWhorter and Sunada, 1977). Specific capacity increases with increasing transmissivity and decreases with increasing time.

It is possible to relate specific capacity to transmissivity by either analytical or empirical equations. However, specific capacity must first be corrected for well loss and partial penetration effects.

Well Loss

Well loss is defined as a loss of hydraulic head in a pumping well because of flow through the well screen and/or turbulent flow of water to the pump intake in the well bore. Therefore, the unit decline in head in the well, Δh_W, is the sum of the head loss in the aquifer at the well, Δh_a, and the well loss, Δh_L:

$$\Delta h_w = \Delta h_a + \Delta h_L \, . \tag{4}$$

Equation 4 can also be presented as

$$\Delta h_w = B\,Q + C\,Q^2 \, , \tag{5}$$

where B is the well function and C is the well loss constant.

The majority of wells in the Edwards aquifer are open completions; they have no well screens, and well bores are in direct contact with the formation. Therefore, frictional well losses at the well face are negligible. However, well losses due to the flow of water to the pump intake are important, especially when pumping rates are high. Another term for this type of well loss is pipe friction loss because the borehole is similar to a pipe. Pipe friction losses for laminar flow are small and can be ignored but can be large for turbulent flow.

If well loss constants were not available for a specific capacity test at a well, well loss owing to turbulent flow was approximated as a pipe friction loss, which was calculated using the Hazel-Williams equation,

$$h_f = \frac{3.022\, v^{1.85}\, L}{C^{1.85}\, d^{1.165}} \, , \tag{6}$$

where v is the velocity of the flow, L is the length of the pipe, C is the Hazel-Williams roughness coefficient (Lindeburg, 1992), and d is the diameter of the pipe. The unit head loss for the aquifer at the well was found using equation 4, and the specific capacity corrected for well loss can be calculated by

$$SC_a = \frac{Q}{\Delta h_a}. \tag{7}$$

Partial Penetration

A well that is not completed over the entire thickness of the aquifer is said to be partially penetrating. When a partially penetrating well is pumped, vertical components of flow result, which can lead to overestimates of transmissivity. The effect of partial penetration can be corrected by using (Walton, 1970):

$$SC_{a,p} = \frac{SC_a}{\left[\frac{L}{b}\left\{1 + 7\left(\frac{r_w}{2L}\right)^{1/2}\cos\left(\frac{\pi L}{2b}\right)\right\}\right]}, \tag{8}$$

where $SC_{a,p}$ is the specific capacity corrected for a partially penetrating well, L is the length of the well screened to the aquifer, b is the thickness of the aquifer, and r_w is the radius of the well. Equation 8 assumes flow is steady state and that the aquifer is an isotropic, homogeneous continuum. Vertical inhomogeneity complicates applying equation 8 to wells in the Edwards aquifer, especially wells with short completion intervals that intersect extremely permeable fractures or conduits. For example, even if one or a few extremely permeable conduits deliver almost all the flow to a well, use of equation 8 assumes that permeability applies to the entire aquifer thickness, which leads to greatly overestimated specific capacities. This is less of a problem where the well face or open interval is long because specific capacity is averaged over the completion length. In order to avoid such difficulties, tests for wells with very short completions (<10 ft [<3 m]) were not included.

Analytical Relationship between Transmissivity and Specific Capacity

Specific capacity can be related to transmissivity using an analytical equation. However, numerous assumptions must be made, some of which might not apply in limestone having

fractures and conduits. The most limiting assumption is that the fractured media approximate a granular aquifer or continuum. However, the hydraulic response of a fractured and/or karst aquifer might appear as a continuum for long periods of pumping (Eagon and Johe, 1972; Gringarten and Witherspoon, 1972). Assuming that tests in the Edwards aquifer were run for a long enough time, analytical equations derived for relating transmissivity to specific capacity in alluvial aquifers can be used.

Brown (1963), Theis (1963), and Theis and others (1963) presented an equation to relate transmissivity to specific capacity in a fully penetrating well with no well loss for transient radial conditions for alluvial aquifers:

$$SC_w = \frac{4\pi T}{\left[-0.5772 - \ln\left(\frac{r^2 S}{4 T t}\right)\right]}, \qquad (9)$$

where T is the transmissivity, r is the well radius, S is the storativity of the aquifer, and t is the length of the specific capacity test. If SC_w is substituted for $SC_{a,p}$ (equation 8), the well loss and partial penetration restriction for equation 9 are of no concern. Because it is difficult to solve equation 9 for T in terms of $SC_{a,p}$ without having to make approximations, a computer program was written to solve for transmissivity iteratively.

Empirical Relationship between Transmissivity and Specific Capacity

Huntley and others (1992) stated that analytical solutions used to predict transmissivity from specific capacity in a continuum do not agree with measured transmissivities in fractured-rock aquifers. Huntley and others showed that analytical solutions overestimate transmissivity. Razack and Huntley (1991) stated that analytical solutions do not hold even in heterogeneous alluvial aquifers because of well losses and that statistically derived empirical relationships are preferred. Huntley and others (1992) used this statistical approach to find an empirical relationship between specific capacity and transmissivity for fractured-rock aquifers. For

transmissivity and specific capacity in units of ft^2/d, transmissivity is related to specific capacity by

$$T = 0.078\,(SC_w)^{1.18}\,. \qquad (10)$$

This empirical relationship was derived using data mostly from aquifer tests in fractured crystalline rock, which has generally very low matrix porosity and permeability. In contrast, the Edwards aquifer is primarily a dual-porosity/dual-permeability aquifer with high matrix porosity and permeability. Therefore, equation 10 might not accurately apply to the Edwards aquifer. Huntley and others (1992) stated that it is unclear whether the relationship holds for other fractured-rock aquifers. For this reason, a relationship similar to equation 10 was determined for the Edwards aquifer using aquifer tests in which both transmissivity and specific capacity were calculated.

Geostatistical Analysis

Specific capacity, transmissivity, and hydraulic conductivity results were statistically analyzed by determining ranges, means, standard deviations, and histograms for the entire study area and for subdivisions within the aquifer. Using ARC/INFO GIS, the data were sorted into unconfined and confined zones, as defined by outcrop, and subdivisions including (1) the Maverick Basin (predominantly Uvalde County), (2) the Devils River Formation (predominantly Medina County), (3) the Kainer and Person Formations, south of the 40-percent-dolomite line defined by Rose (1972) (predominantly Bexar and southern Comal Counties), and (4) the Kainer and Person Formations, north of the 40-percent-dolomite line and south of the Kyle ground-water divide (predominantly northern Comal and southern Hays Counties). Data within these subdivisions were statistically summarized and compared.

Variograms statistically quantify spatial relationships of the data. If the values of a parameter, such as hydraulic conductivity, depend on spatial position, the values of that parameter measured at two points are more likely to be similar if the two points are close

together than if the points are far apart. This measure of similarity can be quantified with a variogram, which is a plot of semivariance versus distance (Journel and Huijbregts, 1978; Clark, 1979; McCuen and Snyder, 1986). For discrete data, the semivariance, γ (for a given separation distance, λ) is defined as

$$\gamma(\lambda) = \frac{1}{2n} \sum \left[X(z_i) - X(z_i+\lambda) \right]^2 , \tag{11}$$

where n is the number of data pairs at a distance λ apart and $X(z_i)$ and $X(z_i+\lambda)$ are the values of the data at the given pairs.

Equation 11 was used to calculate semivariance of measured data (experimental variogram) on specific capacity, transmissivity, and hydraulic conductivity of the Edwards aquifer. Lines were fit to the measured data (theoretical variogram) to evaluate diagnostic spatial statistics. Many possible theoretical variograms might be fit to the measured data. The spherical variogram is a commonly interpreted model, represented mathematically by

$$\gamma(\lambda) = N + W \left(\frac{3\lambda}{2a} - \frac{\lambda^3}{2a^3} \right) \quad \text{for } \lambda \le a, \text{ and} \tag{12}$$

$$\gamma(\lambda) = N + W \quad \text{for } \lambda \ge a, \tag{13}$$

where N is the nugget, or the y-intercept of the variogram, a is the range, or the distance to where the data are spatially uncorrelated (the variogram is flat), and $N + W$ is the sill, or the value at which the semivariance peaks. W represents the difference in variance between the sill and the nugget. The spherical model describes a data set that might have a nugget effect and a spatial correlation that decreases with distance. The nugget denotes a spatially unrelated variance in the data set, which might be due to measurement error, existence of microstructures (Matheron, 1963), or other characteristics of the data (Villaescusa and Brown, 1990).

Assessment of Vertical Variations in Hydraulic Conductivity

Results of tests in 10 wells by Guyton and Associates (1986), Poteet and others (1992), and Waugh (1993) were studied further to determine how hydraulic conductivity varies with depth in the Edwards aquifer at the test locations. We calculated specific capacity from the recovery test data and average pumping rates reported in Poteet and others (1992). Waugh (1993) conducted flow tests, but recovery was so quick (less than 2 minutes) that interpretation of transmissivity was not possible. We calculated a specific capacity from the pressure of the water measured at land surface and the measured rate of flow from the well. Transmissivities for Waugh's (1993) tests were then calculated from specific capacity using the empirical relationship determined for the Edwards aquifer. Hydraulic conductivity was calculated by dividing transmissivity by test interval thickness.

Because the tested intervals for the data sets overlapped each other, a harmonic mean was used to determine the hydraulic conductivity for the intervals. A harmonic mean ($\overline{K}$) for two layers of thicknesses b_a and b_b (Fig. 3) and hydraulic conductivities K_a and K_b is found by

$$\overline{K} = \frac{K_a b_a + K_b b_b}{b}. \qquad (14)$$

The denominator, b, represents the combined thickness of b_a and b_b. The 50-ft flow tests and packer tests were conducted generally with the top of the test interval fixed near the top of the Edwards Formation and the bottom of the test interval at successively greater depth (Fig. 3). In this case, $\overline{K}$, K_a, b, b_a, and b_b are known and equation 14 can be solved for K_b:

$$K_b = \frac{\overline{K} b - K_a b_a}{b_b}. \qquad (15)$$

Using this equation, the hydraulic conductivity was found for interval b_b.

Transmissivity data calculated by Guyton and Associates (1986) and Poteet and others (1992) could not be used because values would sometimes decrease for increasing penetration lengths (Fig. 4a and 4c). It is impossible for transmissivity to decrease with depth, however,

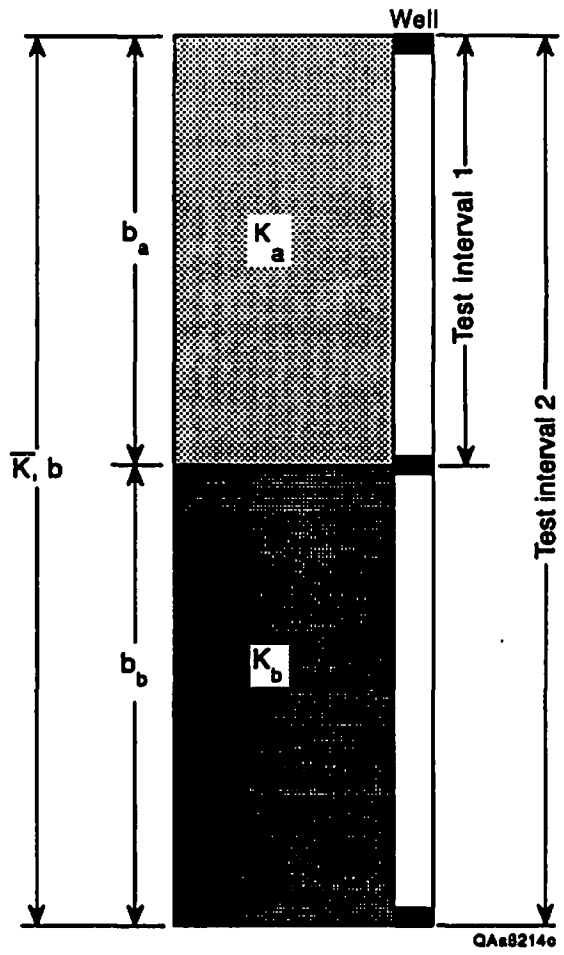

Figure 3. Conceptual models relating the mean hydraulic conductivity to the hydraulic conductivity and thicknesses of two layers for test intervals of increasing length.

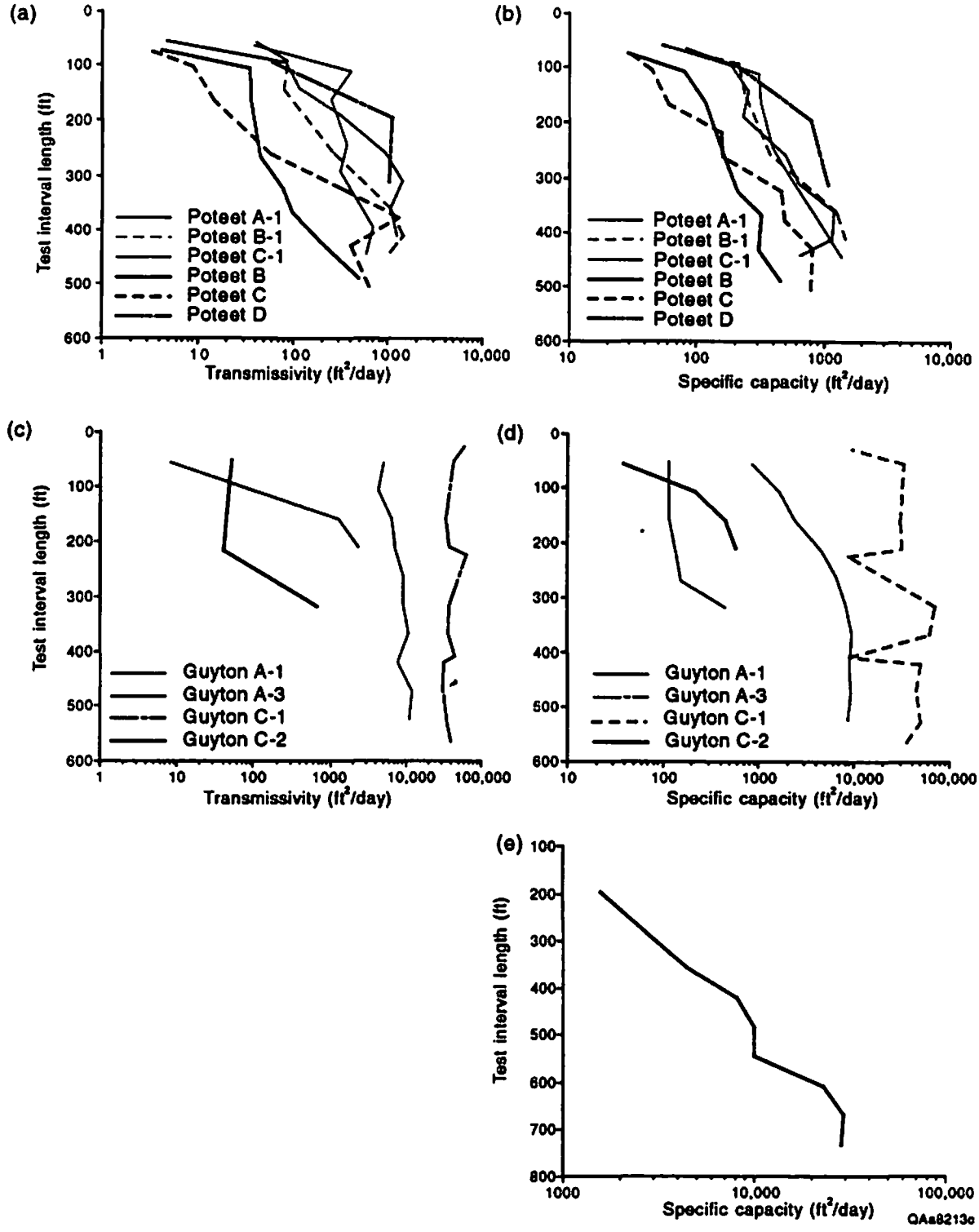

Figure 4. Variation of transmissivity and specific capacity for increasing test-interval length. Variation of (a) transmissivity and (b) specific capacity with interval length at the New Braunfels and San Marcos test wells. Variation of (c) transmissivity and (d) specific capacity with interval length at the San Antonio test wells. Variation of (e) specific capacity with interval length at the South Medina County test well.

because transmissivity of successive layers has an additive effect on the harmonic mean where flow is parallel to the layers. This can be demonstrated by equation 14 in a different form:

$$\overline{K}\,b = K_a b_a + K_b b_b\,, \tag{16a}$$

$$\overline{T} = T_a + T_b\,, \text{ and} \tag{16b}$$

$$\overline{T} = T_a + T_b + T_c + \ldots + T_n\,, \tag{16c}$$

where equation 16b is simplified ($T = Kb$) and equation 16c is generalized for n layers. The transmissivity values reported by Guyton and Associates (1986) and Poteet and others (1992) might be suspect because of errors in assumptions, measurement, interpretation, or analysis.

As with transmissivity, specific capacity should also increase with increasing penetration depth. Specific capacity data from Guyton and Associates (1986) and Poteet and others (1992) generally increase with depth (fig. 4b, 4d, 4e). One notable exception is well C-1 tested by Guyton and Associates (1986), where specific capacity decreases and increases by nearly an order of magnitude with increasing penetration (fig. 4c). Data from this well were excluded from further analysis.

Because reported transmissivities were suspect, the empirical relationship derived for the Edwards aquifer was used to estimate transmissivity from the reported and calculated specific capacity values of Guyton and Associates (1986) and Poteet and others (1992). Because transmissivity and specific capacity are directly related by a power law relationship, increasing values of transmissivity with increasing penetration depth were obtained. These values were used to find hydraulic conductivity at different intervals using equation 15. At the few intervals where specific capacity decreases with increasing interval length, the hydraulic conductivity of successive layers was assumed to be negligible. Hydraulic conductivity was plotted versus depth to determine which stratigraphic intervals of the Edwards aquifer conduct the most water at these well locations.

Average matrix permeability based on core data from these 10 wells was calculated for each interval and, using equation 2, compared with measured hydraulic conductivities determined from well testing. The hydraulic conductivities determined from well testing were assumed to reflect matrix and fracture–conduit permeability. In this manner, the relationship between matrix and fracture–conduit permeability was investigated.

The variation of specific capacity with increasing depth for the entire Edwards aquifer was determined. Percent penetration was calculated for all the confined wells and plotted against specific capacity values uncorrected for effects of partial penetration.

Plug and Log-Based Calculation of Permeability

In addition to specific capacity, other data were examined to provide information about the distribution of permeability within the Edwards aquifer. These data include measurements of the matrix, or rock, permeability. The combination of matrix, fracture, and conduit permeability leads to the measured value of transmissivity at a well, provided that these sources of permeability exist in the tested area.

Porosity and permeability were related to each other so that permeability could be calculated from log-based porosity measurements. First, porosity and permeability were measured using standard core analysis techniques on 1-inch-diameter (2.54-cm) plug samples from representative intervals of each rock type from core or outcrop. Second, empirical relationships between porosity and permeability were determined. Third, these relationships were used to estimate matrix permeability from the log-based porosity calculated by Hovorka and others (1993). SGM StrataModel© software was then used to construct a three-dimensional model of log-based matrix permeability. In addition, the stratigraphic and geographic distribution of large openings (probable conduits), measured in subsurface well bores using a caliper tool was also assessed.

The steps used to determine matrix permeability using geophysical logs were (1) collecting, describing, and classifying suites of representative samples, (2) developing an

understanding of depositional and diagenetic variables that influence porosity by examining cores and outcrops, (3) developing matrix porosity–permeability transforms from core plugs, (4) using these transforms to calculate permeability from porosity logs, (5) averaging the permeability over the logged interval to compare with transmissivities calculated from specific capacity. The permeability data served as input into a three-dimensional structural and stratigraphic model using structure and isopach maps in SGM StrataModel© to define the matrix permeability distribution throughout the model.

Hovorka and others (1993) analyzed 195 plugs and thin sections from 5 cores from the Edwards. During the present permeability study, an additional 195 plugs from 5 additional cores and 7 outcrops were analyzed. The five cores examined during the permeability study are: USGS Feathercrest, TWDB RP2, Landa Park No. 3, USGS San Marcos, and Tenneco No. 1 Ullman. Hovorka and others (1993) examined USGS Castle Hills, USGS Randolph, USGS Sabinal, TWDB YP4, and International Water and Boundary Commission ID22. The location of these cores is shown on Plate 1 and Figure 1, with the exception of the Landa Park No. 3 from New Braunfels (the exact location of which is unknown), the International Water and Boundary Commission ID22 from Val Verde County (see Carr, 1987), and Tenneco No. 1 Ullman from Gonzales County (see Rose, 1972). These cores are stored at the Core Research Center at the Bureau of Economic Geology, The University of Texas at Austin.

The relation between porosity and permeability varies with rock type. In material composed of grains, for example, well-sorted uncemented sand, the exponential relationship between porosity and permeability, depends on grain size. The relationship between porosity and permeability can be more complex for carbonate rocks, such as the Edwards Group, than for granular materials because of (1) nonspherical shapes of shells and other grains, (2) common admixtures of poorly sorted grains with varying amounts of carbonate mud, and (3) complex alteration of the carbonate minerals by dissolution, replacement, and cementation during burial and uplift. One carbonate rock with a porosity of 20 percent can have very well interconnected pores and a permeability of 100 millidarcys (md), whereas another sample with

the same total porosity can have isolated pores and permeability as low as 0.1 md. Carbonate rocks can be grouped on the basis of porosity evolution, rock fabric, or average size of grains, and porosity–permeability transforms can be developed for each group (Lucia, 1983). A rock-fabric specific approach was followed for developing porosity–permeability transforms for the Edwards Group.

Once the relationship between porosity and permeability for each rock type was developed using core-plug permeability measurements, the permeability of rock of a similar type could be calculated from porosity determined from wireline logs. Porosity logs available for the Edwards aquifer include resistivity logs, neutron logs in porosity units, and sonic logs. Porosity was calculated for these logs using the techniques developed by Hovorka and others (1993). A total of 127 logs were used for permeability calculation. Logs from Hovorka and others (1993) were supplemented by sonic and density logs, and additional resistivity and neutron logs were used to improve the areal distribution and quality of the data. The additional logs were digitized using Neuralog, Inc., software for on-screen digitizing. Log values were sampled and porosity calculated at 1-ft (0.3-m) intervals, producing a continuous measurement of the porosity variation through the aquifer. The equations of Schultz (1993, 1994) were used for conversion of sonic log ΔT to porosity. Sonic porosity was cross plotted against other calculated porosity values. Core descriptions were prepared and porosity–permeability plug data were collected from Hays and Kinney Counties and from the saline part of the aquifer. These data were used to calibrate log response in these areas. Anomalously high porosity in shaly intervals, especially at the top of the Georgetown Formation and in the McKnight Formation, was observed by Hovorka and others (1993). Correcting for the influence of shale was not feasible using available logs because of variable gamma-ray log response to shale and karst (Poteet and others, 1992). Shaly intervals at the top of the Georgetown were discarded from the data set. Intervals within the McKnight that were interpreted to be shaly on the basis of log character and core examination were assigned low effective porosity for permeability calculation.

The porosity-log interpretation and porosity–permeability transforms were used to assign a matrix permeability to each 1-ft (.30-m) interval in each logged well. The average permeability of the logged interval was recorded. A three-dimensional geologic model of matrix permeability was constructed using (1) the structure map of the top of the Edwards Group (base Glen Rose) in the confined aquifer, (2) the structure map of the top of the Glen Rose Formation in the unconfined aquifer, (3) an isopach of the Edwards Group, (4) an isopach of the upper Edwards (Person, upper Devils River, Salmon Peak, and Georgetown Formations), and (5) the log-derived matrix permeability estimates.

Quantitative Description of Faults, Fractures, and Karst in Outcrop

Fractures and caves form local and regional conduits for transmitting ground water in carbonate-rock aquifers. The rock matrix of the Edwards aquifer is highly porous and permeable and, therefore, could possibly be significant in transmitting and storing water. Fractures and caves were examined in outcrops to assess the relative contribution to transmissivity of matrix versus conduits. Large outcrops provide a unique opportunity to examine the conduits and quantify the variables that influence their hydraulic conductivity, such as conduit spacing, aperture, roughness, and connectivity. The outcrops are now on upland areas above the active part of the aquifer. During earlier stages of landscape evolution they were part of the aquifer (Woodruff and Abbot, 1986) and thus provide an opportunity to examine features analogous to those still in the subsurface.

During this study seven outcrops were described to help explain the influence of faults and joints on permeability, diagenesis, and karst development (Pl. 1). Long outcrops along road cuts provided large horizontal exposures without significant effects of surface weathering typical of natural exposures. Selected outcrops were studied with the aid of photomosaics and were described in terms of fracture mapping, fracture aperture, porosity, permeability, and roughness. Stratigraphic measured sections and samples for porosity and permeability measurement and thin section analysis were selected from the study outcrops.

Fracture Mapping

For detailed examination of three outcrops, faults and fractures were mapped on photomosaics, fracture strikes were measured, and throws on faults were calculated. A series of color photographs were taken of the outcrop at regularly spaced intervals. The photographs were taped together, overlaid with Mylar, and mapped features were drawn on the Mylar. Fracture zone widths discussed in this report are widths that were measured perpendicular to the strikes of the master faults. Data on fracture spacing were added to an existing data base containing data for other localities within the Balcones Fault Zone.

Fracture Aperture, Porosity, and Permeability

Fracture aperture was measured at the Stone Oak, Wilderness Oak, and San Geronimo exposures. This work involved (1) placing a transect line, (2) making aperture measurements, and (3) calculating porosity and permeability. Fracture aperture was measured using feeler gauges at each fracture encountered along the transect. The feeler gauges could measure a range of apertures 0.038 mm to 0.889 mm. Larger fractures and the width of cavities were measured using a 30-cm metal ruler. Care was taken to measure only natural fractures and not fractures caused by the excavation of road cuts. A vertical transect was measured at the Wilderness Oak exposure.

Porosity, n, was estimated for the vertically oriented fracture set from these aperture measurements using

$$n = \frac{\Sigma e}{L_t} \times 100, \tag{17}$$

where Σe is the sum of fracture apertures and L_t is the length of the sample set. Apertures measured for the vertical transect at the Wilderness Oak exposure were used to determine the porosity for the set of horizontally oriented fractures. Porosity for both vertically and horizontally oriented fractures, n_a, was determined from

$$n_a = \left[\frac{\left(\Sigma e_h L_v + \Sigma e_v L_h - \Sigma e_h \Sigma e_v \right)}{L_h L_v} \right] \times 100 , \qquad (18)$$

where Σe_h is the sum of the apertures collected horizontally (vertical fractures), Σe_v is the sum of the apertures collected vertically (horizontal fractures), L_v is the vertical transect length, and L_h is the horizontal transect length.

Fracture permeability was estimated from aperture measurements by assuming fractures to be parallel plates and all the fractures to be able to transmit fluids. The relationship between hydraulic conductivity, K_f, and fracture aperture is

$$K_f = \frac{\rho g}{\mu} \frac{e^2}{12} , \qquad (19)$$

where e is the fracture aperture, ρ is the density of water, g is the acceleration of gravity, and μ is the dynamic viscosity of water (de Marsily, 1986). An equivalent hydraulic conductivity such as might be measured in a well can be represented as (Snow, 1969)

$$K_e = \frac{\rho g}{\mu} \frac{N e^3}{12} , \qquad (20)$$

where N is the number of fractures per unit distance across the face of the rock. The product of N and e is equivalent to the fractional porosity of the fractures. De Marsily (1986) represented the equivalent hydraulic conductivity as

$$K_e = \frac{\rho g}{\mu} \frac{N e^3}{12} + K_m , \qquad (21)$$

where K_m is the matrix permeability.

These equations provide an upper limit to the permeability of the fractures or fracture system because they do not consider fracture roughness, aperture variability, or discontinuity, all of which have the effect of decreasing permeability.

Fracture and Conduit Roughness

Pipes, conduits, and fractures with rough walls have greater frictional losses than those with smooth walls. In other words, rough surfaces serve to decrease permeability. Specific roughness, ε, quantifies roughness of a surface, or the average size of imperfections on a surface. Specific roughness can be used to find relative roughness, R_r, which is defined as

$$R_r = \frac{\varepsilon}{D_h}, \tag{22}$$

where D_h is the hydraulic diameter. For a fully saturated pipe, D_h equals the pipe diameter. For a fracture,

$$D_h = \frac{4S_a}{P}, \tag{23}$$

where S_a is the cross-sectional area of a fracture and P is the outside perimeter of the cross section. For long fractures, D_h is about twice the fracture aperture width (de Marsily, 1986).

Specific roughness can also be used to define friction factor. Friction factor for a fracture, f_f, is defined as

$$f_f = \frac{96}{R_e}\left[1 + 6.0\left(\frac{\varepsilon}{2e}\right)^{3/2}\right], \tag{24}$$

where e is the fracture aperture and R_e is the Reynolds number.

Fracture and conduit roughness was measured in the field using a 15-cm-long contour gauge and transcribed onto paper. These traces were later scanned and digitized, and digitized files were used to measure imperfection lengths at 1-mm intervals. Specific roughness was calculated from

$$\varepsilon = \frac{\Sigma L_i}{N}, \tag{25}$$

where L_i is the imperfection lengths and N is the number of measurements. In addition to specific roughness, the standard deviation of the imperfection lengths was calculated.

Karst Features

Frequency, size, and geometry of macroscopic, solution-enlarged features transcribed from the seven outcrop photomosaics were measured. The size and location of solution features were traced on Mylar sheets, and the image was scanned into a Macintosh computer. Karst features were interpreted as if projected to a planar surface and the effects of the three-dimensional roughness of the outcrops minimized. Open cavities and features filled with terra rossa were included for analysis. Image analysis was performed on a Macintosh Centris 650 computer using the public domain NIH Image program[3]. This program was used to determine the fraction of the two-dimensional outcrop that was occupied by karst features and the size distribution of the karst features.

Digital Data Coverages

The data collected and interpreted during this study were assembled both as a set of plates that accompany this report and as a set of coverages in an ARC/INFO GIS data base. The content of the GIS data base is summarized in Table 2.

RESULTS

Structural Framework of Edwards Aquifer

The Edwards aquifer occurs within a complex part of the Balcones Fault Zone (Pl. 3). Numerous faults cut the aquifer strata and many structural discontinuities within the water-bearing strata exist regionally and locally. The composite stratigraphic displacement across the aquifer (from the fresh/saline-water interface on the south and southeast edge to the Edwards outcrop on the north and northwest) varies regionally. In the San Antonio area of Bexar

[3]Written by Wayne Rasband at the U.S. National Institutes of Health, available from the Internet by anonymous ftp from zippy.nimh.nih.gov or on disk from NTIS, 5285 Port Royal Rd., Springfield, VA 22161, part number PB93-504868.

Table 2. Content of ARC/INFO GIS data base.

Data set	Information included	Arc/Info file name	File size (bytes)	Coverage type
Stratigraphic data	Include top Edwards (base Del Rio) in feet below KB or land surface, base RDM and stratigraphic equivalents (base Salmon Peak), and base Edwards (top Glen Rose) for each well log. In addition, document well name, Texas State well number, other well numbers from log source, well location, data source, log types, total depth (TD), elevation or KB	stratwellsutm	307,539	points
Hydrologic test data	Include uncorrected and corrected specific capacity (ft^2/day), calculated transmissivity (ft^2/day), and calculated hydraulic conductivity (ft/day). In addition, document type of test, data reference, location source, location in the confined (0), or unconfined (1) aquifer, Texas State well number, well depth, casing diameter, and well diameter	hydroutm	77,153	points
Top Edwards structure	Faults and inferred faults	faults	698,237	arc
	Structure contours	contours	359,289	line
	Edwards outcrop edge	formation	541,872	polygons
Top Glen Rose	In Edwards outcrop			
Isopachs	Isopach of the total Edwards Group	tedwisopach	15,022	arc
	Isopach of the upper Edwards Group (Georgetown, Person, upper Devils River, Salmon Peak Formations)	upedwisopach	29,911	arc
Matrix permeability	Matrix permeability values calculated from wireline logs	porpermutm	10,979	points
	Matrix permeability contours	matrix	5,330	arc
Porosity + matrix permeability	Average total porosity from porosity study (revised 1994); average porosity of the upper Edwards (Georgetown, Person, upper Devils River and Salmon Peak Formations) Average porosity of the lower Edwards (Kainer, lower Devils River, McKnight and West Nueces Formations) Average total permeability, average permeability of the upper Edwards, average permeability of the lower Edwards	stratmod		points

Table 2 (cont.)

Data set	Information included	Arc/Info file name	File size (bytes)	Coverage type
Aquifer boundaries	Saline-freshwater interface (Schultz, 1994)	edwbwl	3,933	arc
	Edwards outcrop edge	formation	541,872	arc
	Updip limit of aquifer (Klemt and others, 1979)	klemt	1,341	arc
	Kyle ground-water divide (Klemt and others, 1979)	kyle	1,074	arc
	Brackettville ground-water divide (Klemt and others, 1979)	brac	826	arc
County lines	Digitized from 1:100,000 New Braunfels and San Antonio sheets, others from TNRCC 1:250000 source	txcnty250utm	454,738	arc
Geographic location grid	7.5-minute quadrangle boundaries from TNRIS	75minutm	1,302,264	polygons

County the composite displacement of aquifer strata is greater than 1,450 ft (442 m). In central Medina County there is about 1,850 ft (564 m) of composite displacement. Near Uvalde, Uvalde County, the composite displacement of aquifer strata is about 1,150 ft (350 m). Near New Braunfels, Comal County, there is more than 1,400 ft (427 m) of composite displacement of aquifer strata.

Faults within and adjacent to the Edwards Group outcrop belt between New Braunfels and San Antonio have been studied in the most detail, and general characteristics of the faults in this area most likely reflect fault characteristics in the Edwards outcrop belt toward the west, where mostly smaller scale mapping has been done. Southeast of the outcrop belt, characteristics of faults interpreted using subsurface well data might also be similar to fault characteristics of the outcrop belt. Between San Antonio and New Braunfels, the fault zone is composed of en echelon normal fault strands that strike mostly N40°–70°E and dip southeastward. Fewer faults dip northwestward. Subsidiary faults strike northwestward, northward, and eastward. The few outcrops containing larger faults indicate that fault surfaces are irregular, have dips between 60° and 85°, and display slickensides parallel to subparallel to the fault dip. Smaller subsidiary faults commonly dip between 45° and 85°. The fault zone consists of multiple, major 2.2- to 7-mile-wide (3.5- to 11-km) fault blocks bound by a long series of southeast-dipping, tight, en echelon large normal faults that have throws ranging between approximately 100 and 850 ft (30 and 260 m) (Fig. 5). Smaller fault blocks occur within the larger fault blocks, and many smaller faults with throws ranging between less than 1 ft (0.3 m) and 100 ft (30 m) cut strata across the fault zone. A series of tight en echelon large faults that bound the large fault blocks consist of individual fault strands that are commonly between 6 and 16 mi (9.7 and 26 km) long. In the New Braunfels area the spacing of the large faults increases away from the largest fault at the Balcones Escarpment. The two largest faults of this area, displaying about 340 and 850 ft (100 and 260 m) of throw, are associated with northwest-dipping antithetic faults that bound narrow grabens 3,000 to 4,000 ft (900 to 1,200 m) wide.

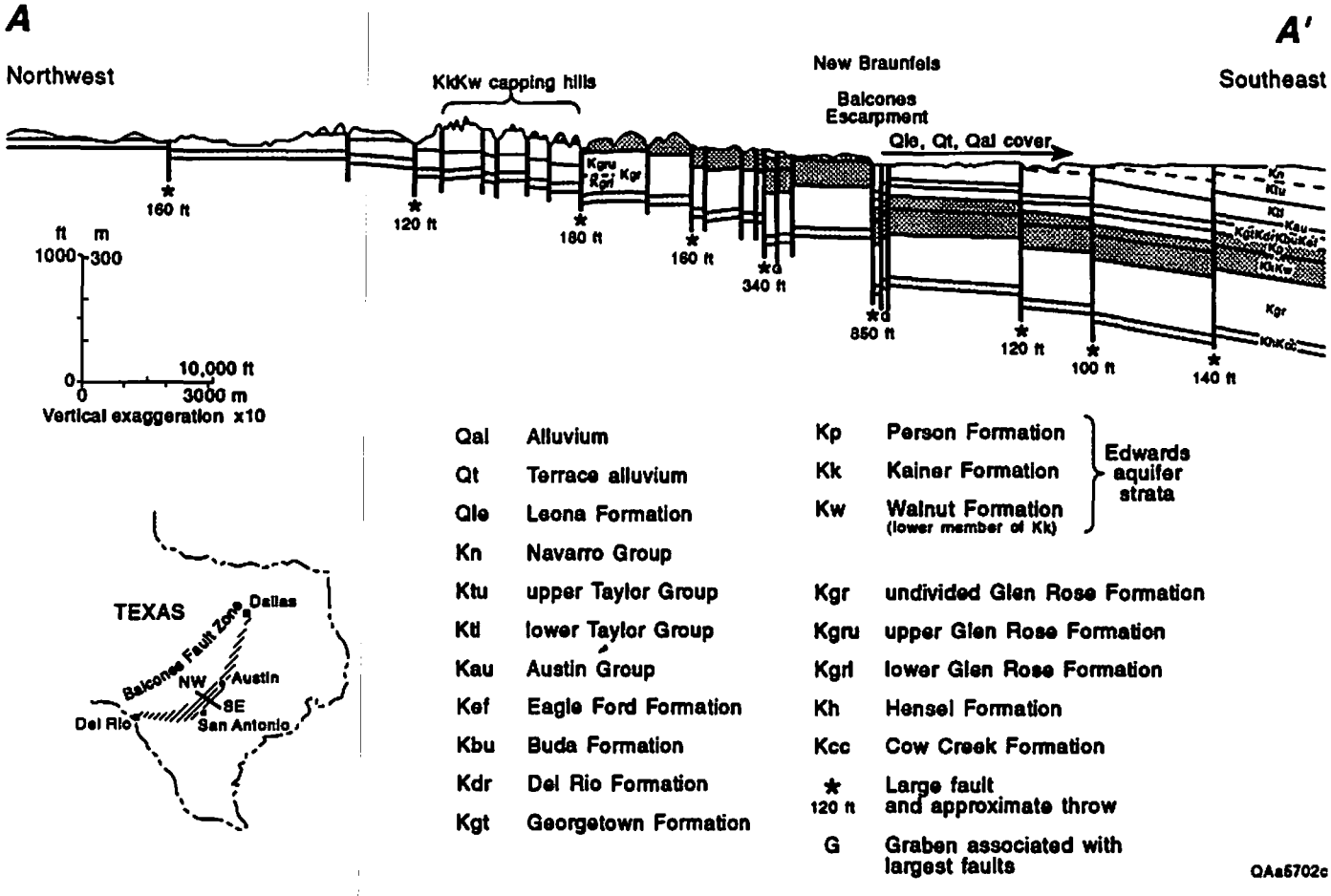

Figure 5. Structural cross section A–A′ of the Balcones Fault Zone at New Braunfels, Texas. Line of section shown in Figure 1.

The Edwards outcrop belt exhibits four large-scale steps along the fault zone. Grimshaw and Woodruff (1986) interpreted a 6-mi-wide (9.7-km) left step of the outcrop belt at San Marcos to be a northeast-dipping ramp structure between large displacement faults. About 50 mi (80 km) toward the southwest at San Antonio, the fault zone and the Edwards outcrop belt are characterized by a composite 4- to 5-mi-wide (6- to 8-km) right step of the largest displacement faults and Edwards outcrop. This area might be a southwest-dipping relay ramp that has formed in this area between the right-stepping large displacement faults. Relay ramps, also called transfer zones, are structures that might form between the tips of two en echelon normal faults dipping in the same direction (Fig. 6) (Larsen, 1988; Peacock and Sanderson, 1991, 1994). The San Marcos and San Antonio step-related structures also might be caused by faulting across the San Marcos Arch. West of San Antonio, two other large right steps occur along the Edwards outcrop belt near Sabinal and Uvalde. Other, smaller steps occur in the outcrop belt, indicating that smaller relay ramps might exist within the fault zone. A narrow 0.6-mi-wide (1.0-km) relay ramp between overlapping en echelon fault strands located north of San Antonio contains numerous fractures that have different strikes (Collins, 1993a).

South and southeast of the Edwards outcrop belt, many faults are inferred in the subsurface (Pl. 3) that generally exhibit map patterns similar to those of the outcrop belt. Most of the inferred subsurface faults strike northeastward and dip southeastward, and multiple series of closely en echelon fault strands cut across the area. Some faults dip northwestward. Preliminary analysis indicates that most of the inferred subsurface faults have throws of less than 250 ft (80 m), although a few faults might have throws that exceed 550 ft (170 m).

Matrix and Conduit Permeability of the Edwards Aquifer

Permeability in the Edwards aquifer is created by four interrelated processes: (1) depositional fabric, (2) diagenetic alteration, (3) dissolution and collapse, and (4) fracturing. Depositional fabric and diagenetic alteration affect the amount of porosity and the relative amounts of connection or separation of the pores that control fluid movement through the

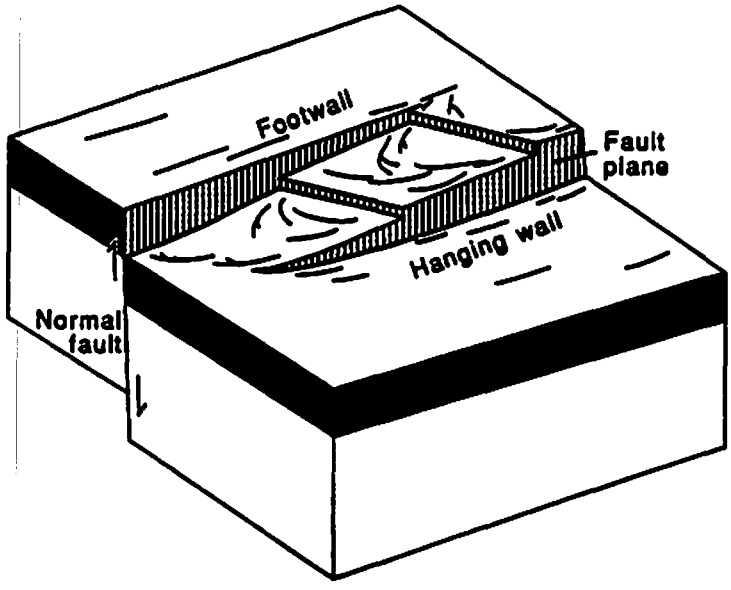

Figure 6. Generalized view of a relay ramp, modified from Collins (1993a) and Peacock and Sanderson (1994). Relay ramps and related features occur on a small scale between en echelon faults and on a regional scale between en echelon fault strands. The folded aquifer strata in the ramp might be fractured and faulted and serve as a high transmissivity pathway across a zone where offset on major faults has reduced transmissivity.

matrix of Edwards carbonate rocks. Carbonate and evaporite solution cavities and breccias have a complex geometry reflecting multiple episodes of dissolution and cavern infilling. Fracture-enhanced hydraulic conductivity depends on fracture aperture, spacing, roughness, and connectivity.

Petrographic and Facies Controls on Permeability

The permeability of a rock matrix on a fine scale depends on porosity, pore-size distribution, and size and tortuosity of the pore throats. The geometry of the pore network depends on the size and shape of the particles of which the rock is composed and on postdepositional modifications of the size and shape of particles and pores as materials dissolved and precipitated.

The initial size of the particles of which a carbonate rock is composed depends on the depositional environment in which the sediment accumulated, and it is used as the basic element in carbonate-rock description (Table 3). Environments of deposition of the Edwards Group varied laterally across the platform and through time (Rose, 1972). Changes in relative sea level caused platformwide changes in environment and corresponding changes in the texture and fabric of the sediment (Hovorka and others, 1993). High-frequency changes in relative sea level caused accumulation of cyclic sequences of low-energy subtidal, high-energy grainstone bar and muddy or grainy tidal flat facies on the San Marcos Platform (Fig. 7). Low-energy subtidal facies, deposited in the deepest water, generally have a carbonate mud matrix (packstones and wackestones), producing a fine particle size. High-energy grainstone bars facies were deposited in shallow water and are composed of well-sorted, sand- and granule-size grains (ooids, coated grains, miliolid forams, and algal or skeletal fragments). Tidal flat facies were deposited in intermittently exposed shoals, islands, and mudflats and are composed of generally thin-bedded muddy or sand-size sediments. Intermittently, marine circulation across parts of the San Marcos platform became restricted, evaporated, and then became hypersaline (Fisher

Table 3. Classification of rock fabrics used in the study of matrix permeability.

Name*	Description	Depositional environment	Porosity and permeability characteristics
Grainstone	Sediment was composed of sand size (average diameter 0.02 to 2 mm) carbonate grains.	Sediment accumulated in high energy bar or channel setting, where finer material was transported away.	Intergranular porosity can be 30 percent, resulting in permeabilities of 10 to 100 md. In dominantly subtidal settings (top of Kainer, Maverick Basin), pores are commonly filled with calcite cement, reducing porosity and permeability. Grains can be leached, especially if they were composed of aragonite, creating moldic separate-vug pores and low permeability.
Grain-dominated packstone	Sediment was composed of sand size carbonate grains, with finer (silt and clay sized) carbonate in laminae and admixed by burrowing.	Sediment accumulated in intermittently high energy bar or channel, episodically finer material accumulated and was admixed by burrowing.	Intergranular porosity is less than grainstones because of finer material partly choking pores. Porosity and permeability enhanced by dissolution of grains, mud, or dolomite.
Mud-dominated packstone	Sediment was composed of sand size and larger carbonate grains with abundant finer (silt and clay size) carbonate matrix that fills all of the intergranular space.	Sediment accumulated in a variety of subtidal environments.	Initial porosity in muddy carbonate matrix commonly reduced during diagenesis by recrystallization of the carbonate mud. Porosity and permeability enhanced by dissolution of dolomite in stratigraphic intervals where dolomitization was intense.
Wackestone	Sediment was composed of silt and clay size carbonate mud with more than 10 percent larger carbonate grains.	Sediment accumulated in low-energy subtidal environments. Large shells commonly autochthonous.	Initial porosity in muddy carbonate matrix commonly reduced during diagenesis by recrystallization of the carbonate mud. Permeability most commonly increased by fracturing.
Mudstone	Sediment was composed of silt and clay size carbonate mud with less than 10 percent carbonate grains.	Sediment accumulated in low-energy environments during platform flooding and in supertidal pond environments.	Initial porosity in muddy carbonate matrix commonly reduced during diagenesis by recrystallization of the carbonate mud. Permeability most commonly increased by fracturing.

* Nomenclature adapted from Dunham (1962) and from Lucia (1983).

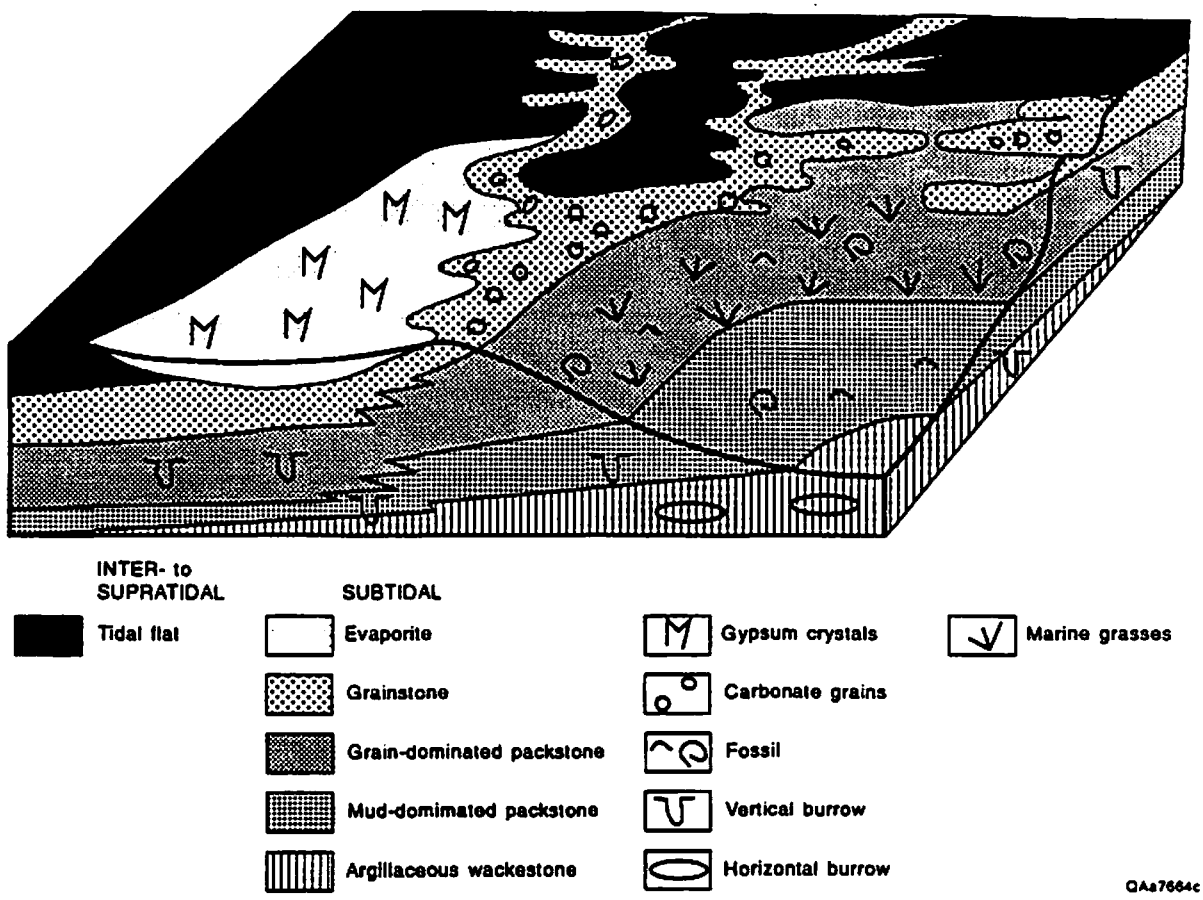

Figure 7. Generalized view of sea-level-controlled depositional facies. Lateral migration of these facies in response to sediment aggradation and sea-level fluctuation creates high-frequency cycles that are the basic component of Edwards deposition. Depositional facies is one of the factors that control the porosity and permeability of carbonates.

and Rodda, 1969; Rose, 1972). Gypsum precipitated on the floors of shallow brine pools (Hovorka and others, 1993).

Cycles created by high-frequency sea-level changes can be recognized across the platform. Minor changes in relative subsidence rates and depositional environment can be recognized in the relative abundances of facies. More tidal flats and more dolomitization can be identified toward the center of the San Marcos Platform, in eastern Bexar, Comal, and Hays Counties (Fig. 8).

In the Maverick Basin, slightly deeper water conditions persisted during Edwards deposition, and sedimentary cycles are less well defined than they are on the platform. The West Nueces Formation is dominated by fine-grained, fossiliferous wackestone and packstone facies, with grainstone beds toward the top (Fig. 8). The McKnight Formation is composed of dark, fine-grained, argillaceous limestone that was originally interbedded with gypsum and anhydrite (Smith, 1964; Carr, 1987; Hovorka and others, 1993). Gypsum and anhydrite have been dissolved from the freshwater Edwards aquifer but are preserved in parts of the saline subsurface. The Salmon Peak Formation overlying the McKnight is composed of burrowed, massive, fine-grained miliolid packstones. Toward the top, the unit is coarser grained and better sorted. This unit is tentatively interpreted as a lowstand wedge equivalent to the pre-Georgetown unconformity (Fig. 8).

Carbonate sediments are commonly altered by a variety of processes during shallow burial, deeper burial, and uplift and exposure (Bathurst, 1975). Preliminary classification of the major types of alteration was made using macroscopic and thin-section microscopic descriptions from core and outcrop. For a more detailed discussion of diagenesis of the Edwards aquifer, see Ellis (1986 a, b). The major diagenetic processes that impact matrix permeability development and porosity–permeability relationships are (1) dolomitization, (2) calcite cementation, (3) gypsum alteration by calcitization and dissolution, and (4) intense freshwater alteration. Diagenesis has modified the pore structure in a variety of ways, which are summarized in Figure 9.

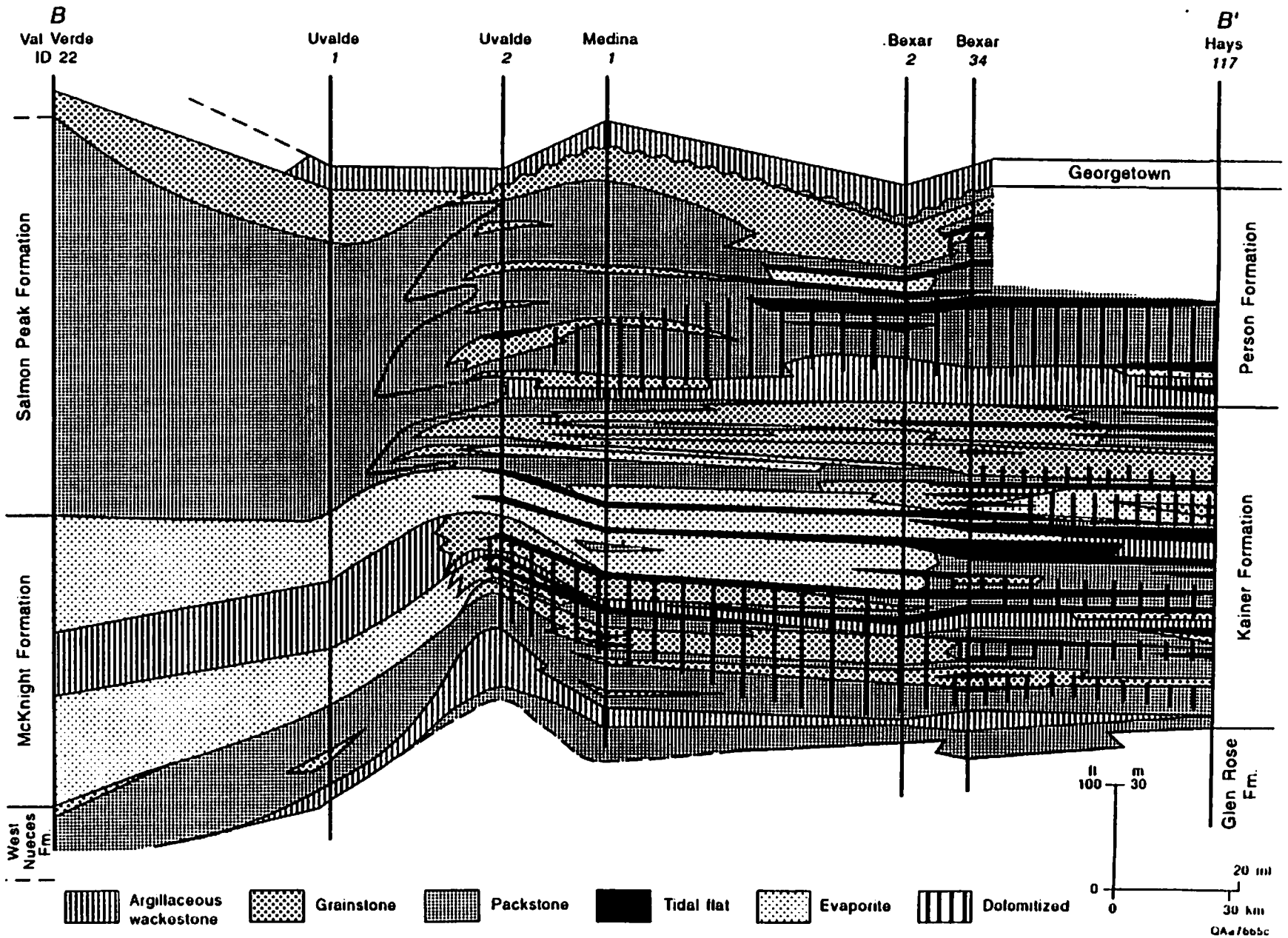

Figure 8. Generalized facies cross section B–B′ of the Edwards Group, showing stacking pattern of high-frequency cycles to form two sequences. The lower sequence is composed of the Kainer Formation, lower Devils River Formation, and basinal equivalent West Nueces and McKnight Formations. The upper sequence is composed of the Person, upper Devils River, and basinal equivalent Salmon Peak Formation. Line of section shown in Figure 1. An interval interpreted as karst dissolution in the Kainer in the Bexar 2 core has been restored to presumed original thickness. See Hovorka and others (1993) for original data.

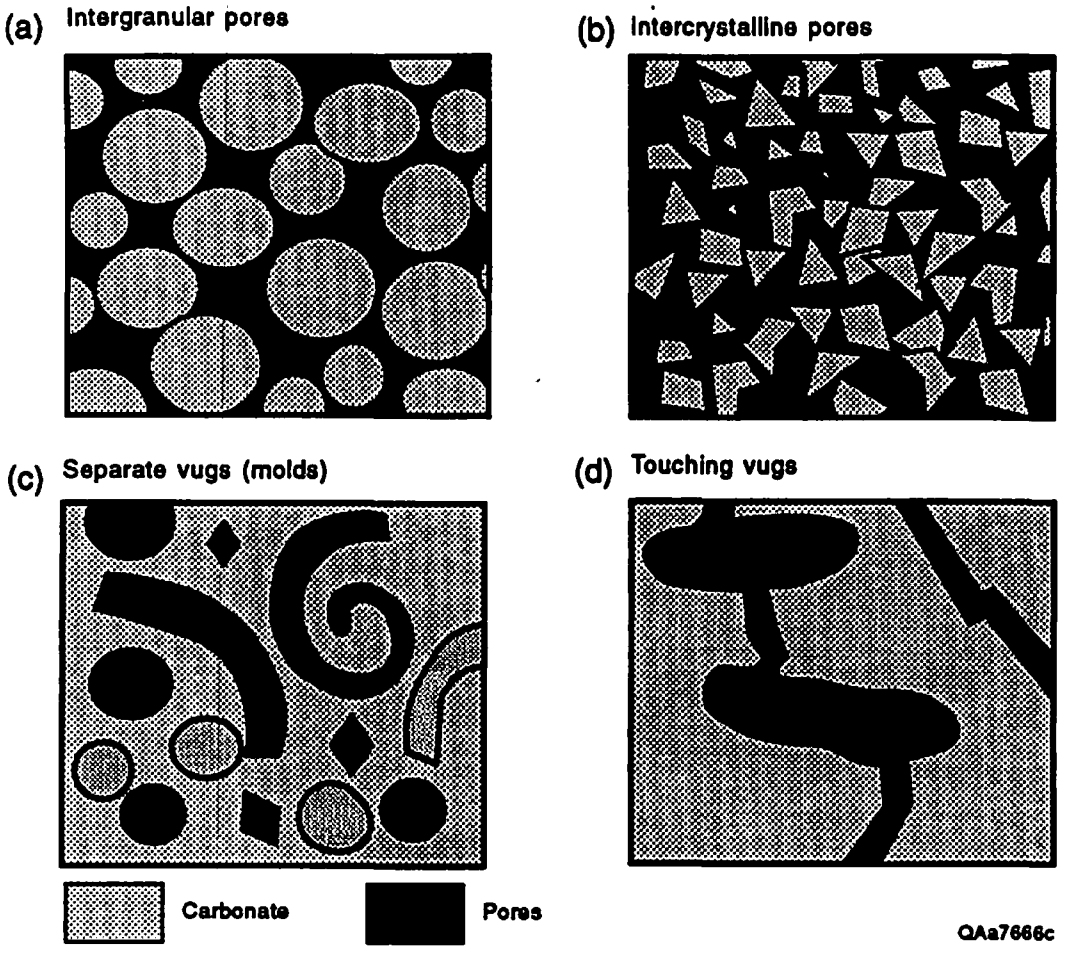

Figure 9. Schematic diagram of several common pore structures resulting from different diagenetic histories. (a) Intergranular pores exist where original grains are the dominant particle controlling pore geometry. (b) Where the original grains have been replaced or highly modified by cement, the pores are intercrystalline. (c) Separate vugs or molds form where particles (grains or crystals) have been dissolved to created pores. These pores are poorly interconnected in three dimensions and, therefore, have low permeability. (d) In contrast, touching vugs are well connected, and have high permeability.

Pore structure defined principally by size, shape, and sorting of the carbonate grains is classified as intergranular (Fig. 9a). If the original carbonate was extensively recrystallized, the pore structure is intercrystalline (Fig. 9b), and permeability depends on the crystal size and packing. Intergranular and intercrystalline pore types can be grouped as interparticle porosity. Separate vugs are pores that are interconnected only through a less porous matrix (Fig. 9c). Separate-vug permeability, limited by pore interconnection, is low relative to the permeability of rocks with similar amounts of interparticle porosity. Skeletal grains or all or parts of dolomite crystals commonly are preferentially dissolved, producing moldic porosity, which is the microscopic equivalent of separate vug porosity. Larger vugs left by dissolution of evaporite crystals and nodules are the other major separate vug types observed in the Edwards Group. If large pores are interconnected, they are classified as touching vugs (Fig. 9d). In the Edwards, touching vugs include small-scale dissolution features, fractures, and large molds that have been interconnected by dissolution of intervening matrix and cement.

Dolomitization is the process by which calcite or aragonite is replaced by dolomite. Dolomitization occurs in a variety of settings (Land, 1985) from shortly after deposition of the sediment to deep burial. In the Edwards Group, preliminary investigation identified two major types of dolomite that appear to play a role in permeability structure: (1) early formed, fine-grained tidal flat dolomite and (2) coarser dolomite that has replaced subtidal packstones. Subtidal dolomite typically has a cloudy center and a clear rim. In many samples, the center of the dolomite rhomb has been preferentially dissolved. In other samples, dolomite crystals have been completely dissolved, creating molds. Moldic pores might be large but poorly connected, and typically they have high porosity but low permeability. Replacement of dolomite by calcite, known as "dedolomitization" has been recognized as an important process in the Edwards aquifer (Abbott, 1974; Ellis, 1986b; Deike, 1990).

Core and thin sections were examined to document the present-day distribution of dolomite, as well as the distribution of calcitized and dissolved dedolomite. Most of the subtidal dolomite and dedolomite are in the middle Kainer and middle Person (Fig. 8). Most of the tidal

flat dolomite is in the middle part of the Kainer Formation and in thin units in the Person Formation that are not regionally correlatable. The most subtidal units, the base of the Kainer Formation, the grainstones at the top of the Kainer Formation, the regional dense member at the base of the Person Formation, the subtidal grainstones at the top of the Person Formation, and most facies in the Maverick Basin are minimally dolomitized. Rose (1972) mapped the distribution of dolomite in the Kainer and Person Formations throughout the Edwards Group, most of the subsurface data being collected from the saline part of the unit. The amount of dolomite increases systematically across the platform, from 20 percent at the Bexar–Medina County line to more than 60 percent dolomite in the center of the San Marcos Arch. This confirms that the dolomite distribution shown in Figure 8 is reasonably consistent with regional trends, even though the original dolomite distribution in the aquifer has been highly modified.

Calcite cementation is an intrinsic part of geochemical stabilization of the initially multimineralic biogenic materials that comprise carbonate sediments. Aragonite and high-Mg calcite shells and mud dissolve and, depending on geochemical variables, precipitate either at the same site on a microscopic scale (neomorphic replacement) or in other sites as cements. In the Edwards Formation, many of the large aragonitic skeletal grains, especially rudists, have been dissolved, and calcite cement has precipitated between the grains, creating moldic pores. Abundant calcite cement has reduced the porosity in grainstones. Cement is especially important where the grainstones are beneath thick subtidal units, for example, in the top of the Kainer, the top of the West Nueces, and the upper Salmon Peak Formations (Fig. 8). This calcite cement reduces both the porosity and the permeability in what would otherwise be highly transmissive units. Calcite cement beneath thick subtidal units might have prevented extensive dolomitization of these units. Additional calcite cement is interpreted to have precipitated during dolomite dissolution (Deike, 1990).

Gypsum was initially a volumetrically significant component of sediments in the Kainer and Person Formation on the San Marcos Platform and in the McKnight Formation in the McKnight Basin. On the San Marcos Platform, gypsum has been entirely removed by

calcitization and dissolution. Gypsum dissolution is a cause of regionally correlated breccias in Edwards platformal rocks (Fisher and Rodda, 1969; Rose, 1972). Hovorka and others (1993) identified abundant pseudomorphs after bottom-grown gypsum, demonstrating the original distribution of gypsum. Mapping the distribution of breccia and pseudomorphs shows an interval of recurrent establishment of gypsum precipitating brine pools over much of the San Marcos Platform and in the Devils River facies (Fig. 8). Most of the breccia where gypsum has been dissolved has been cemented by very coarse calcite cement, and it therefore has low porosity. Poikilotopic calcite spar also fills porosity where grainstones interfinger and are interbedded with calcitized gypsum (middle Kainer, lower Devils River Formation). Partial replacement of gypsum crystals by calcite creates vuggy porosity.

In the Maverick Basin, anhydrite is preserved in the deeper subsurface. In the aquifer, local silicification and calcitization of sulfates preserve textures; otherwise, gypsum has been removed and the permeability of the overlying strata increased by fracturing. Several episodes of gypsum dissolution and brecciation both before and after asphalt migration can be recognized in the TWDB RP-2 core.

Intense alteration in the freshwater aquifer has produced three major diagenetic alterations: dolomite dissolution, calcite precipitation, and calcite dissolution. The effect of freshwater alteration on dolomite can be observed along a transect from the saline part of the Edwards to the outcrop. Progressively more complete dolomite dissolution, as well as enhancement of porosity by karst, fracture, and intergranular calcite dissolution, is observed. In the Tenneco No. 1 Ullman core, from Austin Pierce field in the saline, hydrocarbon-bearing Edwards at depths greater than 11,700 ft (3,566 m), dolomite is preserved and porosity ranges from 6 to 24 percent. The contrast with the vuggy, bleached, and oxidized character of the aquifer is striking. Dark colors are derived from oil staining, fractures are present but not enlarged by solution, and large vugs are rare. However, even in the most downdip parts of the Edwards platformal rocks, paleokarst collapse breccias are recognized, and bedded sulfates are

not preserved, demonstrating that the present freshwater alteration in the aquifer is only the latest and most intense of a series of dissolution events (Rose, 1972; Abbott, 1975).

Updip, just south of the fresh/saline-water interface (USGS Randolph core), the center of dolomite crystals in subtidal facies has been dissolved, creating abundant partial dolomite molds. Porosity in this core averages 23 percent, higher than in the Ullman No. 1 core. The porosity in partly leached dolomite intervals is as high as 40 percent. Dolomite dissolution and porosity enhancement might be related to proximity to the freshwater aquifer. South of the fresh/saline-water interface, plumes of moderately saline water mapped by Schultz (1993) and mixing of water of various compositions (Prezbindowski, 1981; Clement, 1989) might indicate slow flux of fresh water into the saline zone or migration of the interface over geologic time. Solution-enhanced fractures, terra rossa infills, or large caverns were found neither in core nor boreholes in the saline part of the Edwards.

Within the aquifer, dolomite alteration is complex and variable on a fine scale, reflecting multiple episodes of alteration. However, most commonly dolomite has been partly or wholly dissolved from subtidal facies, but it is preserved in fine-grained tidal flats. Calcite dissolution is abundant at various scales. Many boreholes intersect large caverns. Evidence of caverns includes driller's records of drop in the drill string (Sieh, 1975), poor core recovery, recovery of cave-fill materials such as solution-pitted limestone, travertine, and terra rossa, high porosity-log response, high gamma response indicating terra rossa fills, and large or off-scale caliper log. At a smaller scale, solution modification of fractures and vugs is evident in core. In thin section, partial leaching of calcite grains and cements is evident in many samples of highly porous rocks. Well-connected pores have been further enlarged by dissolution where flow rates are faster. Connection of pores is especially evident in coarse-grained moldic rudist grainstone, where some molds have been connected by dissolution of cement between them.

In outcrop, dolomite has been extensively dissolved so that dolomitized tidal flat and dolomitized subtidal rocks contain large and small vugs and caves and terra rossa fills. These units vary in thickness, suggesting loss of volume in some parts of the bed because of dissolution.

Porosity–Permeability Relationships

Before estimating the distribution of matrix permeability in many parts of the aquifer where it cannot be measured directly, the relationship between porosity and permeability must be derived for each rock type. The porosity–permeability plugs were classified by stratigraphic unit, depositional facies, petrographic characteristics, mineralogic composition, and geologic and hydrologic setting, and the relationships between porosity and permeability were plotted for subsets. A small number of samples with greater than 1,000 md permeability were removed because they might have microfractures (touching vug permeability) and, thus, not represent matrix permeability. Grouping the samples by depositional setting and setting within the aquifer and then considering the mineralogy and petrographic characteristics reduced the scatter and provided usable relationships for calculating matrix permeability (Fig. 10). Six porosity–permeability relationships were derived (Table 4). Permeability is calculated from porosity using the linear linear relationship

$$\log k = m\phi + b\,, \tag{26}$$

where k is permeability in md, ϕ is porosity in percent, and m and b are slope and intercept (presented in Table 4). Permeabilities were not calculated for porosities greater than 35 percent because, according to examination of samples, porosities greater than 35 percent generally contain abundant large vugs, and the matrix porosity–permeability relationship developed from plugs is probably invalid where large vugs predominate.

Permeability of the saline part of the aquifer is closely related to porosity. The data trend for the USGS Randolph FM1604 core from the saline Edwards near the fresh/saline-water interface coincides with that for the deep hydrocarbon reservoir core (Tenneco No. 1 Ullman), although the deep samples have systematically lower average porosity (Fig. 10a). This suggests that the range of pore sizes is similar in both settings. A separate porosity–permeability trend is defined for the highly moldic rocks sampled in the Randolph well. These samples include both

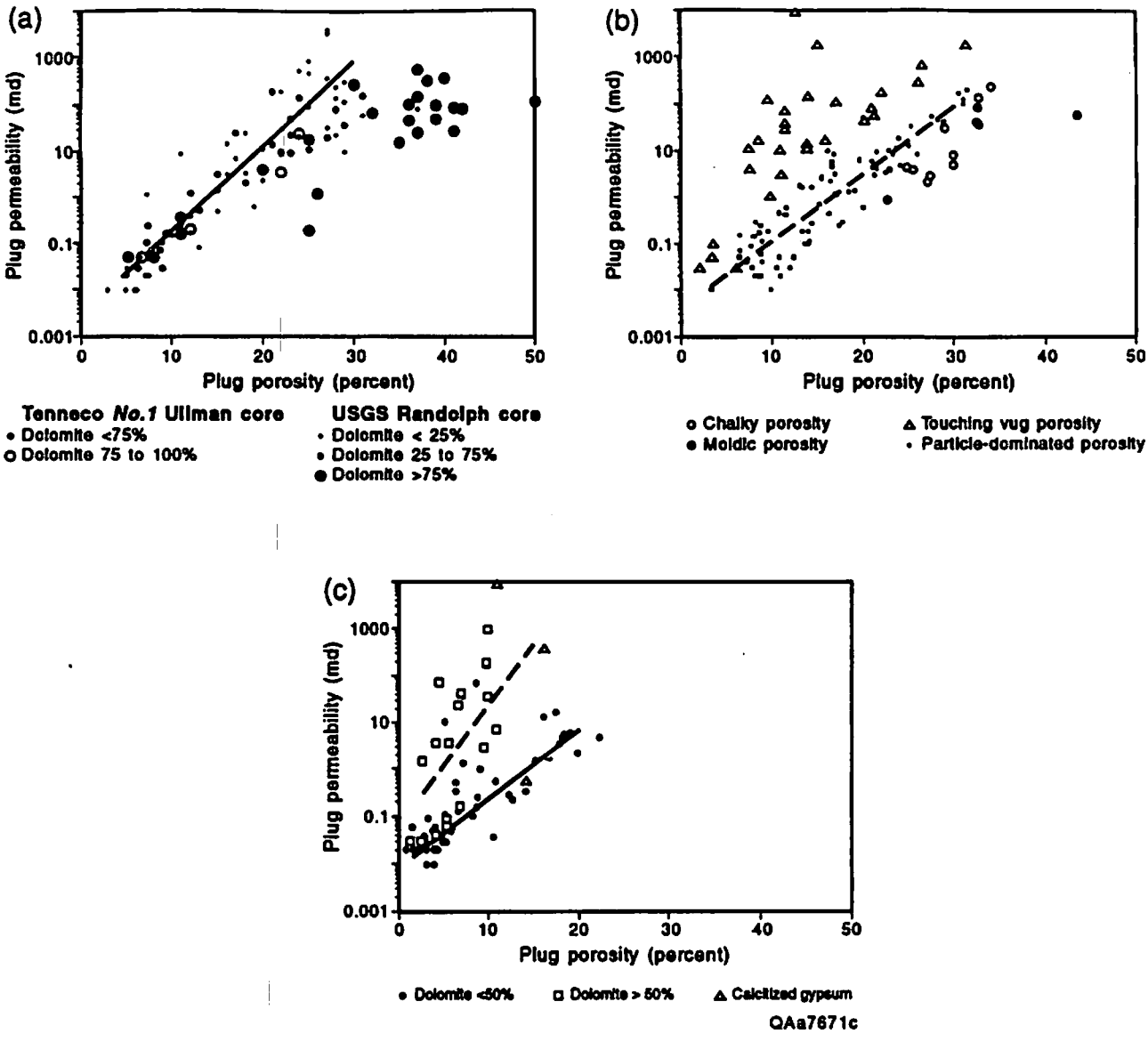

Figure 10. Relation of measured plug permeability to porosity and calculated permeability. (a) Saline part of the Edwards, showing the relationship between porosity, permeability, and dolomite. Samples from the deep subsurface hydrocarbon reservoir (Tenneco No. 1 Ullman core) and from the saline Edwards just south of the fresh/saline-water interface (USGS Randolph FM 1604 core). (b) Confined aquifer on the San Marcos Platform, showing the relationship between porosity, permeability, and pore type. Samples from the USGS Castle Hills, USGS Feathercrest, and USGS San Marcos cores. (c) Outcrops on the San Marcos Platform, showing the relationship between porosity, permeability, and dolomite and dedolomite. Samples from New Braunfels, Stone Oak, Wilderness Oak, FM 1604 at Bitters Road, FM 1604 at Blanco Road, and Lake Medina outcrops.

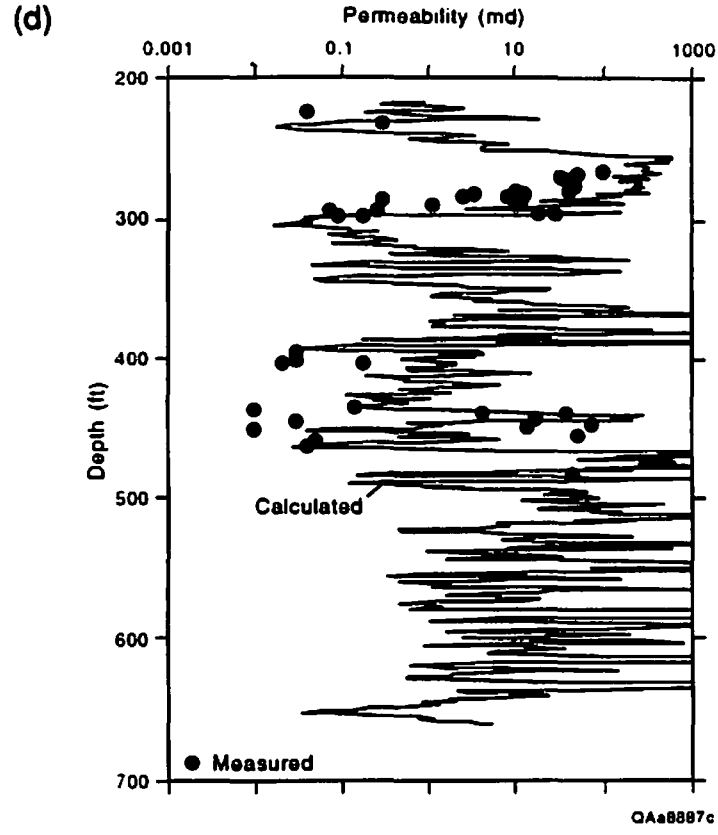

Figure 10. (d) Permeability calculated from inferred porosity log of the USGS Castle Hills well using regression coefficients in Table 4, showing generally good match with measured plug permeability.

Table 4. Empirically derived porosity–log permeability relationships for various components of the Edwards Group.

Facies	Source	Area applied	*m*	*b*	R^2
Outcrop	Plugs from all outcrops	Unconfined aquifer, Bexar and Medina Counties	0.143	–2.06	0.94
San Marcos Platform	USGS Castle Hills, USGS Feathercrest, USGS San Marcos cores	Confined aquifer, Hays, Comal, Bexar, and eastern Medina Counties	0.150	–2.36	0.90
Devils River Formation	USGS Sabinal and TWDB TD3 cores	Aquifer in the mapped (Rose, 1972) Devils River trend, western Medina and eastern Uvalde Counties	0.157	–2.30	0.91
Salmon Peak	USGS RP2 core, TWDB YP4 core	Maverick Basin, Salmon Peak Formation	0.127	–2.02	0.96
West Nueces Formation	TWDB RP2 core, TWDB YP4 core	Maverick Basin, West Nueces and McKnight Formation	0.155	–2.79	0.95
Saline Edwards	USGS Randolph FM 1604, Tenneco No. 1 Ullman cores	Saline Edwards	0.183	–2.64	0.95

highly porous rocks with abundant partly hollow dolomite rhombs and rudist grainstones with highly moldic porosity resulting from leached aragonitic shells. Although these moldic rocks are very porous, the permeability is lower than it would be in particle-dominated rocks with the same porosity because the moldic pores are poorly connected. These data were not used to derive the average trend for the particle-dominated cross plot of the saline part of the Edwards Group.

Samples from the aquifer on the San Marcos Platform provide the bulk of the data and the most complex porosity–permeability relationships (Fig. 10b and 10d). The main trend corresponds to the particle-dominated trend from the saline part of the Edwards Formation, but it has larger scatter. Separation of samples by depositional facies, stratigraphic position, or location within the aquifer did not explain the variance. A large group of samples have high permeability relative to porosity and include most of the calcitized evaporites and associated coarse calcite-cemented grainstones, some of the tidal flat facies, especially those that were dolomitized, and some grainstones and grain-dominated packstones. The fabric and permeability characteristics suggest that the pore structure of these samples is dominated by touching vugs. In thin section, vugs appear to be small caves originating from dissolution of calcite, dolomite, or gypsum, and, like large caves, are locally filled with travertine and terra rossa. Additional petrographic examination might further separate these rock fabrics by quantifying particle sizes and alteration by dolomitization and dedolomitization.

Samples collected from outcrop also have several porosity–permeability relationships (Fig. 10c). In spite of attempts to sample the most porous units systematically within the outcrop, the range and average porosity are low. One set of data mostly from limestones (less than 50 percent dolomite) has a porosity–permeability coincident with the particle-dominated samples from the saline Edwards and the San Marcos Platform; however, outcrop samples have more scatter. This scatter could not be removed by separating the samples according to any petrographic criteria and might record heterogeneities in pore microstructure developed during the complex aquifer history. A second group with a very large scatter has higher permeability at

a given porosity than the particle-dominated group. Samples in this set include many subtidal and tidal flat dolomites (now partly dedolomite). Petrographic examination of these samples identifies highly altered fabrics.

Samples from the Devils River trend in the aquifer (Fig. 11a) have similar but slightly higher and more varied permeability as compared with samples from the San Marcos Platform (Fig. 10b). The main trend is similar to the particle-dominated trend from other facies, demonstrating that the cyclic rock types from the Devils River Formation are similar to other Edwards platformal rocks. Like those from the platform, the second porosity–permeability trend for Devils River samples is dominated by touching vugs. The rock types with porosity–permeability relationships that plot in the touching-vug trend include many of the calcitized evaporites and associated coarse calcite-cemented grainstones, some of the dolomitized tidal flat facies, and some grainstones and grain-dominated packstones.

The generally fine grained wackestone and packstone facies in the Maverick Basin yield two additional porosity–permeability relationships (Fig. 11b). Many of the grainstones within this setting contain abundant calcite cement, as is typical of grainstones overlain by transgressive subtidal units, and make minimal contribution to permeability. The fine-grained packstones of the Salmon Peak Formation in Uvalde and Kinney Counties have (1) fine porosity developed between fine grains and within fine mud matrix and (2) some leaching of grains and cement, giving them a chalky appearance in core. Rocks of the West Nueces Formation have generally low porosity developed in micritic limestones (crystal size less than 15 microns). The permeability of these rocks with fine effective particle sizes is low compared with that of rocks having a larger particle size and the same porosity. The McKnight Formation is heterogeneous, containing fine-grained limestone, argillaceous and organic-rich carbonate, and evaporite breccia. No porosity–permeability relationship was developed for the McKnight Formation because of poor sample recovery in core.

The main particle-dominated porosity–permeability relationship from each of the plots was used for calculation of matrix permeability from logs. The higher permeabilities typical of

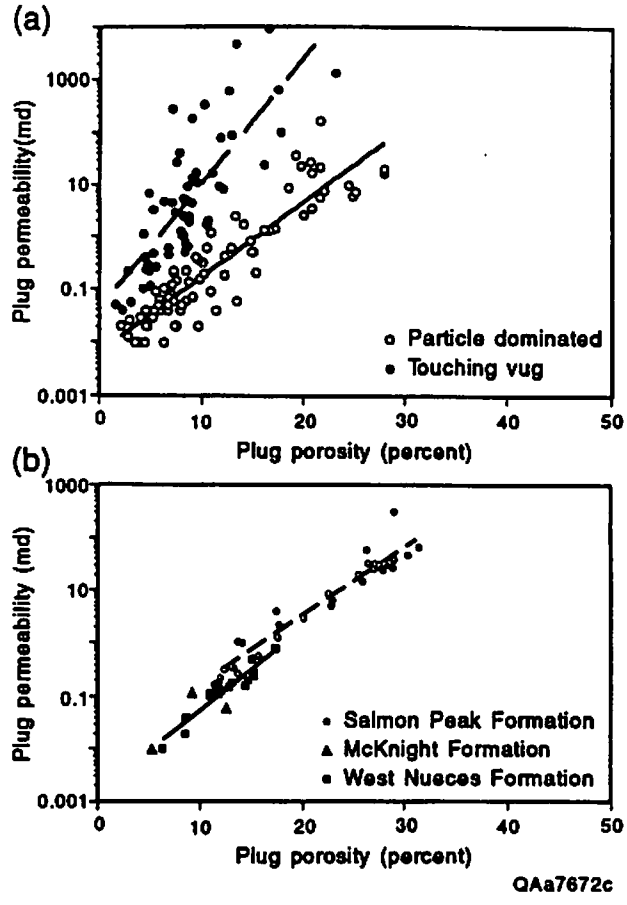

Figure 11. Semilog scatter plot of plug porosity versus log of plug permeability. (a) Devils River Formation in the confined aquifer, showing the relationship between porosity, permeability, and pore structure. Samples from the TWDB TD-3 and USGS Sabinal cores are included on this plot. (b) Maverick Basin, samples from the TWDB YP-4 and USGS RP-2 cores are included on this plot.

touching-vug porosity might reflect incipient formation of conduits. The effect of karst conduits on transmissivity is discussed later. Log porosities higher than 35 percent were not calculated using the matrix porosity–permeability relationship because many of these high-porosity intervals contain conduits. Calculated average permeability at each well was plotted in Plate 6.

Transmissivity from Aquifer Tests

Over 680 specific capacity and/or aquifer tests were compiled for the Edwards aquifer in the study area. Of these tests, 45 percent were performed in wells with greater than 50 percent completions.

Relationship between Transmissivity and Specific Capacity

Figure 12 shows a plot of transmissivity versus specific capacity calculated on the basis of aquifer tests (Fig. 12a), the analytical relationship (equation 9) (Fig. 12b), and the Huntley and others (1992) relationship between transmissivity and specific capacity for fractured rock (equation 10) (Fig. 12c). The Huntley and others (1992) relationship underestimates transmissivities in the Edwards aquifer. Transmissivities calculated from specific capacities using equation 9 agree with the aquifer test data for the most part, although some values are much higher than predicted for a given specific capacity. The difference might be due to the contribution/effect of matrix permeability of the Edwards aquifer. The Huntley and others (1992) relationship was developed for a crystalline fractured rock that has little matrix permeability.

An empirical equation relating transmissivity to specific capacity was derived on the basis of the Edwards aquifer test data (Fig. 12). The best-fit line has an R^2 value of 0.89 (Fig. 13):

$$T = 0.206\,(SC_{a,p})^{1.22}\,. \qquad (27)$$

Transmissivities and hydraulic conductivities were calculated using this relationship.

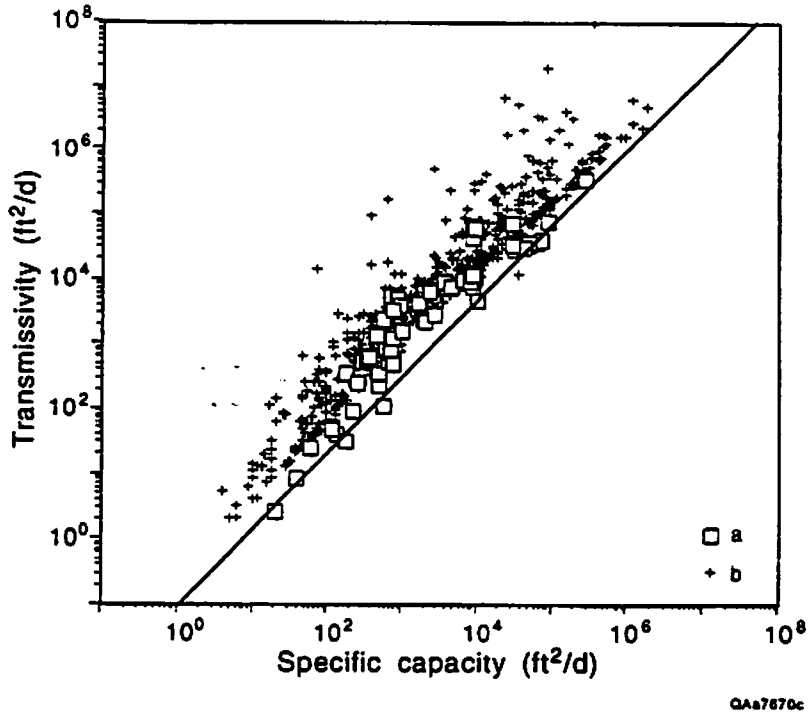

Figure 12. Plot of (a) transmissivity versus specific capacity at wells in which aquifer tests were conducted, (b) transmissivity versus specific capacity for transmissivities calculated from the analytical relationship (equation 8), and (c) the calculated linear relationship between transmissivity and specific capacity for fractured rock offered by Huntley and others (1992) (equation 9).

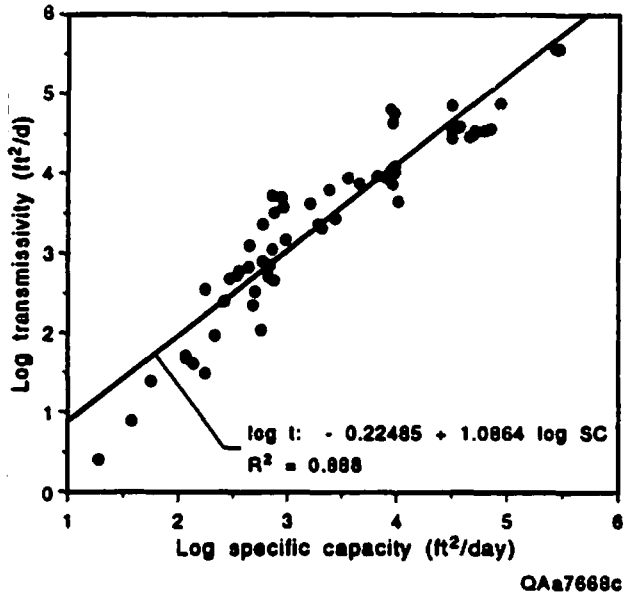

Figure 13. Best-fit line between measured transmissivity and specific capacity data.

Analysis of Data

Specific capacity, transmissivity, and hydraulic conductivity values were analyzed and summarized using different statistical and geostatistical procedures.

Statistical Description of Data

Histograms of the original specific capacity data are shown in Figure 14a. Two histograms each are presented for corrected specific capacity (Fig. 14b and 14c), transmissivity (Fig. 14d and 14e), and hydraulic conductivity (Fig. 14f and 14g). One histogram of the pair includes only tests with measurable drawdown, and the other consists of these tests plus estimates of minimum specific capacity, transmissivity, or hydraulic conductivity based on the zero-drawdown tests. Specific capacity, transmissivity, and hydraulic conductivity are graphed on a logarithmic scale because the data appear log-normally distributed. Data distribution is summarized in Table 5.

Specific capacity, transmissivity, and hydraulic conductivity of the Edwards aquifer each vary over several orders of magnitude. Specific capacity and transmissivity range from 10^{-1} to 10^{7} ft^2/d (10^{-2} to 10^{6} m^2/d) and hydraulic conductivity ranges from 10^{-3} to 10^{5} ft/d ($10^{-3.5}$ to $10^{-4.5}$ m/d). The distributions of these parameters are essentially log-normal, although the histograms suggest the possibility of multiple populations (Fig. 14). Specific capacity might have modal values of both 300 and 10,000 ft^2/d (30 and 1,000 m^2/d) (Fig. 14). The unevenness of the transmissivity and hydraulic conductivity distributions also suggests the possibility of multiple modes. These multiple modes might reflect distinct but overlapping data populations controlled by fracture and matrix permeability or even more complexly overlapping populations controlled by the previously discussed geologic and hydrologic settings.

Estimates of average specific capacity, transmissivity, and hydraulic conductivity are increased by a factor of five if specific capacity tests with no measurable drawdown are

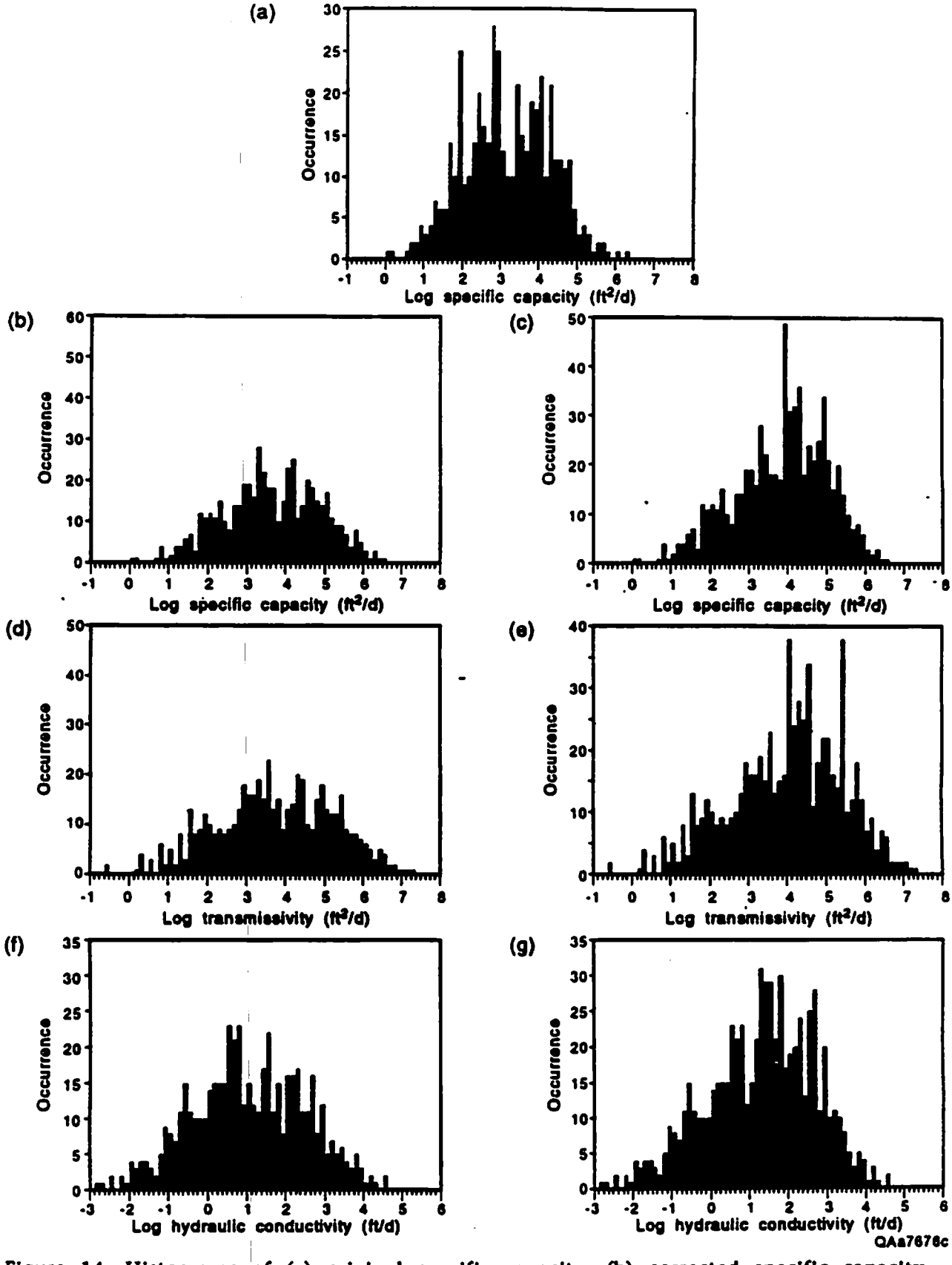

Figure 14. Histograms of (a) original specific capacity, (b) corrected specific capacity, (d) transmissivity, and (f) hydraulic conductivity data. Histograms on the right include (c) estimates of minimum specific capacity, (e) transmissivity, and (g) hydraulic conductivity values based on zero-drawdown tests.

Table 5. Summary of specific capacity, transmissivity, and hydraulic conductivity measurements.

Parameter	Units	Number of measurements	Mean[1] value (units)	Standard deviation range[2] (units)	Variance (log[units])^2	Minimum value (units)	Maximum value (units)
Only tests with measurable drawdown							
Uncorrected specific capacity	ft^2/day	525	1,479	110 - 20,000	1.27	1.3	1,860,000
Corrected specific capacity	ft^2/day	525	4,365	245 - 77,600	1.56	1.3	3,400,000
Transmissivity	ft^2/day	525	5,370	170 - 170,000	2.26	0.28	19,000,000
Hydraulic conductivity	ft/day	525	11.3	0.4 - 300	2.07	0.0016	40,000
Includes tests with zero drawdown							
Corrected specific capacity	ft^2/day	679	6,918	450 - 107,000	1.42	1.3	3,400,000
Transmissivity	ft^2/day	681	10,000	350 - 282,000	2.11	0.28	19,000,000
Hydraulic conductivity	ft/day	677	19.6	0.8 - 470	1.91	0.0016	40,000

[1] Geometric mean.
[2] Range of +/- one standard deviation.

included. Because these data were calculated as minimum possible values, a true average value could be greater. Accuracy of determining minimum specific capacities from these tests is limited by several assumptions. However, a data base that does not consider these tests is biased toward lower values.

Areal Distribution of Transmissivity

Local and regional scale variability makes it very difficult to contour specific capacity, transmissivity, and hydraulic conductivity. Maclay and Small (1986) solved this problem by grouping values into different zones having generally similar values. Klemt and others (1979) contoured transmissivities to use in their numerical ground-water flow model. However, this required a substantial amount of data "smoothing" because local-scale variability can range over three orders of magnitude. Individual tests represent hydraulic parameters at particular wells, not necessarily conditions at a larger scale simulated in a model.

Plate 5 shows transmissivity values represented by circles, where the diameter of the circle corresponds to the magnitude of the transmissivity value. Qualitatively, the outcrop appears to have values of transmissivity lower than the confined portion of the aquifer. Bexar and Medina Counties appear to have values of transmissivity larger than those of Uvalde, Comal, and Hays Counties. To test this observation, geologic and hydrologic subdivisions of the aquifer (Fig. 1) were used as polygons in ARC/INFO to subdivide hydraulic conductivity and transmissivity. For each area, the number of measurements, mean, standard deviation range, and variance were calculated.

Statistical data on transmissivity and hydraulic conductivity are summarized in Tables 6 and 7, respectively, for the outcrop and subsurface areas including (1) the Maverick Basin, (2) the Devils River Formation, (3) the Kainer and Person Formations in the Bexar County area, and (4) the Kainer and Person Formations in the Hays and Comal Counties area. Selected histograms of transmissivity for these areas and for the entire aquifer are shown in Figure 15. Table 6 shows that the mean transmissivity of the confined zone (Fig. 15b) is more than 240 times greater

Table 6. Summary of transmissivity values[1] for subdivisions of the aquifer.

Area of interest	Number of measurements	Mean[2] value (ft^2/d)	Standard deviation range[3] (ft^2/d)	Variance (log [ft^2/d])^2
All	525	5,370	170 - 170,000	2.26
Outcrop (unconfined)	50	75	9 - 630	0.87
Subcrop (confined)	399	18,200	720 - 460,000	1.97
Maverick Basin[4]	30	4,300	120 - 150,000	2.42
Devils River Formation[4]	140	22,000	1,500 - 320,000	1.34
Bexar County area[4]	207	29,000	1,100 - 760,000	2.01
Hays–Comal County area[4]	22	440	26 - 7,400	1.51

[1] Does not include zero drawdown tests.
[2] Geometric mean.
[3] Range of +/- one standard deviation.
[4] Values for the confined portion.

Table 7. Summary of matrix and aquifer test hydraulic conductivity values[1] for subdivisions of the aquifer

Area of interest	Number of measurements	Mean[2] value (ft/d)	Standard deviation range[3] (ft/d)	Variance (log [ft/d])[2]
All	525	11.3	0.4 - 300	2.07
Outcrop (unconfined)	399	0.28	0.04 - 2.1	0.78
Subcrop (confined)	50	34	1.4 - 832	1.92
Hydraulic conductivity of matrix	129	0.09	0.02 - 0.36	0.34

[1] Does not include zero drawdown tests.
[2] Geometric mean.
[3] Range of +/- one standard deviation.

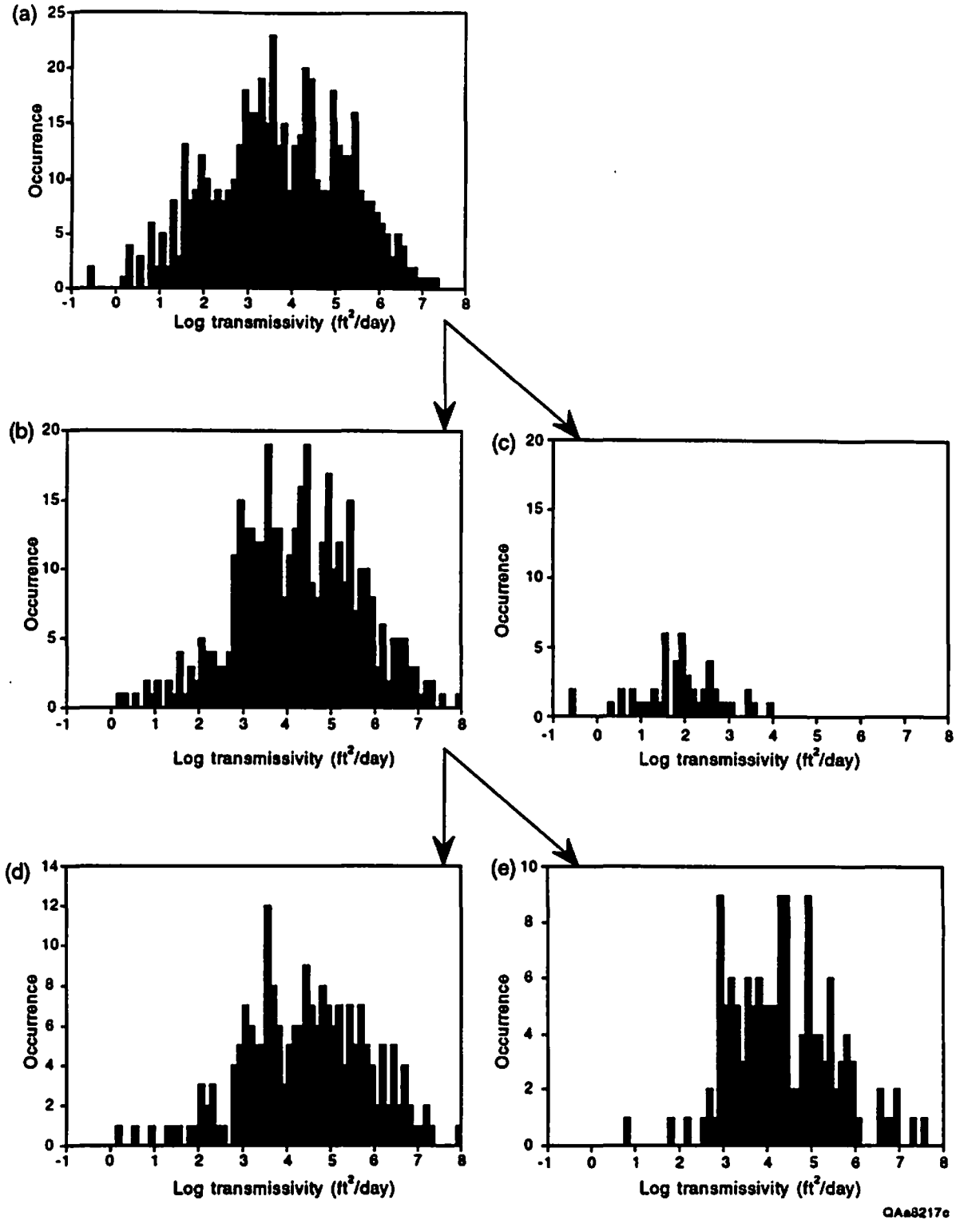

Figure 15. Transmissivity histograms of (a) all data, (b) data from the confined zone, (c) data from the unconfined, or outcrop, zone, (d) data from the confined portion of the Bexar County area, and (e) data from the confined portion of the Devils River Formation.

than mean transmissivity in the unconfined zone (Fig. 15c and Table 6). Smaller aquifer thickness in the outcrop might account for some of this difference. However, hydraulic conductivity, which is independent of aquifer thickness, is also much lower in the unconfined than the confined zone (Fig. 16b and 16c), which would lead to smaller transmissivities. Mean hydraulic conductivity of the confined zone is more than 120 times greater than mean hydraulic conductivity in the unconfined, or outcrop, zone (Table 7). The distributions of transmissivity in the Devils River Formation and in the Bexar County area are similar. The mean and standard deviation of transmissivities in the Bexar County area are slightly greater than those in the Devils River Formation. However, these differences might not be statistically significant. Statistics for the outcrop areas of the Maverick Basin, Devils River Formation, and the Bexar County area were not calculated because the majority (76 percent) of the tests conducted in the outcrop zone were done in the Hays and Comal County area. Data are also limited in the confined portion of the Maverick Basin and the Hays and Comal County area (Table 6). Although the distribution in Maverick Basin is ill defined, it is clear there is a large range of variability (Table 6). The mean transmissivity and standard deviation are lower in the confined portion of the Hays and Comal County area, but there are too few data points to state this conclusively (Table 6).

Spatial Relationships

Experimental and theoretical variograms calculated for specific capacity, transmissivity, and hydraulic conductivity data using equation 11 are shown in Figure 17. Spherical variograms calculated using equations 12 and 13 were visually fit to the experimental variograms. The parameters of equations 12 and 13 for defining the spherical variogram are summarized in Table 8.

Variograms confirm that there is a spatial relationship in specific capacity, transmissivity, and hydraulic conductivity (Fig. 17). Maclay and Small (1986) recognized this by grouping specific capacities into different zones of similar values. The variograms also show that small-

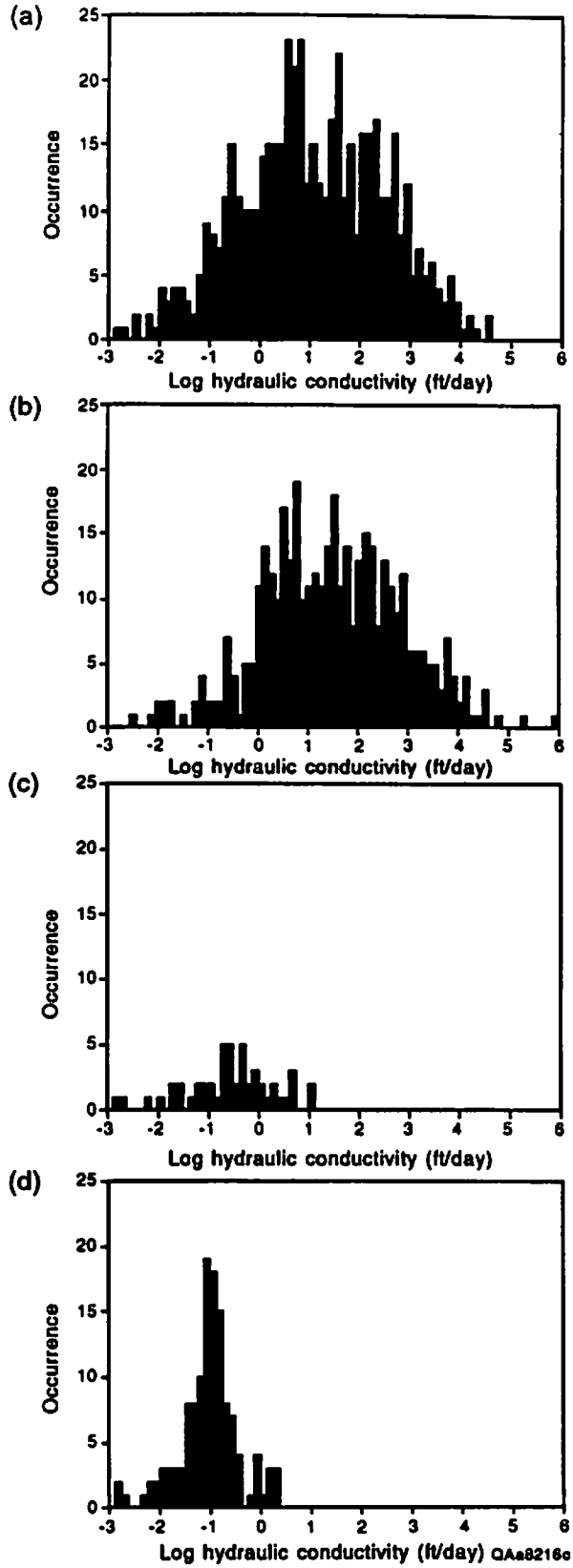

Figure 16. Hydraulic conductivity histograms of (a) all data, (b) data from the confined zone, (c) data from the unconfined, or outcrop, zone, and (d) matrix data.

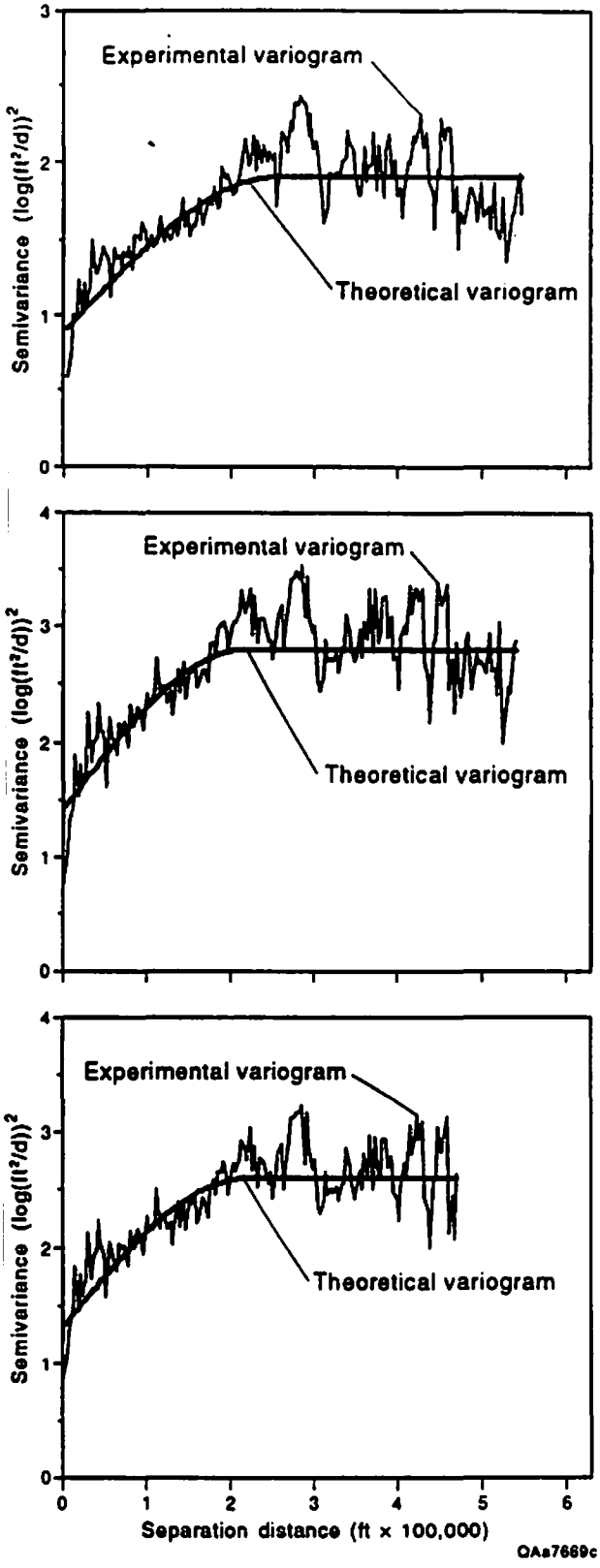

Figure 17. Experimental and theoretical variograms for (a) specific capacity, (b) transmissivity, and (c) hydraulic conductivity data.

Table 8. Parameters for theoretical spherical variograms.

Parameter:	N (nugget) $(\log[ft^2/d])^2$	W $(\log[ft^2/d])^2$	a (range) (ft)	(mi)
Specific capacity	0.9	1	260,000	15
Transmissivity	1.4	1.4	230,000	13
Hydraulic conductivity	1.3	1.3	230,000	13

scale variability (nugget) in specific capacity, transmissibility, and hydraulic conductivity is large; even closely spaced measurements might differ by a factor of 1,000. The small-scale randomness most likely reflects the variable contribution of matrix, fracture, and conduit permeability to the measured average value obtained in well tests. The size of the nugget would be smaller in aquifers that had only matrix permeability or only matrix plus fracture permeability. Because of this small-scale variability, two wells drilled close together can have markedly different hydraulic properties. However, the data do appear to be somewhat spatially related. The ranges, or correlation lengths, for the variograms suggest that specific capacity, transmissivity, and hydraulic conductivity data are spatially related within 13 to 15 miles (22 to 25 km) of a given point (Fig. 17).

Vertical Variation of Hydraulic Conductivity

The tested intervals, reported and calculated specific capacities and transmissivities, and the calculated hydraulic conductivities for the-separate intervals are summarized in Table 9. Figures 18 through 21 show plots of hydraulic conductivity for separate intervals of the flow and packer tests. Superposed on these plots is the average matrix permeability for each interval. The stratigraphic intervals of the Person and Kainer and the location of the regional dense member (RDM) are also shown.

Differences in hydraulic conductivity between tested intervals in each of the wells are as much as 10- to 100-fold (Table 9, Figs. 18 to 21). The vertical differences most likely would be even greater if length of the tested intervals were shorter. The wells in New Braunfels show good lateral correlation of permeable intervals (Fig. 18), with the highest hydraulic conductivities in the Kainer Formation. Wells B and C in San Marcos also show correlation of permeable intervals (Fig. 19) and higher permeability in the Kainer. Hydraulic conductivity in well D does not appear to correlate to wells B and C, but this might be due to longer and fewer tested intervals. Hydraulic conductivity values of the wells in San Antonio do not appear to be correlated between wells, although higher values for wells A-1 and A-3 occur at the elevation of

Table 9. Summary of 50-ft flow tests and packer tests made at the bad water line experiment test sites in San Marcos, New Braunfels, San Antonio, and the test well in South Medina County and hydraulic conductivities calculated for the intervals.

	Tested interval Top (ft)[1]	Bottom (ft)[1]	Specific capacity (ft^2/d)	Reported trans. (ft^2/d)	Calc. trans.[2] (ft^2/d)	Hyd. cond.[3] (ft/d)	Hyd. cond. for interval (ft/d)	Interval From (ft)[1]	To (ft)[1]
A-1[4]	444	506	83	38	46	0.73	0.73	444	506
	444	556	309	395	229	2.04	3.66	506	556
	444	606	313	248	232	1.43	0.07	556	606
	444	687	392	362	306	1.26	0.91	606	687
	444	737	524	304	436	1.49	2.62	687	737
	444	837	998	686	959	2.44	5.23	737	837
	444	887	1,386	594	1,433	3.24	9.48	837	887
B-1[4]	472	530	50	40	25	0.43	0.43	472	530
	472	564	215	85	147	1.59	3.54	530	564
	472	617	234	80	163	1.13	0.31	564	617
	472	727	378	258	293	1.15	1.18	617	727
	472	832	1,258	1,054	1,272	3.54	9.33	727	832
	472	881	1,498	1,235	1,575	3.85	6.15	832	881
C-1[4]	518	577	54	4.7	27	0.46	0.46	518	577
	518	613	186	83	123	1.30	2.66	577	613
	518	661	252	114	178	1.24	1.12	613	661
	518	706	230	298	160	0.85	0	661	706
	518	776	499	910	411	1.59	3.59	706	776
	518	827	632	1,386	548	1.77	2.71	776	827
	518	877	1,204	1,058	1,206	3.36	13.26	827	877
	518	928	1,179	1,463	1,176	2.87	0	877	928
	518	959	659	1,059	577	1.31	0	928	959
B[5]	403	477	29	4.1	13	0.17	0.17	403	477
	403	509	81	35	44	0.42	0.99	477	509
	403	566	117	36	70	0.43	0.44	509	566
	403	669	169	45	109	0.41	0.39	566	669
	403	727	207	76	140	0.43	0.53	669	727
	403	770	323	97	241	0.66	2.34	727	770
	403	833	307	216	227	0.53	0	770	833
	403	891	457	490	369	0.76	2.49	833	891
C[5]	416	489	29	2.8	13	0.17	0.17	416	489
	416	520	44	8.8	21	0.20	0.28	489	520
	416	584	61	15	32	0.19	0.17	520	584
	416	633	156	31	99	0.46	1.37	584	633
	416	676	161	58	103	0.40	0.10	633	676
	416	740	463	319	375	1.16	4.30	676	740
	416	791	490	1,254	401	1.07	0.52	740	791
	416	844	816	401	750	1.75	6.60	791	844
	416	920	801	623	732	1.45	0	844	920
D[5]	462	556	204	60	137	1.46	1.46	462	556
	462	658	797	1,087	728	3.72	5.80	556	658
	462	774	1,087	1,023	1,064	3.41	2.90	658	774

[1] Measured below ground surface.
[2] Calculated with equation 26.
[3] Calculated from transmissivities in previous column.
[4] New Braunfels test wells, data from Poteet and others (1992).
[5] San Marcos test wells, data from Poteet and others (1992).

Table 9 (continued).

	Tested interval Top (ft)[1]	Bottom (ft)[1]	Specific capacity (ft^2/d)	Reported trans. (ft^2/d)	Calc. trans.[2] (ft^2/d)	Hyd. cond.[3] (ft/d)	Hyd. cond. for interval (ft/d)	Interval From (ft)[1]	To (ft)[1]
A-1[6]	965	1,021	864	5,013	804	14.36	14.36	965	1,021
	965	1,071	1,613	4,333	1,725	16.27	18.42	1,021	1,071
	965	1,123	2,381	6,493	2,777	17.58	20.24	1,071	1,123
	965	1,180	4,608	7,333	6,228	28.97	60.54	1,123	1,180
	965	1,228	6,566	9,453	9,604	36.52	70.34	1,180	1,228
	965	1,279	8,064	9,200	12,347	39.32	53.79	1,228	1,279
	965	1,331	9,562	10,720	15,207	41.55	55.00	1,279	1,331
	965	1,384	8,986	7,787	14,095	33.64	0	1,331	1,384
	965	1,437	9,370	12,360	14,835	31.43	13.96	1,384	1,437
	965	1,489	8,640	11,573	13,435	25.64	0	1,437	1,489
A-3[6]	964	1,019	38	8.0	18	0.32	0.32	964	1,019
	964	1,071	211	93	144	1.34	2.42	1,019	1,071
	964	1,123	442	1,307	354	2.23	4.04	1,071	1,123
	964	1,174	576	2,387	490	2.33	2.66	1,123	1,174
C-1[6]	832	859	9,523	59,200	-	-	-	-	-
	832	885	33,216	42,267	-	-	-	-	-
	832	991	30,720	33,067	-	-	-	-	-
	832	1,042	31,488	38,400	-	-	-	-	-
	832	1,056	8,736	65,067	-	-	-	-	-
	832	1,147	70,272	38,800	-	-	-	-	-
	832	1,199	61,440	36,533	-	-	-	-	-
	832	1,240	8,928	44,667	-	-	-	-	-
	832	1,251	48,768	32,533	-	-	-	-	-
	832	1,300	44,160	30,667	-	-	-	-	-
	832	1,360	49,920	35,600	-	-	-	-	-
	832	1,396	36,096	39,467	-	-	-	-	-
C-2[6]	832	882	115	52	68	1.37	1.37	832	882
	832	932	115	48	68	0.68	0	882	932
	832	986	115	-	68	0.44	0	932	986
	832	1,049	134	41	83	0.38	0.23	986	1,049
	832	1,101	154	-	97	0.36	0.28	1,049	1,101
	832	1,150	442	692	354	1.11	5.24	1,101	1,150
SM[7]	2,623	2,822	1,572	-	1,672	8.4	8.4	2,623	2,822
	2,623	2,978	4,458	-	5,982	16.9	27.6	2,822	2,978
	2,623	3,043	8,165	-	12,537	29.9	101	2,978	3,043
	2,623	3,104	9,960	-	15,987	33.2	56.6	3,043	3,104
	2,623	3,168	9,960	-	15,987	29.3	0	3,104	3,168
	2,623	3,231	23,166	-	44,882	73.8	459	3,168	3,231
	2,623	3,291	29,426	-	60,135	90.0	254	3,231	3,291
	2,623	3,356	28,496	-	57,817	78.9	0	3,291	3,356

[6] San Antonio test wells, data from Guyton and Associates (1986).
[7] South Medina County well, data from Waugh (1993).
- Not calculated.

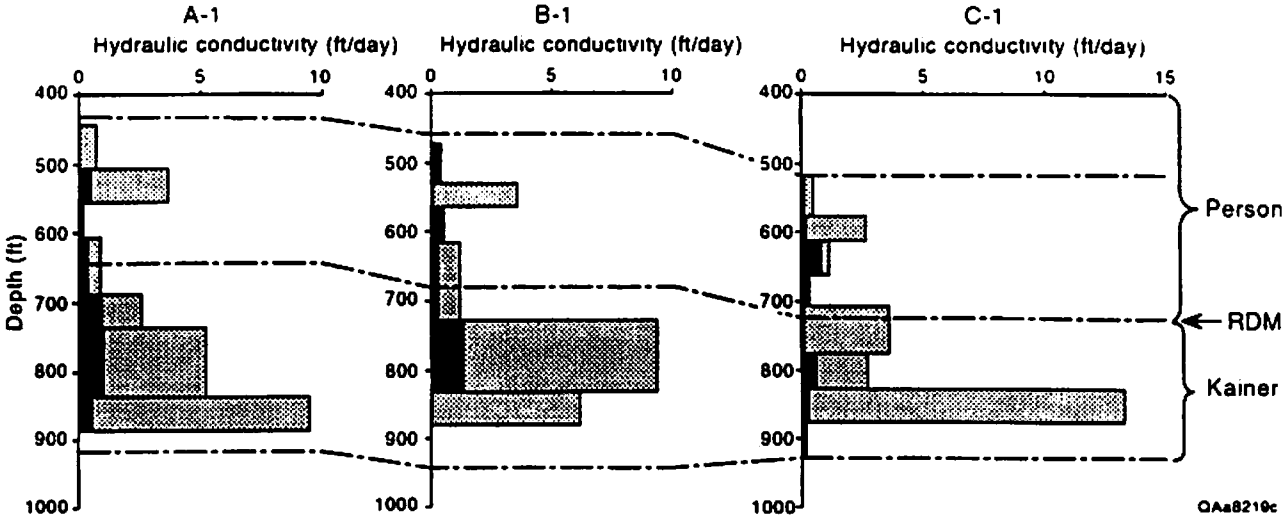

Figure 18. Vertical variation of aquifer test and matrix permeability for test wells at New Braunfels. Darker bars represent matrix permeability.

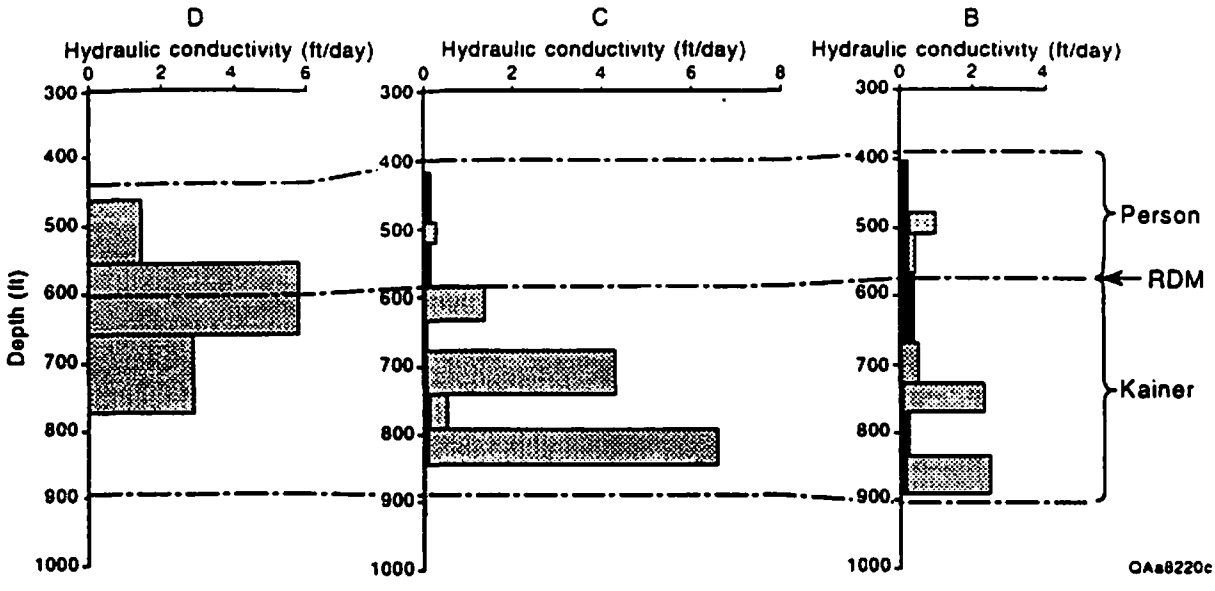

Figure 19. Vertical variation of aquifer test and matrix permeability for test wells at San Marcos. Darker bars represent matrix permeability.

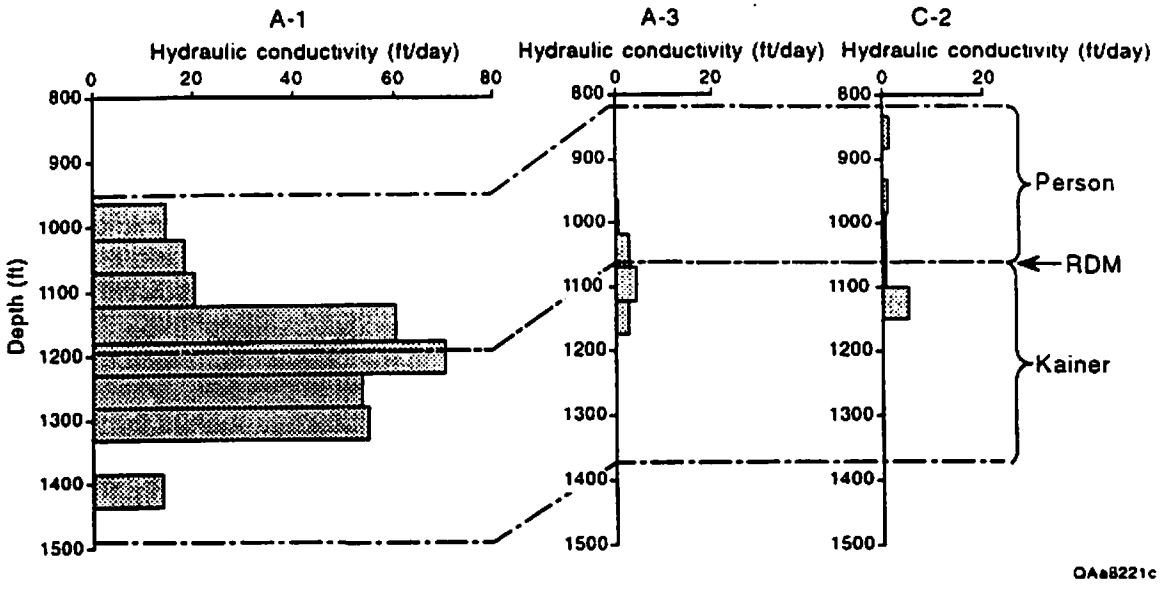

Figure 20. Vertical variation of aquifer test and matrix permeability for test wells at San Antonio. Darker bars represent matrix permeability.

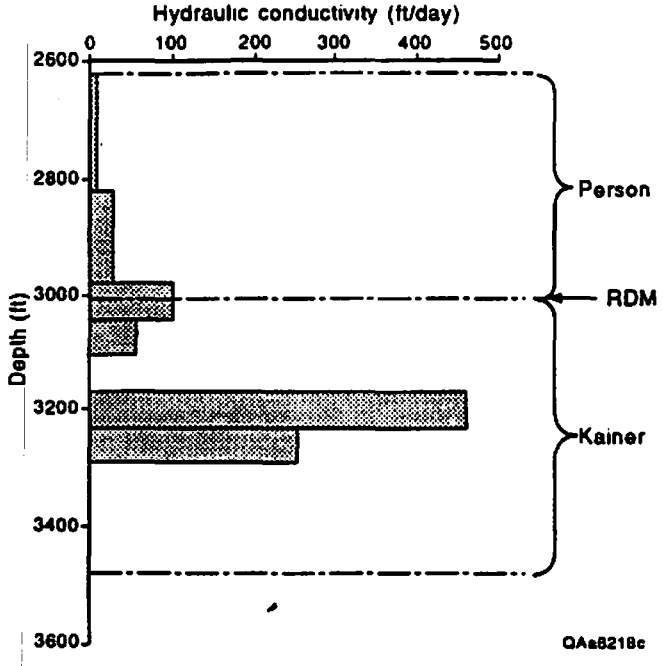

Figure 21. Vertical variation of aquifer test and matrix permeability for test well in south Medina County. Darker bars represent matrix permeability.

the regional dense member (Fig. 20). Well A-1 has much higher hydraulic conductivity than wells A-3 or C-2, with higher values in the bottom part of the Edwards aquifer. The well tested in south Medina County had the highest hydraulic conductivity of the wells shown, with the highest values in the Kainer/lower Devils River Formation (Fig. 21).

Figure 22 shows that specific capacity is not statistically correlated to percent penetration of wells in the Edwards aquifer. The lack of statistical relationship is probably due to the large variability of specific capacity. Similar plots for the different zones show the same result.

Relationship to Matrix Permeability

Vertically averaged matrix permeabilities were compared with hydraulic conductivities derived from aquifer tests. Mean matrix permeability is considerably lower (over 100 times) than mean hydraulic conductivities determined from aquifer tests (Fig. 16a and 16d). This suggests that the contribution of matrix permeability to regional scale hydraulic conductivity is minor and that the majority of Edwards water most likely flows through fractures and conduits. Matrix permeability is more comparable to hydraulic conductivity based on aquifer tests in the outcrop (Fig. 16c and 16d). Therefore, the unconfined aquifer might behave as a dual-permeability system, where the permeability of the matrix and the fractures are similar. Most of the matrix permeability measurements, however, come from the confined portion of the aquifer. Matrix values for the unconfined aquifer might also be low, similar to those of samples from outcrops. Also, hydraulic conductivity data for the outcrop area are limited to aquifer tests in the Hays and Comal County area.

Matrix permeability is plotted in figures 18 through 21 as dark stippled areas. Matrix permeability does not appear on the plots for the San Antonio (Fig. 20) or south Medina County (Fig. 21) wells because the values are low compared with the high aquifer test hydraulic conductivity. Matrix permeability does appear on results for the New Braunfels and San Marcos wells because the aquifer test hydraulic conductivities were low. Matrix permeability accounted for a large fraction of the permeability in intervals with low hydraulic conductivities

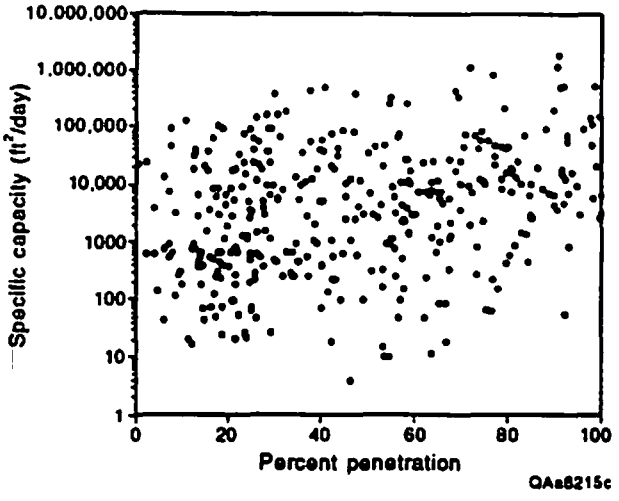

Figure 22. Plot between specific capacity uncorrected for partial penetration and percent penetration.

determined from aquifer tests. In intervals with higher tested hydraulic conductivity, the matrix contribution was low (< 1 percent). A plot of matrix permeability against tested hydraulic conductivity for these wells showed no correlation.

Outcrop Investigations

Seven large outcrops were examined to characterize the types and distribution of conduits in a variety of structural settings (Table 10). Large photomosaics were prepared of each outcrop, and a variety of data were collected. The stratigraphic interval based on measured sections and general structural setting based on regional mapping were defined. Detailed structure mapping, fracture aperture and roughness, and quantification of the amount and distribution of karst features were undertaken at selected outcrops.

Structural Description of Fractures

Normal faults of the Balcones Fault Zone are commonly surrounded by zones of highly fractured strata, although few data on fractures associated with faulted Edwards limestone exist for the study area (Collins, 1987, 1993a; Reaser and Collins, 1988; Collins and Laubach, 1990; Collins and others, 1992). Abundant fractures (mostly small faults and some joints) adjacent to faults are well connected both laterally and vertically by numerous intersecting and crosscutting fractures. Locally anastomosing fault arrays grade into breccia. In general, faults with larger throws have wider, highly fractured zones or breccia zones (Fig. 23). Fracture spacing and connectivity decrease away from master faults. Fracture zones associated with smaller faults have larger fracture spacings and poorer fracture connectivity than the highly fractured zones that occur directly adjacent to the master faults.

The Fiesta outcrop (Fig. 24a) is an example of an approximately 20-ft-wide (6.1-m) fracture–breccia zone associated with a fault that has an estimated throw of 170 ft (51.8 m). The 20-ft-wide (6.1-m) highly fractured–brecciated zone includes about 6 ft (1.8 m) of brecciated

Table 10. Outcrops analyzed for this study.

Outcrop	Location	Unit exposed	Structural setting within Balcones Fault Zone
New Braunfels	Comal County, south of New Braunfels on Loop 337 1.5 miles west of I35, W98° 9' 28", N29° 42' 5"	lower Person	On footwall block about 600 ft from large fault having about 850 ft of throw
Stone Oak	Bexar County, on Stone Oak Parkway west of intersection with Route 281, W98° 27' 6", N29° 38' 7"	middle Kainer	Strata adjacent to a fault having about 22 ft of throw
Wilderness Oak	Bexar County, Wilderness Oak 0.9 mile east of Blanco Road, W98° 32' 29" N29° 38' 2"	upper Kainer	Small faults typical of the area within a 1.8-mile-wide block bounded by large faults
1604 at Blanco Road	Bexar County, on FM 1604 west of Panther Springs Creek, W98° 31' 30" N29° 36' 20"	upper to middle Person	Roadcut parallel to and 0.5 mile south of large fault with about 200 ft of throw
1604 at Bitters Road	Bexar County, on FM 1906 east of Salado Creek, W98° 32' 0" N29°36' 17"	lower Person	Roadcut parallel to and 0.2 mile south of large fault with about 250 ft of throw
Fiesta, Texas	Bexar County, above main gate to Fiesta Texas, 0.6 mile west of highway 87 north of 1604, W98° 36' 52", N29° 36' 17"	lower Kainer	A large fault with an estimated throw of 170 ft is exposed in the outcrop
San Geronimo	Easternmost Medina County, north end of bridge over San Geronimo Creek, FM 211 0.6 mile north of FM 471 W98° 48' 38" N29° 32' 0"	middle Kainer	On the footwall block of a large fault with displacement between 850 and 1200 ft. Outcrop about 600 ft from fault
Lake Medina	Medina County, FM 1283 1.8 miles north of turn to Mico, W98° 54' 10" N29° 34' 45"	lower Kainer	Small faults typical of a 4-mile-wide block bounded large faults

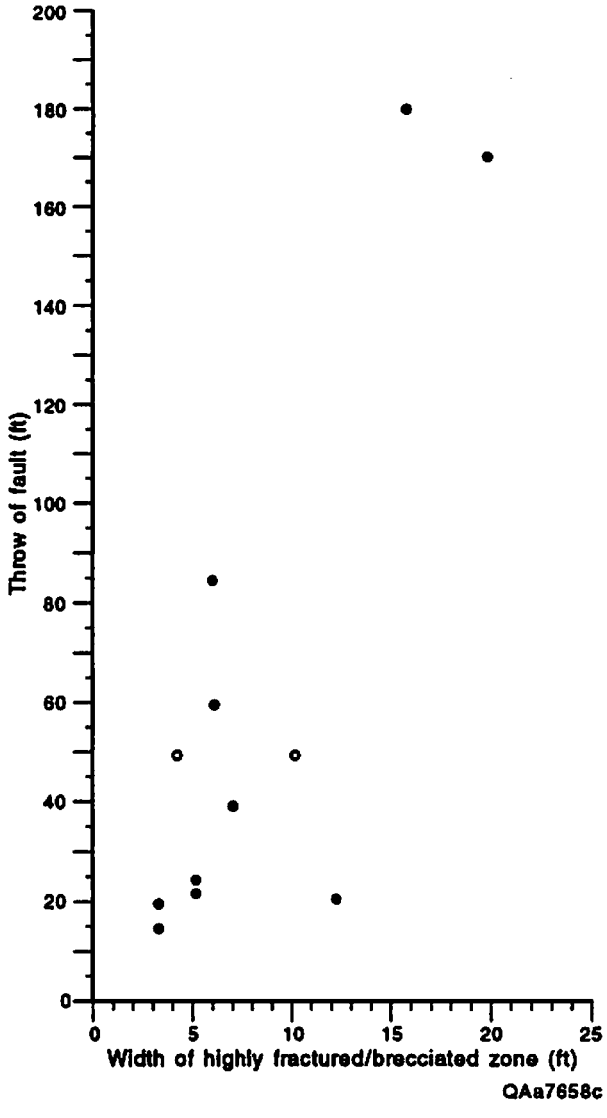

Figure 23. Preliminary data comparing throws of faults and widths of highly fractured/brecciated zones associated with faults of the Balcones Fault Zone. Data are from Edwards, Glen Rose, and Austin limestones. Open circles indicate approximate minimum throw value.

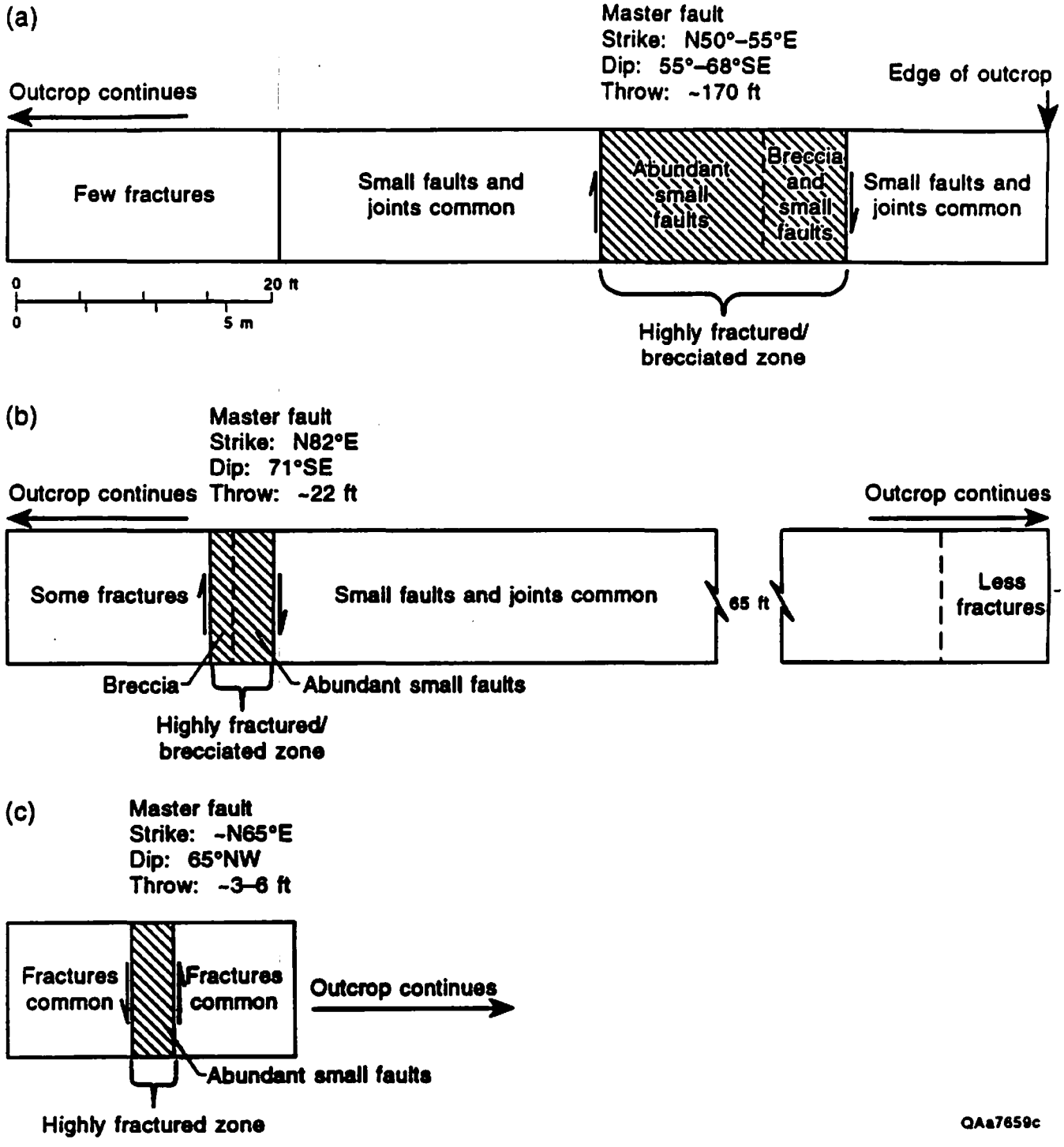

Figure 24. Fracture zones at faults cutting the Kainer Formation of the Edwards Group. Simplified zone section of (a) Fiesta outcrop, (b) Stone Oak outcrop, and (c) Wilderness Oak outcrop.

strata and 14 ft (4.3 m) of anastomosing well-connected small faults and joints. As many as nine fractures occur across 3 ft (1 m) within this zone. Subsidiary fracture zones also occur adjacent to the highly fractured–brecciated zone.

The Stone Oak outcrop (Fig. 24b) contains an approximately 5 ft (1.5 m) wide highly fractured–brecciated zone associated with a fault with an estimated throw of about 22 ft (6.7 m). Adjacent to the highly fractured zone is an approximately 130 ft (39.6 m) wide fracture zone characterized by common small faults (throws of less than 2 ft [0.6 m]) and some joints.

The Wilderness Oak outcrop, (Fig. 24c) is an example of a fault with a small amount of throw. Throw is estimated to be between 3 and 6 ft (1 and 2 m) and is difficult to measure precisely because of the limited outcrop dimensions. The 3-ft-wide (1-m) fracture zone adjacent to the fault is not brecciated like some of the larger faults; however, the zone contains abundant well-connected small faults (throws less than 1 ft [0.3 m]) and joints having different strikes and dips. As many as 8 to 10 fractures occur across 3 ft (1 m) within this zone.

Fracture Aperture, Porosity, and Permeability

Aperture measurements were made at the Stone Oak, Wilderness Oak, and San Geronimo exposures. Exactly 32 fractures were measured at Stone Oak on a 65-ft (20-m) scanline, 289 fractures were measured at Wilderness Oak on a 96-ft (29-m) scanline, and 481 fractures were measured at San Geronimo on a 100-ft (30-m) scanline. Many of the fractures had very small apertures, which were below the measuring threshold of the instrument. For porosity and permeability calculations, it was assumed that the aperture for these hairline fractures was 0.038 mm. Of the fractures measured at the Stone Oak, Wilderness Oak, and San Geronimo exposures, 25, 73, and 84 percent, respectively, had apertures equal to or less than 0.038 mm. Figure 25 shows the cumulative distribution of apertures at each of the outcrops. Ninety-five percent of the apertures for the San Geronimo and Wilderness Oak exposures are smaller than 1 mm. Ninety percent of the apertures at Stone Oak are smaller than 1 mm. The San Geronimo

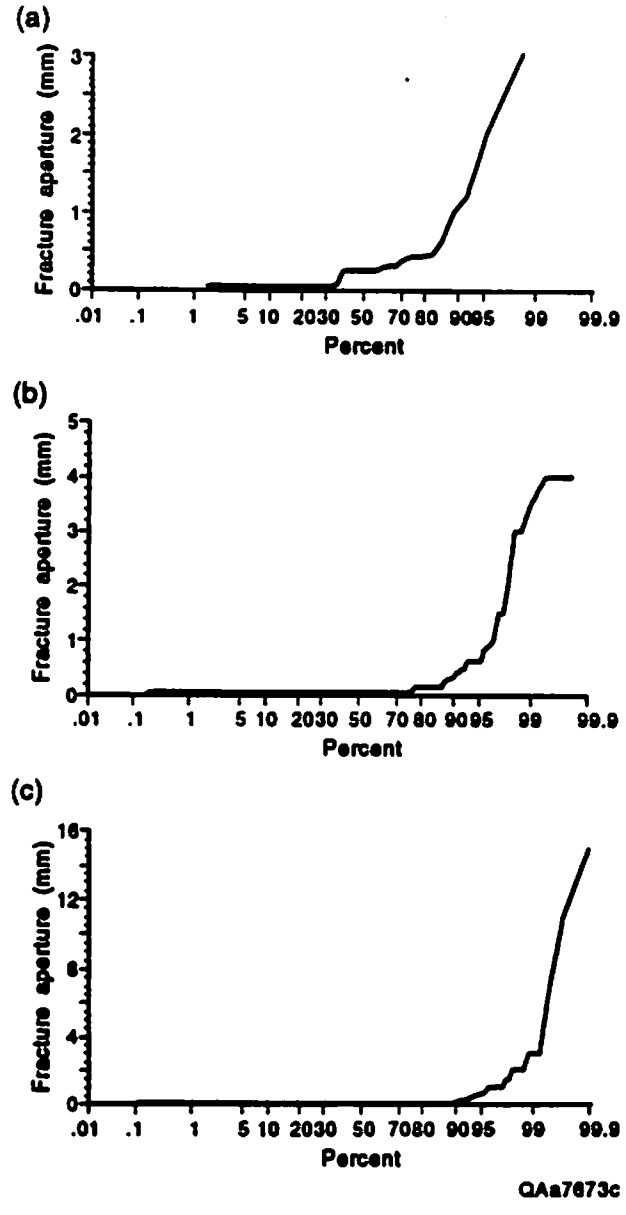

Figure 25. Cumulative distribution functions for fracture apertures measured at the (a) Stone Oak, (b) Wilderness Oak, and (c) San Geronimo exposures.

exposure had apertures as large as 15 mm. In contrast, the largest apertures measured at Stone Oak and Wilderness Oak are 3 mm and 4 mm, respectively.

Porosities calculated on the basis of aperture measurements are summarized in Table 11. Porosity of the vertical fractures is greatest for the San Geronimo exposure (0.29 percent) but less for the Stone Oak (0.07 percent) and the Wilderness Oak (0.16 percent) outcrops. This suggests that the San Geronimo site has increased fracture porosity. It is important to note that the San Geronimo site also has higher fracture frequency than the Stone Oak or Wilderness Oak site. The San Geronimo site is near a fault with more than 800 ft (60 m) of throw. At the Wilderness Oak site the porosity for horizontally oriented fractures was 1.25 percent, almost eight times greater than the porosity for the vertically oriented fractures.

Karst porosity calculated from scanlines was greater for the Wilderness Oak exposure than the San Geronimo outcrop (Table 11). However, the San Geronimo exposure had many open caves with dimensions of 0.5 by 3 ft (0.1 by 1 m) that the scanline did not cross because the caves were situated along a dolomitized interval. The Wilderness Oak exposure also had some larger karst features, although they appeared to have been filled with terra rossa. No karst was encountered on the scanline at the Stone Oak exposure.

Porosity values calculated from scanline measurements of aperture or karst length are estimates of the true values. These calculations assume that the fractures and karst features measured on the scanline are representative of the outcrop in three dimensions, which might not be true due to different fracture patterns in different directions. Porosity values are biased toward conditions encountered along the scanline. Estimates of fracture porosity are probably more accurate than estimates of karst porosities because of the larger number of fractures encountered. Taylor and Fleming (1988) found that fracture porosity measured in this manner reasonably agreed with porosity determined from resistivity measurements of the formation.

Hydraulic conductivities and equivalent hydraulic conductivities for the fractured outcrop were very high (Table 11) and represent an upper limit for the outcrops. As stated earlier,

Table 11. Summary of porosity calculations from aperture measurements at outcrops.

	Stone Oak	Wilderness Oak	San Geronimo
Length of horizontal scanline (ft)	64.8	101.2	100.0
Length of vertical scanline (ft)	-	10.9	-
Number of apertures measured on horizontal scanline	32	260	481
Number of apertures measured on vertical scanline	-	29	-
Sum of the apertures for vertical fractures (mm)	13.1	46.8	88.5
Sum of the apertures for horizontal fractures (mm)	-	21.8	-
Mean aperture for vertical fractures (mm)	0.41	0.18	0.18
Mean aperture for horizontal fractures (mm)	-	0.75	-
Horizontal fracture frequency (fractures/ft)	0.5	2.6	4.8
Vertical fracture frequency	-	2.7	-
Porosity of vertical fractures (%)	0.07	0.16	0.29
Porosity of horizontal fractures (%)	-	1.25	-
Porosity of vertical and horizontal fractures (%)	-	1.41	-
Porosity of karst (%)	None	1.13	0.50
Hydraulic conductivity of the fractures (ft/day)	3.99×10^{7}	1.10×10^{8}	1.81×10^{9}
Equivalent hydraulic conductivity of the fractures (ft/day)	2.80×10^{4}	1.76×10^{5}	5.25×10^{6}

these calculations do not consider fracture connectivity. A more accurate determination of hydraulic conductivity would come from a field-scale hydrologic test.

Fracture and Conduit Roughness

Fracture and conduit surfaces measured at the Wilderness Oak and San Geronimo exposures are shown in Figures 26 and 27. Specific roughnesses calculated for the 27 measurements at the San Geronimo and Wilderness Oak sites are summarized in Table 12. As expected, fractures that had not been modified by solution had the lowest specific roughness (average of 2.3 mm), and karst conduits had the highest specific roughness: fractures with mild and heavy solution enhancement had mean specific roughnesses of 4.4 mm and 4.9 mm, respectively, and solution cavities had a mean specific roughness of 10.0 mm.

Although specific roughness is higher for karst conduits than for unaltered fractures, relative roughness is higher for fractures than for conduits. This is because the hydraulic diameter of a fracture is usually much smaller than the hydraulic diameter of a conduit. For instance, many fractures with no solution enhancement had small apertures (~ 0.038 mm), whereas conduits had large diameters (~ 200 mm). Using these aperture and conduit diameters, the relative roughnesses for a fracture and a conduit are 30 and 0.1, respectively. Therefore, more frictional head loss would occur in the smoother fracture than in the rougher conduit.

Karst

The volume, size, shape, and distribution of macroscopic solution features reflect the complex geologic history of the Edwards Group. Solution features can be related to stratigraphic, structural, and fabric influences on preferential solution of some areas of the rock. In addition, comparison of outcrops, cores from the aquifer, and cores from the saline part of the Edwards helps explain when and how the solution features formed. Paleokarst, near-surface

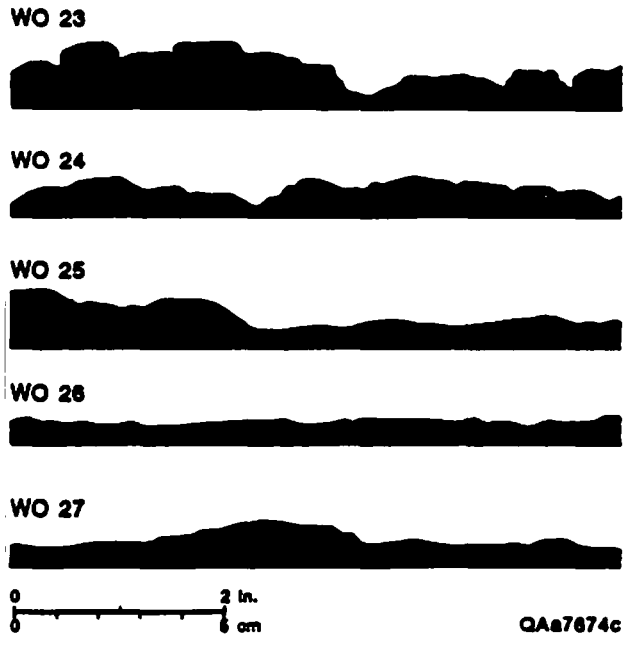

Figure 26. Fracture and conduit surfaces measured at the Wilderness Oak exposure.

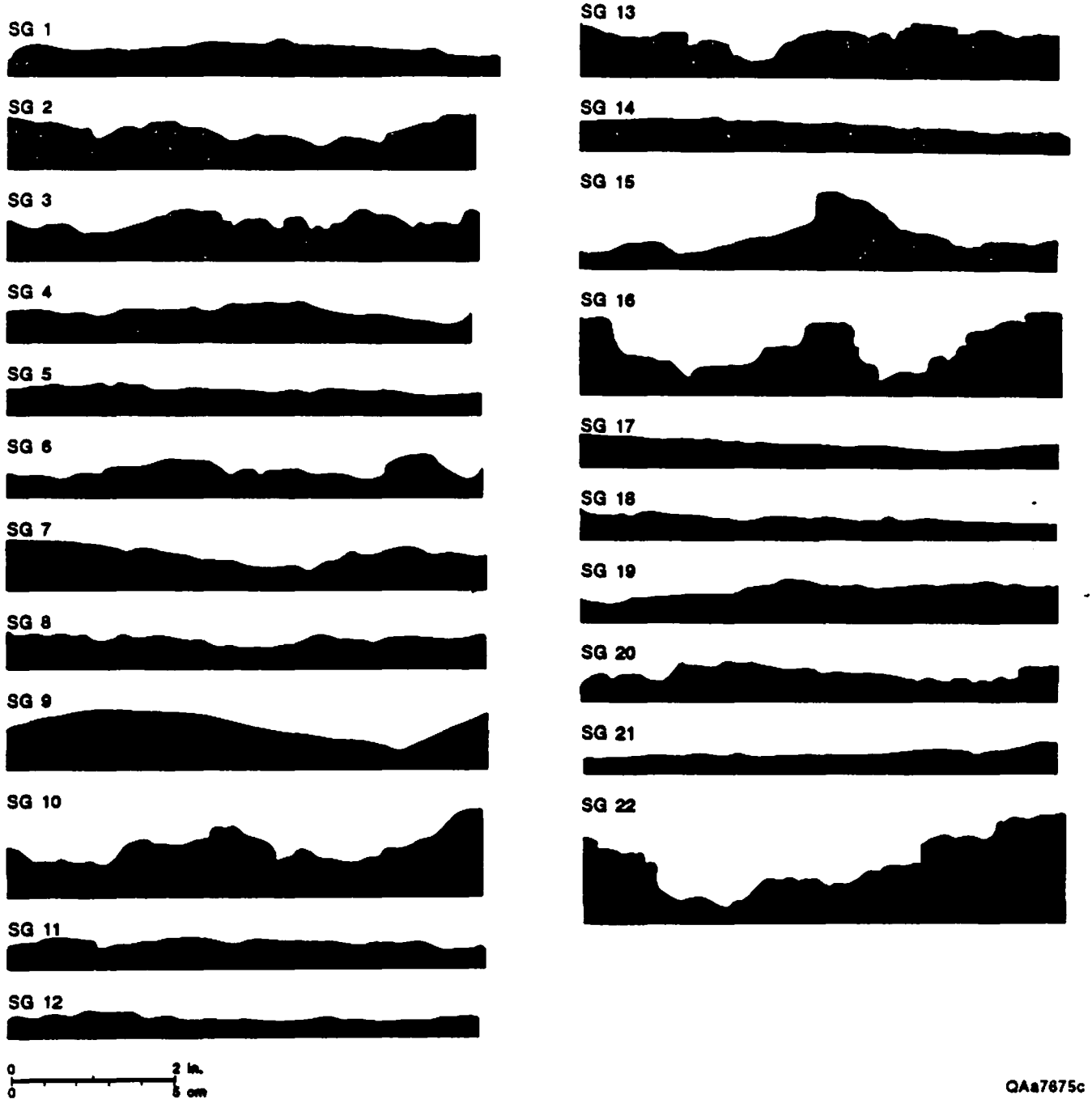

Figure 27. Fracture and conduit surfaces measured at the San Geronimo exposure.

Table 12. Specific roughness of fractures and conduits measured at the San Geronimo and Wilderness Oak sites

Sample	Specific roughness (mm)	Standard deviation (mm)	Location	Feature measured	Solution enhancement?
SG 1	3.7	1.3	San Geronimo	Fracture	None
SG 2	4.7	2.7	San Geronimo	Fracture	Minor
SG 3	3.3	2.0	San Geronimo	Fracture	Yes
SG 4	2.7	1.6	San Geronimo	Fracture	None
SG 5	1.4	0.6	San Geronimo	Fracture	None
SG 6	4.1	2.2	San Geronimo	Fracture	Yes
SG 7	5.3	2.5	San Geronimo	Fracture	Minor
SG 8	2.8	1.3	San Geronimo	Fracture	None
SG 9	5.3	2.9	San Geronimo	Fracture	None
SG 10	5.8	4.2	San Geronimo	Fracture	Yes
SG 11	2.9	1.1	San Geronimo	Fracture	None
SG 12	1.1	0.8	San Geronimo	Fracture	None
SG 13	7.8	2.8	San Geronimo	Conduit	Yes
SG 14	1.3	0.5	San Geronimo	Fracture	None
SG 15	6.6	5.5	San Geronimo	Conduit	Yes
SG 16	11.4	6.7	San Geronimo	Conduit	Yes
SG 17	1.0	0.8	San Geronimo	Fracture	None
SG 18	1.2	0.6	San Geronimo	Fracture	None
SG 19	2.3	1.3	San Geronimo	Fracture	None
SG 20	3.4	1.8	San Geronimo	Fracture	Minor
SG 21	1.1	0.7	San Geronimo	Fracture	None
SG 22	14.3	8.7	San Geronimo	Conduit	Yes
WO 23	6.5	2.7	Wilderness Oak	Fracture	Yes
WO 24	4.2	1.7	Wilderness Oak	Fracture	Minor
WO 25	4.4	2.0	Wilderness Oak	Fracture	None
WO 26	1.3	0.7	Wilderness Oak	Fracture	None
WO 27	2.5	2.0	Wilderness Oak	Fracture	None

effects, and collapse because of dissolution of underlying horizons are also recognized as factors that influence the amount and distribution of solution features in outcrop.

The major post-Miocene to Holocene episode of karstification occurred during development of the freshwater aquifer. Valley incision and development of springs played a major role in draining saline pore fluids and setting up a karstic hydrologic system that circulated large volumes of fresh water through the Edwards (Woodruff and Abbott, 1986; Deike, 1990).

Karst porosity and the distribution of karst feature size were determined at several sites. Karst porosities are summarized in Table 13. Histograms of karst feature size are shown in Figure 28. The number of karst features, geometric mean size, variance, and largest size are summarized for each location in Table 14. Drawings of fracture and karst features of three representative exposures are shown in Figures 29, 30, and 31.

Stratigraphic control on karst formation is evident where caves, soft porous carbonate, and terra rossa infills occur preferentially at one horizon. Stratigraphic controls on dissolution include (1) preferential dissolution of dolomite, (2) focusing dissolution in breccia zones, and, possibly, (3) preferential dissolution of calcitized evaporite zones with abundant touching vugs. In almost all outcrops, caverns have developed preferentially in former dolostones—both dolomitized subtidal packstones and dolomitized tidal flat facies (for example, Figs. 29 through 31).

Examples of leached subtidal rocks were abundant at the New Braunfels, Stone Oak, Highway FM 1604, and San Geronimo outcrops. Partly dolomitized subtidal packstones and wackestones have been intensely altered in outcrop and form thick, laterally continuous honeycombed beds. Vugs developed as a result of preferential dissolution of one material, leaving a knobby, fossiliferous limestone matrix with a honeycombed texture. In outcrop, these beds are dark colored or stained red with terra rossa. Intensity of alteration varies laterally within many beds and might reflect the amount of dolomitization, the amount of replacement of dolomite by late calcite (dedolomitization), and proximity to conduits. Comparison of

Table 13. Karst porosities measured using image analysis of selected parts of outcrops.

Site	Structural setting	Porosity (%)
Lake Medina	Small faults typical of a 4-mile-wide block bounded by large faults	3.01
1604 at Bitters Road	Roadcut parallel to and 0.2 mile south of large fault with about 250 ft of throw	2.83
Wilderness Oak	Small faults typical of the area within a 1.8-mile-wide block bounded by large faults	1.48
1604 at Blanco Road[1]	Roadcut parallel to and 0.5 mile south of large fault with about 200 ft of throw	9.43
1604 at Blanco Road[2]	See above	1.08
Fiesta, Texas	A large fault with an estimated throw of 170 ft is exposed in the outcrop	1.75
New Braunfels	On footwall block about 600 ft from large fault having about 850 ft of throw	5.68
San Geronimo	On the footwall block of a large fault with displacement between 850 and 1200 ft. Outcrop about 600 ft from fault	2.61
Stone Oak	Strata adjacent to a fault having about 22 ft of throw	2.6

[1] With large cave included.
[2] Without large cave.

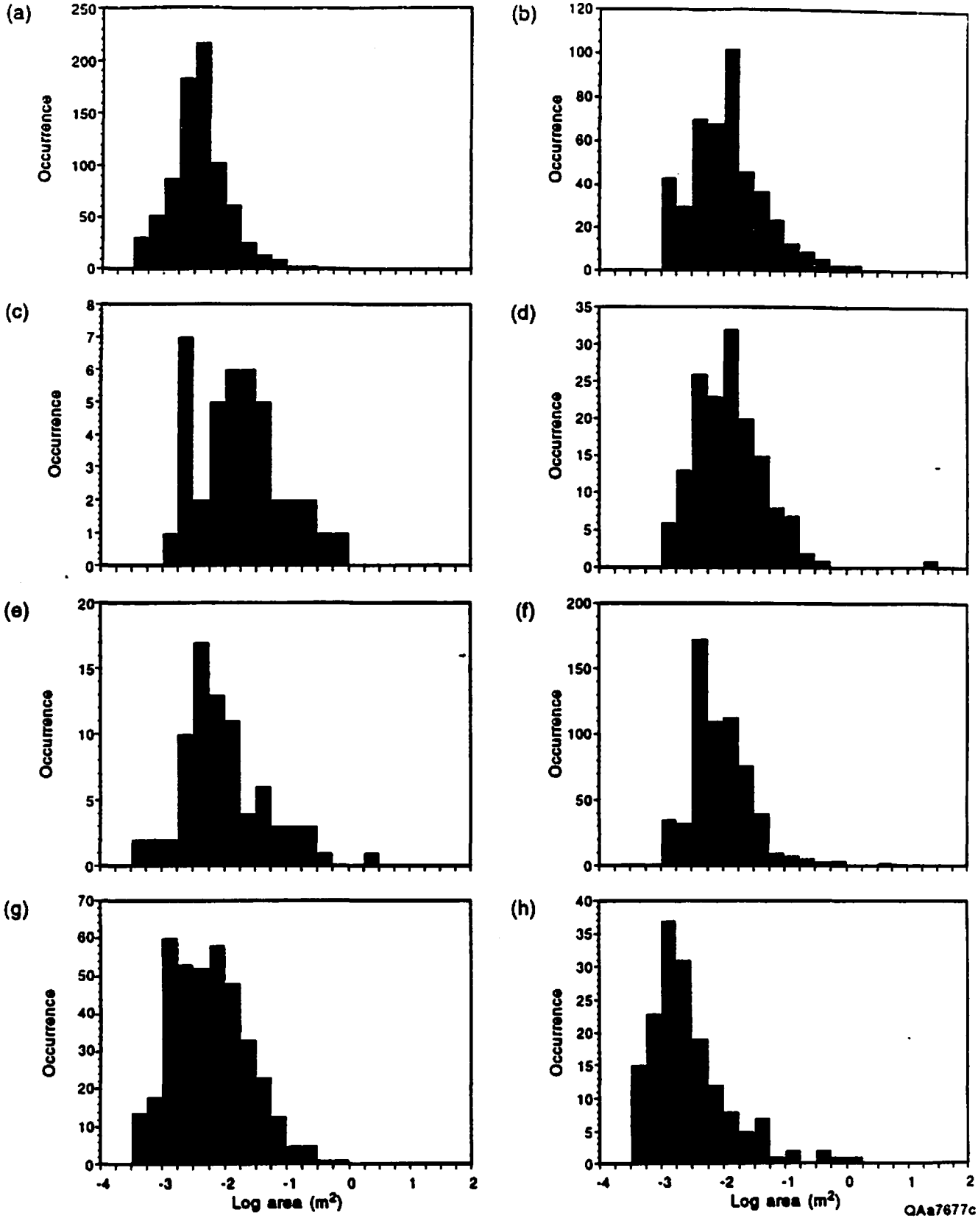

Figure 28. Histograms of karst feature size distribution for (a) Lake Medina, (b) FM 1604 at Bitters Road, (c) Wilderness Oaks, (d) FM 1604 at Blanco Road, (e) Fiesta, Texas, (f) New Braunfels, (g) San Geronimo, and (h) Stone Oak.

Table 14. Size distribution of karst features.

Site	Number of features	Mean[1] size (m^2)	Variance $(\log[m^2])^2$	Maximum size (m^2)
Lake Medina	796	0.004	0.252	3.89
1604 at Bitters Road	455	0.012	0.401	2.01
Wilderness Oaks	40	0.017	0.457	0.83
1604 at Blanco Street	154	0.013	0.324	19.72
Fiesta, Texas	78	0.010	0.464	2.40
New Braunfels	614	0.009	0.287	9.55
San Geronimo	384	0.006	0.411	0.59
Stone Oak	164	0.003	0.436	1.10

[1] Geometric mean.

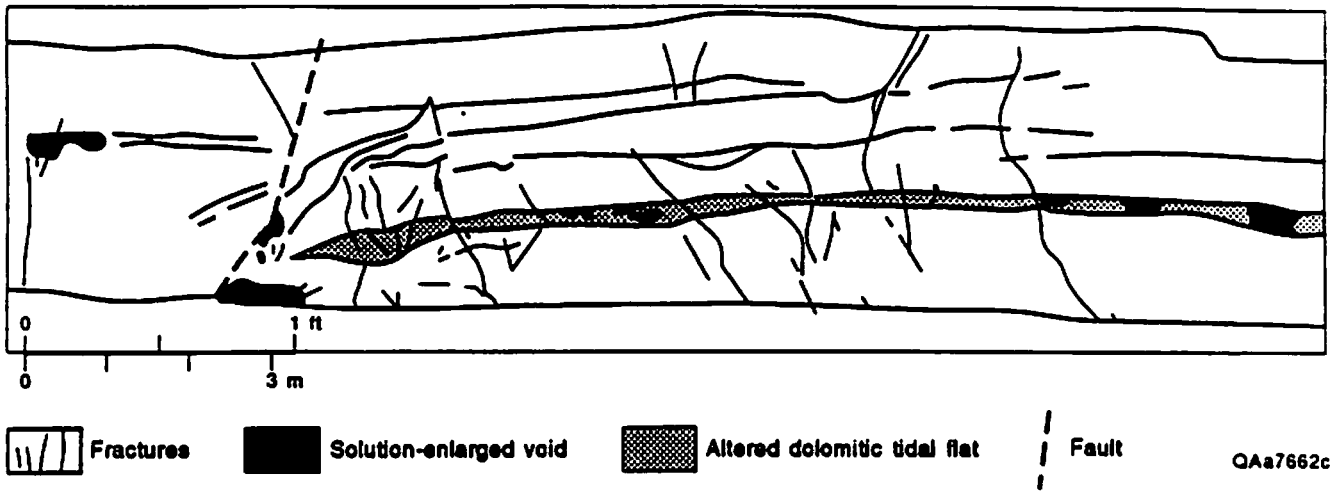

Figure 29. Faults, fractures, and solution-enlarged voids at the Wilderness Oak exposure, drawn from a photomosaic. Both open and terra-rossa-filled solution features are shown.

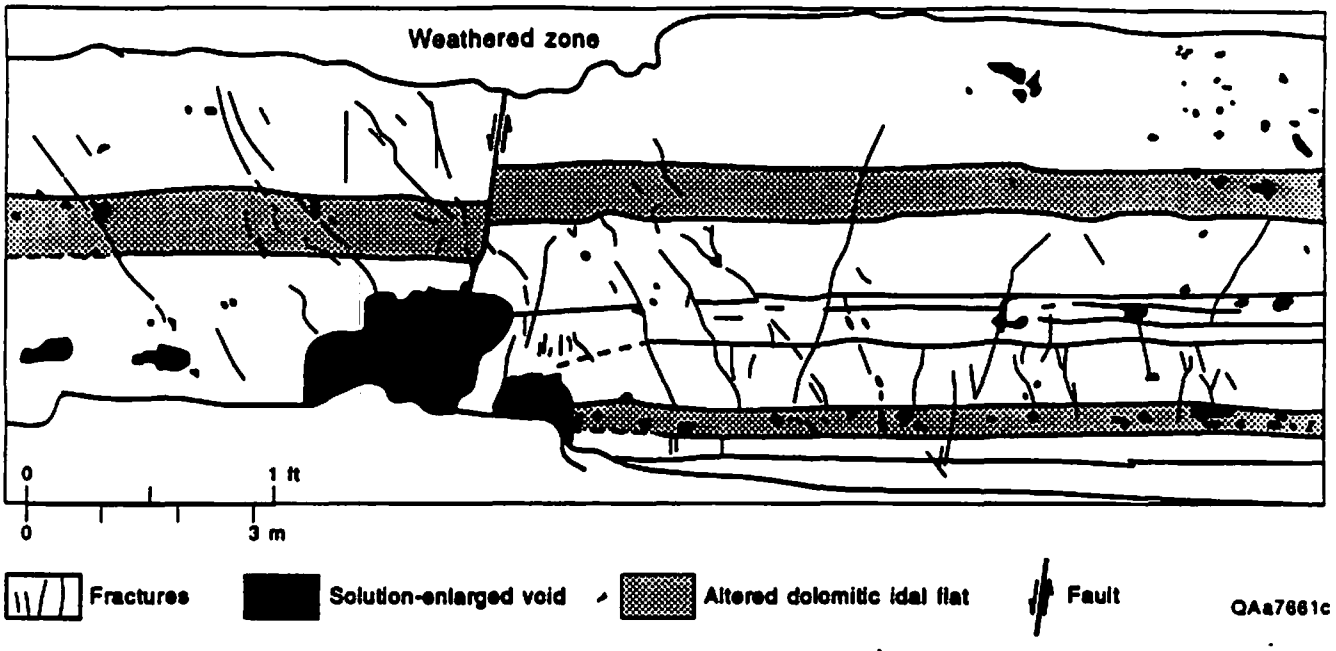

Figure 30. Faults, fractures, and solution-enlarged voids at the Lake Medina exposure, drawn from a photomosaic.

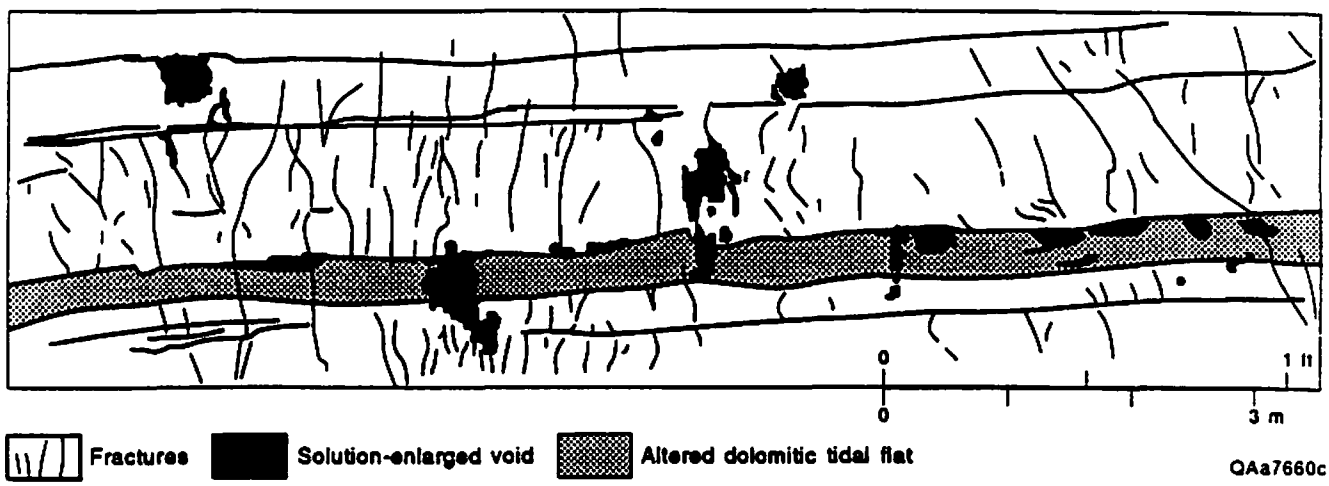

Figure 31. Faults, fractures, and solution-enlarged voids at the San Geronimo exposure, drawn from a photomosaic. Both open and terra-rossa-filled solution features are shown.

honeycombed texture in outcrops with less altered fabrics in cores suggests that many of the dissolved areas were burrows that were preferentially dolomitized and then leached. The presence of abundant burrows and diverse shelly fauna in the altered beds demonstrates that these beds were deposited under normal marine conditions and suggests that gypsum was not the mineral dissolved.

Partial dissolution of burrowed subtidal dolomitic beds in a folded footwall block of a large fault has created additional folding and fracturing in the New Braunfels outcrop. Large caves have developed in the breccia. Large, widely spaced collapse features are observed in both Highway FM 1604 outcrops. The base of the collapse zones is not exposed, but a honeycomb subtidal dolomite unit exposed toward Panther Springs Creek might be the unit that dissolved and led to collapse. Collapse features (dissolved bed not exposed) also increase the amount of brecciation and karst apparent at the San Geronimo exposure.

Thin-bedded dolomitic tidal flat facies have also been altered in outcrops and form zones of soft porous carbonate and terra rossa. The thickness of tidal flat sequences is substantially decreased in some areas where dolomite has been altered and indicates volume loss. In other areas, horizontal caves lie within leached tidal flat units. The thin-bedded character and the dolomitic mineralogy of the tidal flat units might contribute to dissolution. Leached tidal flat dolomite is common at the Wilderness Oak, San Geronimo, and Lake Medina outcrops. In contrast, in the cores from the aquifer, tidal flat dolomite is generally preserved, whereas subtidal dolomite has been leached, producing lost core and high-caliper response.

Structural control on karst development is very important. Apertures of solution-enlarged fractures were previously described. Solution enlargement of conduits along faults was seen in the Wilderness Oak (Fig. 29), Fiesta, Texas, and Lake Medina (Fig. 30) exposures. Solution enlargement along fractures was seen in all exposures. Intensely fractured and gently folded strata on the footwall of a fault with more than 800 ft (243 m) of throw at the San Geronimo exposure (Fig. 31) show the effect of fractures on focusing dissolution. The relationship between lineaments and fractures in the Edwards, transmissivity, and cave orientation has been

studied by Wermund and others (1978) and Alexander (1990). Preferential development of small caves in dolomitic beds or at the junction of fractures and dolomitic beds is well displayed in the Lake Medina (Fig. 30), Wilderness Oak (Fig. 29), and San Geronimo (Fig. 31) outcrops. Caves are localized along faults or within fault breccias, as observed at the Wilderness Oak, Fiesta, Texas, San Geronimo, and Lake Medina exposures. In each of these settings, the largest caves are found in the highly brecciated zone along the fault plane. In contrast, other fault breccias, such as the one at the Stone Oak outcrop, are cemented by calcite, and permeability appears low. Examination of these outcrops emphasizes that faults can either increase or decrease the total transmissivity. Abundant, interconnected fractures in the intensely fractured zone adjacent to the fault might be enlarged, and they focus flow, possibly parallel to the fault. Where calcite cement fills the breccia, cross-fault flow might be decreased. Stratigraphic offset of permeable zones along faults might also decrease the cross-fault flow (Maclay and Small, 1983). Additional research is needed to define the relative importance and potential interactions between these effects.

Fabric control of dissolution is illustrated where vugs initially created by alteration and dissolution of gypsum or dissolution of large rudist fossils have been further enlarged by dissolution of matrix carbonate. Large vugs seen in outcrop are similar in occurrence and probable genesis to the touching vugs that are observed in plugs and thin sections. Fabric-controlled vugs are well displayed at the Stone Oaks outcrop.

Paleokarst has long been recognized as an important feature in the evolution of Edwards permeability (Cronin, 1932; Fisher and Rodda, 1969; Rose, 1972; Abbott, 1975; Woodruff and Abbott, 1986). Paleokarst features can be related to episodes of subaerial exposure during accumulation of the Edwards sediments, to relative sea-level fall and exposure at the end of Edwards deposition, and to phases of aquifer development.

Syndepositional solution of carbonate and especially sulfate minerals most likely occurred during relative sea-level lowstands at the end of some cycles. Such early dissolution of sulfate beds has been proposed where beds overlying sulfate breccias are undisturbed (Fisher and

Rodda, 1969). Top of cycle exposure events are recognized on the San Marcos Platform in many depositional cycles in the middle Kainer Formation and some cycles in the middle Person Formation. During more prolonged exposure at sequence boundaries, diagnostic altered and karstic fabrics in carbonates formed (Esteban and Klappa, 1983), and remaining sulfates calcitized or dissolved. Such exposure is widely recognized on an altered surface at the top of the Person Formation prior to Georgetown deposition. Multiple exposure events preceding Georgetown deposition are evidenced in the USGS Randolph FM 1604 core and the USGS Castle Hills core. Large carbonate-filled karst pits, tentatively assigned to the same post-Person exposure, were observed at the Highway FM 1604–Bitters Road exposure. Pre-Georgetown exposure played a role in enhancing matrix and touching-vug porosity in some upper Person rudist grainstones.

In the subsurface, large caves corresponding to a section of lost core within the Kainer in the Castle Hills core are attributed to preferential development of caves within breccias. Correlation of cycles shows that the lost section probably originally contained evaporite. High gamma-ray response is commonly seen in the Kirschberg evaporitic interval of the Kainer Formation, suggesting that higher clay concentration corresponding to terra rossa might be developed in this interval. Dissolution and collapse of the McKnight gypsum beds have increased permeability of the breccia interval, as well as the overlying Salmon Peak Formation. The porosity of the McKnight and the lower Salmon Peak appears on logs to be high locally, although uncertainties resulting from log response to shale and asphalt make the porosity of these intervals difficult to determine. Solution enlargement of fractures in the largely calcitic Maverick Basin section is much less than in the dolomitized platform.

Another variable influencing the development of karst is the hydrologic setting. Only paleokarst is identified in the saline Edwards, although enhancement of micropores might occur near the fresh/saline-water interface, as observed in the USGS Randolph FM 1604 core. The amount of karst is highest in the outcrop (Table 13). Outcrops include solution that occurred within the phreatic aquifer as well as the unsaturated zone. Vertical karst pipes filled with terra

rossa soils are noted near the present surface. These features might have formed during earlier stages of aquifer development; however, their present geometry suggests that they have been enlarged and straightened by near-surface karst processes. They are commonly filled with roots, which might also play a role in their formation. Other near-surface effects include formation of dolines at the surface, precipitation of pedogenic carbonates, and other modifications such as down-slope creep. Areas most strongly affected by these processes were avoided for quantitative studies, although some near-surface effects are noted in all outcrops. Within the aquifer, it is difficult to separate the effects of hydrologic setting from other variables. For example, more karstic vugs and terra rossa are noted in the Kainer Formation in the Landa Park core than in the Kainer Formation of the Castle Hills and Feathercrest cores. This might be because of (1) the proximity of the Landa Park to large springs, and therefore high flow rates, (2) the shallow depth of the Kainer in the Landa Park core (surface to 200 ft [60.1 m] at Landa Park, 300 to 600 ft [91.4 to 182.9 m] in the other cores), (3) depositional facies control of increase in dolomitization toward the northeast (Rose, 1972), or (4) the large fault in Landa Park. Examination of outcrop suggests that all four contribute (Table 13). The outcrop having the highest karst porosity is New Braunfels, with large caves developed in collapse breccia from dissolution of subtidal dolomite adjacent to a large fault. The outcrop at Highway FM 1604 at Bitters Road has abundant large and small solution features related to preferential dolomite dissolution and brecciation and collapse, and it is within a block between large faults. The Lake Medina outcrop has high cave porosity because of abundant smaller vugs in dolomitic beds and abundant fractures, but it has a fault with only a small amount of throw. The San Geronimo outcrop has less dolomite, and therefore less stratigraphically controlled dissolution, but enlargement of abundant fractures. Stone Oak, Wilderness Oak, and Fiesta, Texas, have less dolomite, and therefore less solution enlargement, in spite of abundant fractures and faults.

DISCUSSION

Previous hydrologic models have generalized the Edwards aquifer as a single flow unit with discrete subareas that have uniform transmissivities and that are subdivided by single-line fault barriers (Klemt and others, 1979; Maclay and Land, 1988; Kuniansky, 1994). These simplifications do not describe real aquifer complexities and may not be adequate to model some important characteristics of the aquifer. For example, vertical variations in salinity in the aquifer, especially but not exclusively near the fresh/saline-water interface, might reflect stratigraphic and structural heterogeneity. Small-scale aquifer heterogeneity may also be important in modeling aquifer behavior on a local scale, especially in a contaminant transport model.

Data sets collected during this study document the spatial distribution of permeability through the aquifer. Structure and isopach maps (Pls. 3 and 4) show the geometry of the aquifer and the distribution of and displacement on faults. Maps of transmissivity (Pl. 5), as well as specific capacity and hydraulic conductivity, show strong lateral heterogeneity. Maps of matrix permeability based on wireline logs minimize the contribution of conduits, such as fractures and faults, and therefore show lower values and less variability. Strong vertical heterogeneity in the distribution of hydraulic conductivity was documented from analysis of aquifer tests reported from 10 of the wells from various fresh/saline-water interface experiments (Figs. 18 through 21). Calculated matrix permeability based on wireline logs from these wells shows vertical variation in the total, and percent contribution from the matrix varies from layer to layer. Some of the possible causes of variation can be considered by integrating the various data sets.

Vertical variation in hydraulic conductivity near the fresh/saline-water interface shows high transmissivity in the middle of the Kainer Formation in most wells and moderate transmissivity in the middle of the Person Formation in many wells (Figs. 18 and 19). Matrix permeability accounts for only a fraction of the total; therefore, conduits appear to have developed preferentially in these intervals. Preferential dissolution of dolomite to produce caves and honeycomb fabric, as well as their microfabric equivalent, touching-vug porosity, was

observed both in outcrop and in core plugs from the aquifer. Figure 5 shows abundant dolomitized tidal flat and subtidal faces in the middle Kainer Formation and somewhat lesser amounts in the Person Formation. The amount and distribution of these dolomitized facies (Fig. 7) correspond to the intervals with increased hydraulic conductivity in the New Braunfels and San Marcos fresh/saline-water interface transects (Figs. 18 and 19). Mid-Kainer (Kirschberg equivalent) calcitized evaporites, which play a role in creation of touching-vug porosity and breccia may also contribute to the high conduit porosity. In the south Medina well (Fig. 21), the Kainer–lower Devils River preferentially leached zone is present, but the Person interval is not evident. Matrix porosity in the Person throughout this area is lower than elsewhere on the platform (Hovorka and others, 1993), which may be related to the off-platform decrease in amount and thickness of tidal flat facies and associated subtidal dolomite. Decreased dolomite in the Person may be the reason that conduit porosity is not preferentially developed in this unit in southern Medina County. The poorest relationship between the amount of dolomite and development of conduits is in the wells that have higher hydraulic conductivity than do adjacent wells, the San Marcos well D (Fig. 19) and San Antonio well A (Fig. 20). Comparison with outcrop analogs would suggest that these wells may intersect fracture sets that dominate conduit development and conduit flow and overwhelm any stratigraphic effects.

On a regional scale, an element of systematic lateral variation in transmissivity can be identified. Spatial relationships over 13-mile areas are indicated by variograms. Examining cores and outcrops helps in understanding the factors contributing to heterogeneous distribution of permeability in the aquifer.

Comparing transmissivity (Pl. 5) and mapped faults (Pl. 3) shows no strong relationship between high transmissivity and proximity to faults. High transmissivity values are found in areas between major faults. Moderate and low transmissivity values are found in parts of the outcrop with abundant faults. This result contrasts with that of Alexander (1990), who found a relationship between specific capacity and distance of the well from lineaments in the Barton Springs part of the Edwards. In the Alexander study, the specific capacity of wells increased

several orders of magnitude for wells southwest of lineaments as compared with those more than 1,000 ft (300 m) from a fault. In the present outcrop studies, an increase in the abundance and connectivity of fractures near faults was observed, as well as preferential development of large caves in fault zones. The width of the highly brecciated zones adjacent to faults increases with throw on the fault (Fig. 23). These factors suggest that transmissivity increases near faults in the study area. Several factors may obscure relationships between mapped faults and transmissivity. Many small faults and fractures are found within the blocks between the large mapped faults. Three of the outcrops studied, more than 1,000 ft (300 m) from large faults, contain small faults, fractures, and abundant karst. Wells that intersect small faults or karst systems may account for some of the high transmissivities away from faults. Abundant fractures and small faults localized by structural features other than faults, such as folds and relay ramps, may account for others. Variables other than structure that contribute to increasing transmissivity, such as karst development, may also obscure relationships between transmissivity and faulting. Well locations are extracted from various sources, and well-location errors may obscure structurally controlled trends. Because the width of the highly fractured zone adjacent to large faults is only 25 ft (7.6 m), and many faults dip steeply, minor uncertainties in well location can be a significant factor in identifying the effect of distance from the fault on transmissivity.

A strong contrast in the average and distribution of transmissivity is noted between the confined and unconfined parts of the aquifer, with a lower average and range of transmissivities in the unconfined aquifer (Fig. 15). A trend of high matrix permeability is observed on both sides for the fresh/saline-water interface (Pl. 6). Comparing transmissivities with structural position shows that this pattern (Pls. 3 and 4) can also be recognized within the confined aquifer, with more high transmissivities in the deeper parts of the aquifer than in the parts where the top of the aquifer is higher than about 200 ft (60 m) above sea level. This is somewhat counterintuitive because fast flow of undersaturated water might be expected in the shallowest part of the aquifer. Outcrops, at the highest elevations, show abundant dissolution

features and additional karst features that have developed in near-surface settings. No sharp change in depositional facies or diagenetic alteration corresponds to the confined–unconfined boundary because the major depositional facies boundaries are nearly perpendicular to the Balcones Fault trend. Examination of Plate 3 shows that structural setting with respect to throw on faults or fault frequency does not appear to be the major cause of increased transmissivity of the deeper part of the aquifer because in much of Bexar County, the largest faults define the updip edge of the confined aquifer. An explanation involving karst development is therefore suggested.

One factor that might account for greater development of both conduit and matrix permeability in the deeper parts of the aquifer is dynamics of the geochemical processes that favor dissolution. Deike (1990) modeled the role of mixing saline and fresh water in driving dolomite dissolution in the Edwards aquifer. Deike's observations of the role of dolomite dissolution in porosity creation are supported by the relationships between conduits and touching vugs and dolomitized facies documented in this study. It is possible that the setting for rapid dolomite dissolution lies in a mixing zone found near the fresh/saline-water interface, as well as at various stratigraphic positions located vertically within the Edwards Group. The amount of dolomite dissolved would correspond to the length of time that the mixing zone remained in an area. Woodruff and Abbott (1986) described evolution of the aquifer through time, with freshwater circulation related to intersection of the aquifer by downcutting valleys, allowing saline water to drain. If the area of the freshwater aquifer initially expanded rapidly and has slowed toward the present, greater dolomite dissolution might result in the deeper parts of the aquifer. This might be supported by greater calcitization and dissolution of dolomite in the Selma core from the confined aquifer (Deike, 1990) than was observed in the cores from near the updip edge of the confined aquifer that were examined during this study.

Another possible explanation for the lower transmissivities observed in the unconfined aquifer is that the areas where recharge may be focused, such as stream beds or sink holes, are

not represented in either the aquifer test or outcrop study data set. Preferential flow through these areas may reduce porosity enhancement in other parts of the unconfined aquifer.

Another area with a number of low transmissivities from aquifer tests is the Maverick Basin (Pl. 5). However, some high transmissivities are present, and the total number of aquifer tests is inadequate to define a distribution. Matrix permeability in the Maverick Basin is lower than the regional average. Dolomite dissolution, which plays a dominant role in permeability enhancement elsewhere in the Edwards Group, is minimal in the Maverick Basin because of the dolomite content of these dominantly subtidal rocks. Core and plug analysis and thin-section examination show only minor carbonate dissolution and few samples with abundant touching vugs, suggesting that karst may be less important in this area than elsewhere in the Edwards aquifer. However, evidence of multiple stages of brecciation as a result of dissolution of thick sulfate beds from the McKnight Formation can be documented in core. In addition, many of the Maverick Basin facies in Uvalde County have been deformed into a complex dome intruded by Cretaceous volcanics. Increased hydraulic conductivity of breccia, overlying fractured carbonate, and structural deformation may partly or wholly offset the decrease in solution-enhanced conduit development in this area. Original thickening of the Edwards section into the Maverick Basin has been offset by evaporite dissolution throughout the aquifer; however, the vertical lithologic heterogeneity may mean that the thickness of the highly transmissive part of the aquifer is substantively reduced.

One key area not adequately characterized by aquifer tests is the confined aquifer in Hays and Comal County. Several sets of high-quality data from transects of research wells are available from this area (Poteet and others, 1992); however, few other aquifer tests from this area were located. Inverse modeling of the Barton Springs portion of the Edwards aquifer (Slade and others, 1985) identified high transmissivities near Barton Springs. Proximity to large faults, shown on Plate 3, and high dolomite content indicated by facies distribution (Fig. 7) and mapped by Rose (1972) in the confined Edwards aquifer in Hays and Comal Counties suggest that karstic conduits are major contributors to flow in this part of the aquifer.

CONCLUSIONS

Three sets of data were compiled to describe the characteristics of the Edwards aquifer: (1) structure and thickness of the aquifer, (2) distribution of transmissivities calculated from specific capacity and pump tests of wells penetrating the aquifer, and (3) distribution of matrix permeability. Each of these data sets was prepared in a digital format for ARC/INFO GIS to facilitate future analysis. These data sets build on previous studies of the Edwards aquifer and include incremental improvements. The structural map includes well log data collected by EUWD over the past several years and draws on recent mapping of the Edwards outcrop for subsurface interpretations. A statistical relationship for relating specific capacity to transmissivity was developed specifically for the Edwards aquifer and applied to determine the distribution of transmissivity and hydraulic conductivity. A facies model based on high-frequency cyclicity was developed for the Edwards and applied to the interpretation of hydrologic data. Core and outcrop examination documented and quantified relationships between faults, fractures, karst, and rock matrix. Aquifer tests previously conducted along four fresh/saline-water interface transects were further interpreted to define these relationships for the subsurface.

Hydraulic conductivity of the Edwards aquifer is highly heterogeneous at several scales. Detailed description of heterogeneity provided by this report allows selection of the appropriate techniques for generalizing, averaging, or lumping data for future specific models or calculations.

At the smallest scale, two general rock fabric types are identified: particle-dominated fabrics and touching-vug-dominated fabrics. For particle-dominated rocks, a relationship between porosity and permeability was developed for geologically and hydrologically defined parts of the aquifer. Vertical variation in the matrix permeability shows high permeabilities in dolomitized units that occur in the middle Kainer and middle Person on the crest of the San Marcos Platform. Lateral changes show high matrix permeability near the fresh/saline-water interface and lower permeability where dolomitic units thin off the San Marcos Platform. The

lowest matrix permeability is found in the undolomitized rocks of the Maverick Basin. Touching vugs, indicating dissolution and fracturing at a small scale, develop preferentially in dolomitized subtidal rocks, dolomitized tidal flats, and in calcitized evaporites.

At a single-well or outcrop scale, fractures, faults, and karst features are the dominant control on hydraulic conductivity. In most wells, hydraulic conductivity from aquifer tests is over a hundred times higher than that of the matrix. High hydraulic conductivity is observed in the dolomitized intervals of the Kainer and Person Formations. Outcrop studies show preferential development of karst in dolomitic zones, paralleling small-scale dissolution of these rocks. Some of the highest hydraulic conductivity, however, is not stratigraphically limited and may be structurally controlled. In outcrop, a relationship between throw on faults and the width of the adjacent highly fractured zone is noted. Brecciation related to carbonate or evaporite dissolution was also noted in core and outcrop. The largest caves were located in highly brecciated zones. Additional analysis is needed to determine whether a relationship between increased hydraulic conductivity and faults can be identified throughout the aquifer. The variable hydraulic conductivity between nearby wells quantified in the nugget on variograms shows the hydrologic effect of the karst and fractures.

Variograms show that hydraulic conductivity is spatially related at a regional scale. The areas of highest hydraulic conductivity are found in the downdip parts of the confined aquifer on the San Marcos Platform and the Devils River trend. The distribution of aquifer tests is inadequate to demonstrate this relationship in the northeastern part of the confined aquifer in Hays and Comal Counties. The unconfined aquifer in Hays and Comal Counties is an area of low hydraulic conductivity. The origin of this low hydraulic conductivity is unknown, but several hypotheses relating to the evolution of the aquifer are presented. Data distribution in the Maverick Basin is inadequate to determine whether this area has lower than average hydraulic conductivity, as suggested by the low dolomite content and reduced carbonate dissolution and low matrix permeability, or whether this low potential for formation of karstic conduits is

compensated for by fracturing and brecciation related to evaporite dissolution and structural deformation.

FURTHER WORK

As a result of this study, additional data and topics requiring further analysis have been recognized that could improve the quality of hydraulic conductivity data input into a hydrologic model.

- Additional aquifer test data are needed from areas with sparse data. In particular, test data are needed from the unconfined aquifer in Bexar and Medina Counties to determine whether low transmissivities and hydraulic conductivities are found in this part of the aquifer as they are in the unconfined aquifer in Hays and Comal Counties.

- Additional data on the vertical distribution of hydraulic conductivity are needed in the unconfined aquifer and updip parts of the confined aquifer. These data would complement the data available from the fresh/saline-water interface studies. Data might be used to better assign transmissivity vertically within the aquifer. Quantitative data on stratigraphic controls on conduit development in the recharge zone are needed.

- Further analysis of transmissivity is needed. Because numerical models require a value of transmissivity for input into a cell, individual test results must be averaged or extrapolated. This might include kriging or other types of contouring, construction of directional variograms, iterative and probabilistic simulations to determine the effects of lateral and vertical variability, additional analysis of geologic controls on transmissivity, or a combination of these analyses. Additional statistical analysis of the GIS data bases has the potential to determine the contribution of large faults to hydraulic conductivity.

- Compilation and interpretation of tracer tests are needed. Tracers could be used to better predict the fate and transport of possible contaminants in the Edwards aquifer and to refine the transmissivity distribution. Chemical species from spills or artificial recharge, natural

tracers such as salinity, environmental tracers such as tritium and chlorofluorocarbons, and controlled tracer tests could serve as tracers.

• Inverse modeling is needed. In areas with little data control, inverse modeling can determine a probable transmissivity. This approach might eliminate potential errors resulting from the bias of insufficient testing of the aquifer. For example, large karst conduits can have a large impact on flow but because of limited areal cross section, not be penetrated by wells. This might be especially important in areas with few aquifer tests, particularly the confined part of the aquifer in Comal and Hays Counties and areas of preferential recharge along streams.

ACKNOWLEDGMENTS

This work was performed for and funded by the Edwards Underground Water District under contract No. 93-17-FO. We thank EUWD staff members John Waugh and Steve Walthour for their support and assistance in data collection. Bill Stein of W. F. Guyton Associates, Ted Small of USGS, San Antonio office, and Bob Maclay contributed helpful insights to numerous discussions. Core-plug analysis was carried out by Reservoirs, Inc., Midland, Texas. Thin sections were prepared by National Petrographic Service, Houston, Texas. Dianne Spinney, Tom Tremblay, and Patrice Porter provided GIS support. Figures were drafted by Maria Saenz.

REFERENCES

Abbott, P. L., 1973, The Edwards Limestone in the Balcones Fault Zone, South-Central Texas: The University of Texas at Austin, Ph.D. dissertation, 122 p.

_____ 1974, Calcitization of Edwards Group dolomites in the Balcones zone aquifer, South-Central Texas: Geology, v. 2., p. 359–362.

_____ 1975, On the hydrology of the Edwards Limestone, South-Central Texas: Journal of Hydrology, v. 24, p. 251–269.

Alexander, K. B., 1990, Correlation of structural lineaments and fracture traces to water-well yields in the Edwards aquifer, Central Texas: The University of Texas at Austin, Master's thesis, 113 p.

Bathurst, R. G. C., 1975, Carbonate sediments and their diagenesis: developments in sedimentology 12: New York, Elsevier Scientific Publishing Company, 658 p.

Baumgardner, R. W., Jr., and Collins, E. W., 1991, Geologic map of the Hunter 7.5-minute quadrangle, Texas: The University of Texas at Austin, Bureau of Economic Geology, open-file map prepared for U.S. Geological Survey under cooperative agreement, scale 1:24,000.

Bentall, Ray, 1963, Methods of determining permeability, transmissivity, and drawdown: U.S. Geological Survey Water-Supply Paper 1536-I, 99 p.

Bisroy, Y. K., and Summers, W. K., 1980, Determination of aquifer parameters from step tests and intermittent pumping data: Ground_Water, v. 18, no. 2, p. 137–146.

Brown, R. H., 1963, Estimating the transmissivity of an artesian aquifer from the specific capacity of a well: U.S. Geological Survey Water Supply Paper 1536-I, p. 336–338.

Brown, T. E., Waechter, N. B., Rose, P. R., and Barnes, V. E., 1974, San Antonio sheet: The University of Texas at Austin, Bureau of Economic Geology, Geologic Atlas of Texas, scale 1:24,000.

Campana, M. E., and Mahin, D. A., 1985, Model-derived estimates of ground-water mean ages, recharge rates, effective porosities and storage in a limestone aquifer: Journal of Hydrology, v. 76, p. 247–264.

Carr, M. M., 1987, Facies and depositional environments of evaporites of the Lower Cretaceous McKnight Formation, Maverick Basin, southwest Texas: The University of Texas at Arlington, Master's thesis, 144 p.

Clark, Isobel, 1979, Practical geostatistics: London, Applied Science Publishers, Limited, 129 p.

Clement, T. J., 1989, Hydrochemical facies in the bad water zone of the Edwards aquifer, Central Texas: The University of Texas at Austin, Master's thesis, 168 p.

Collins, E. W., 1987, Characterization of fractures in limestones, northern segment of the Edwards aquifer and Balcones Fault Zone, Central Texas: Gulf Coast Association of Geological Societies Transactions, v. 37, p. 43–53.

_____ 1992a, Geologic map of the Anhalt 7.5-minute quadrangle, Texas: The University of Texas at Austin, Bureau of Economic Geology, open-file map prepared for U.S. Geological Survey under cooperative agreement 14-08-0001-A0885, scale 1:24,000.

_____ 1992b, Geologic map of the Fischer 7.5-minute quadrangle, Texas: The University of Texas at Austin, Bureau of Economic Geology, Open-file map prepared for U.S. Geological Survey under cooperative agreement 14-08-0001-A0885, scale 1:24,000.

_____ 1992c, Geologic map of the Smithson Valley 7.5-minute quadrangle, Texas: The University of Texas at Austin, Bureau of Economic Geology, open-file map prepared for U.S. Geological Survey under cooperative agreement 14-08-0001-A0885, scale 1:24,000.

_____ 1992d, Geologic map of the Spring Branch 7.5-minute quadrangle, Texas: The University of Texas at Austin, Bureau of Economic Geology, open-file map prepared for U.S. Geological Survey under cooperative agreement 14-08-0001-A0885, scale 1:24,000.

_____ 1993a, Fracture zones between overlapping en echelon fault strands: outcrop analogs within the Balcones Fault Zone, Central Texas: Gulf Coast Association of Geological Societies Transactions, v. 43, p. 77–85.

_____ 1993b, Geologic map of the Bat Cave 7.5-minute quadrangle, Texas: The University of Texas at Austin, Bureau of Economic Geology, open-file map prepared for U.S. Geological Survey under cooperative agreement 1434-92-A-1085, scale 1:24,000.

_____ 1993c, Geologic map of the Bulverde 7.5-minute quadrangle, Texas: The University of Texas at Austin, Bureau of Economic Geology, open-file map prepared for U.S. Geological Survey under cooperative agreement 1434-92-A-1085, scale 1:24,000.

_____ 1993d, Geologic map of the Marion 7.5-minute quadrangle, Texas: The University of Texas at Austin, Bureau of Economic Geology, open-file map prepared for U.S. Geological Survey under cooperative agreement 1434-92-A-1085, scale 1:24,000.

_____ 1993e, Geologic map of the McQueeney 7.5-minute quadrangle, Texas: The University of Texas at Austin, Bureau of Economic Geology, open-file map prepared for U.S. Geological Survey under cooperative agreement 1434-92-A-1085, scale 1:24,000.

_____ 1993f, Geologic map of the New Braunfels East 7.5-minute quadrangle, Texas: The University of Texas at Austin, Bureau of Economic Geology, open-file map prepared for U.S. Geological Survey under cooperative agreement 1434-92-A-1085, scale 1:24,000.

_____ 1993g, Geologic map of the New Braunfels West 7.5-minute quadrangle, Texas: The University of Texas at Austin, Bureau of Economic Geology, open-file map prepared for U.S. Geological Survey under cooperative agreement 1434-92-A-1085, scale 1:24,000.

_____ 1993h, Geologic map of the Schertz 7.5-minute quadrangle, Texas: The University of Texas at Austin, Bureau of Economic Geology, open-file map prepared for U.S. Geological Survey under cooperative agreement 1434-92-A-1085, scale 1:24,000.

_____ 1994a, Geologic map of the Bergheim 7.5-minute quadrangle, Texas: The University of Texas at Austin, Bureau of Economic Geology, open-file map prepared for U.S. Geological Survey under cooperative agreement 1434-93-A-1174, scale 1:24,000.

_____ 1994b, Geologic map of the Camp Bullis 7.5-minute quadrangle, Texas: The University of Texas at Austin, Bureau of Economic Geology, open-file map prepared for U.S. Geological Survey under cooperative agreement 1434-93-A-1174, scale 1:24,000.

_____ 1994c, Geologic map of the Castle Hills 7.5-minute quadrangle, Texas: The University of Texas at Austin, Bureau of Economic Geology, open-file map prepared for U.S. Geological Survey under cooperative agreement 1434-93-A-1174, scale 1:24,000.

_____ 1994d, Geologic map of the Kendalia 7.5-minute quadrangle, Texas: The University of Texas at Austin, Bureau of Economic Geology, open-file map prepared for U.S. Geological Survey under cooperative agreement 1434-93-A-1174, scale 1:24,000.

_____ 1994e, Geologic map of the Longhorn 7.5-minute quadrangle, Texas: The University of Texas at Austin, Bureau of Economic Geology, open-file map prepared for U.S. Geological Survey under cooperative agreement 1434-93-A-1174, scale 1:24,000.

Collins, E. W., Baumgardner, R. W., Jr., and Raney, J. A., 1991a, Geologic map of the Sattler 7.5-minute quadrangle, Texas: The University of Texas at Austin, Bureau of Economic Geology, open-file map prepared for U.S. Geological Survey under cooperative agreement, scale 1:24,000.

_____ 1991b, Geologic map of the Wimberly 7.5-minute quadrangle, Texas: The University of Texas at Austin, Bureau of Economic Geology, open-file map prepared for U.S. Geological Survey under cooperative agreement, scale 1:24,000.

Collins, E. W., Hovorka, S. D., and Laubach, S. E., 1992, Fracture systems of the Austin Chalk, North-Central Texas, *in* Schmoker, J. W., Coalson, E. B., and Brown, C. A., eds., Geological studies relevant to horizontal drilling: examples from western North America: Rocky Mountain Association of Geologists, p. 129–142.

Collins, E. W., and Laubach, S. E., 1990, Faults and fractures in the Balcones Fault Zone, Austin region, Central Texas: Austin Geological Society Guidebook 13, 34 p.

Cronin, K. S., 1932, An Edwards Georgetown erosional interval: The University of Texas at Austin, Master's thesis.

Darcy, H. P. G., 1856, Les fontaines publiques de la Ville de Dijon: Paris, Victor Dalmont.

de Marsily, G., 1986, Quantitative hydrogeology: San Diego, Academic Press, Inc., 440 p.

Deike, R. G., 1990, Dolomite dissolution rates and possible Holocene dedolomitization of water-bearing units in the Edwards aquifer, South-Central Texas: Journal of Hydrology, v. 112, no. 3–4, p. 335–373.

Domenico, P. A., and Schwartz, F. W., 1990, Physical and chemical hydrology: New York, John Wiley and Sons, 824 p.

Driscoll, F. G., 1986, Ground water and wells: St. Paul, Minnesota, Johnson Division, 1089 p.

Dunham, R. J., 1962, Classification of carbonate rocks according to depositional texture: American Association of Petroleum Geologists Memoir 1, p. 108–121.

Eagon, H. B., Jr., and Johe, D. E., 1972, Practical solutions for pumping tests in carbonate-rock aquifers: Ground Water, v. 10, no. 4, p. 6–13.

Ellis, P. M., 1986a, Diagenesis of the Lower Cretaceous Edwards Group in the Balcones Fault Zone area: The University of Texas at Austin, Ph.D. dissertation, 327 p.

_____ 1986b, Post-Miocene carbonate diagenesis of the Lower Cretaceous Edwards Group in the Balcones Fault Zone area, South-Central Texas, *in* Abbot, P. L., and Woodruff, C. M., Jr., eds., The Balcones Escarpment, geology, hydrology, ecology, and social development in Central Texas: Geological Society of America Annual Meeting, p. 101–114.

Esteban, Manteu, and Klappa, C. F., 1983, Subaerial exposure environment, *in* Scholle, P. A., Bebout, D. G., and Moore, C. H., eds., Carbonate depositional environments: American Association of Petroleum Geologists Memoir 33, p. 1–54.

Fisher, W. L., and Rodda, P. U., 1969, Edwards Formation (Lower Cretaceous), Texas: Dolomitization in a carbonate platform system: American Association of Petroleum Geologists Bulletin, v. 53, p. 55–72.

Freeze, R. A., and Cherry, J. A., 1979, Ground water: Englewood Cliffs, New Jersey, Prentice-Hall, Inc., 604 p.

Garza, Sergio, 1968, Aquifer characteristics from well-field production records, Edwards Limestone, San Antonio area, Texas: University of Arizona, Master's thesis, 46 p.

Grimshaw, T. W., 1976, Environmental geology of urban and urbanizing areas: a case study from the San Marcos area, Texas: The University of Texas at Austin, Ph.D. dissertation, 244 p.

Grimshaw, T. W., and Woodruff, C. M., Jr., 1986, Structural style in an en echelon fault system, Balcones Fault Zone, Central Texas: geomorphologic and hydrologic implications, *in* Abbott, P. L., and Woodruff, C. M., Jr., eds., The Balcones Escarpment, geology, hydrology, ecology, and social development in Central Texas: Geological Society of America Annual Meeting, p. 71–75.

Gringarten, A. C., and Witherspoon, P. A., 1972, A method of analyzing pump test data from fractured rock aquifers, *in* Proceedings of the Symposium on Percolation through Fissured Rock: Stuttgart, Germany, International Association of Rock Mechanics, p. T3-B1–T3-B8.

Guyton, W. F., and Associates, 1986, Drilling, construction, and testing of monitor wells for the Edwards aquifer bad-water line experiment: Consultant Report, 56 p.

Hovorka, S. D., Ruppel, S. C., Dutton, A. R., and Yeh, Joseph, 1993, Edwards aquifer storage assessment, Kinney County to Hays County, Texas: The University of Texas at Austin, Bureau of Economic Geology, contract report prepared for the Edwards Underground Water District, 101 p.

Huntley, David, Nommensen, Roger, and Steffey, Duane, 1992, The use of specific capacity to assess transmissivity in fractured-rock aquifers: Ground Water, v. 30, no. 3, p. 396–402.

Jacob, C. E., 1950, Flow of ground water, *in* Rouse, Hunter, ed., Engineering hydraulic: New York, John Wiley and Sons, p. 321–386.

Journel, A. G., and Huijbregts, C. J., 1978, Mining geostatistics: New York, Academic Press, 600 p.

Kastning, E. H., Jr., 1983, Geomorphology and hydrogeology of the Edwards Plateau karst, Central Texas: The University of Texas at Austin, Ph.D. dissertation, 714 p.

_____ 1986, Cavern development in the New Braunfels area, Central Texas, *in* Abbott, P. L., and Woodruff, C. M., Jr., eds., The Balcones Escarpment, geology, hydrology, ecology, and social development in Central Texas: Geological Society of America Annual Meeting, p. 91–100.

Klemt, W. B., Knowles, T. R., Elder, G. and Sieh, T., 1979, Ground-water resources and model applications for the Edwards (Balcones Fault Zone) aquifer in the San Antonio region, Texas: Texas Department of Water Resources Report 239, 88 p.

Kuniansky, E. L., 1994, Multilayer finite-element model of the Edwards and Trinity aquifers, Central Texas, *in* Dutton, A. R., ed., Toxic substances and the hydrologic sciences: American Institute of Hydrology, p. 234–249.

Kuniansky, E. L., and Holligan, K. Q., in press, Simulations of flow in the Edwards–Trinity aquifer system and contiguous hydraulically connected units, west-central Texas: U. S. Geological Survey Water-Resources Investigations Report 93-4039, 40 p.

Land, L. S., 1985, Origin of massive dolomite: Journal of Geological Education, v. 33, p. 112.

Langford, O. F., 1942, Collapsed caverns as modifiers of older structures in the vicinity of the Balcones faults in Uvalde County, Texas: The University of Texas at Austin, Master's thesis.

Larson, P. H., 1988, Relay structures in a Lower Permian basement-involved extension system, East Greenland: Journal of Structural Geology, v. 10, no. 1, p. 3–8.

Lindeburg, M. R., 1992, Engineer-in-training reference manual: Belmont, California, Professional Publications, Inc., variously paginated.

Lucia, F. J., 1983, Petrophysical parameters estimated from visual descriptions of carbonate rocks: a field classification of carbonate pore space: Journal of Petroleum Technology, v. 35, no. 3, p. 629–637.

Maclay, R. W., and Land, L. F., 1988, Simulation of flow in the Edwards aquifer, San Antonio region, Texas, and refinements of storage and flow concepts: U.S. Geological Survey Report Water-Supply Paper 2336, 48 p.

Maclay, R. W., and Rettman, P. L., 1973, Regional specific yield of the Edwards and associated limestones in the San Antonio, Texas, area: Edwards Underground Water District, 10 p.

Maclay, R. W., and Small, T. A., 1976, Progress report on geology of the Edwards aquifer, San Antonio area, Texas, and preliminary interpretation of borehole geophysical and laboratory data on carbonate rocks: U.S. Geological Survey Open-File Report 76-627, 65 p.

_____ 1983, Hydrostratigraphic subdivisions and fault barriers of the Edwards aquifer, South-Central Texas, U.S.A.: Journal of Hydrology, v. 61, p. 127–146.

_____ 1984, Carbonate geology and hydrology of the Edwards aquifer in the San Antonio area, Texas: U.S. Geological Survey Open-File Report 83-537, 72 p.

_____ 1986, Carbonate geology and hydrology of the Edwards aquifer in the San Antonio area, Texas: Texas Water Development Board Report 296, 90 p.

Maclay, R. W., Small, T. A., and Rettman, P. L., 1980, Water-level, recharge, discharge, specific-capacity, well-yield, and aquifer test data for the Edwards aquifer in the San Antonio area, Texas: Texas Department of Water Resources LP-133, 83 p.

Mahin, D. A., and Campana, M. E., 1983, Discrete-state compartment model of a limestone ground-water reservoir—the Edwards aquifer near San Antonio, Texas: University of Nevada, Desert Research Institute Water Resources Center Publication 41077, 41 p.

Marquardt, G. L., and Elder, G. R., 1979, Records of wells, chemical analyses, and water levels of selected Edwards wells, Bexar County, Texas: Texas Department of Water Resources Report 237, 458 p.

Matheron, G., 1963, Principles of geostatistics: Economic Geology, v. 58, p. 1246–1266.

McCuen, R. H., and Snyder, W. M., 1986, Hydrologic modeling: statistical methods and applications: Englewood Cliffs, New Jersey, Prentice-Hall, 568 p.

McWhorter, D. B., and Sunada, D. K., 1977, Ground-water hydrology and hydraulics: Fort Collins, Colorado, Water Resources Publications, 290 p.

Miller, B. C., 1983, Physical stratigraphy and facies analysis, Lower Cretaceous, Maverick Basin and Devils River Trend, Uvalde and Real Counties, Texas: The University of Texas at Arlington, Master's thesis, 217 p.

Moore, C. H., Jr., 1964, Stratigraphy of the Fredericksburg division, South-Central Texas: The University of Texas at Austin, Bureau of Economic Geology, Report of Investigations No. 52, 48 p.

Myers, B. N., 1969, Compilation of results of aquifer tests in Texas: Austin, Texas, Texas Water Development Board, Report 98, 532 p.

Ogden, A. E., Quick, R. A., Rothermel, S. R., and Lundsford, D. L., 1986, Hydrological and hydrochemical investigation of the Edwards aquifer in the San Marcos area, Hays County, Texas: San Marcos, Texas, Edwards Aquifer Research and Data Center, 364 p.

Peacock, D. C. P., and Sanderson, D. J., 1991, Displacements, segment linkage, and relay ramps in normal fault zones: Journal of Structural Geology, v. 13, no. 6, p. 721–733.

_____ 1994, Geometry and development of relay ramps in normal fault systems: American Association of Petroleum Geologists Bulletin, v. 78, no. 2, p. 147–165.

Poteet, Diane, Collier, Hughbert, and Maclay, Robert, 1992, Investigation of the fresh/saline-water interface in the Edwards aquifer in New Braunfels and San Marcos, Texas: Edwards Underground Water District Report 92-02, report and appendix variously paginated.

Prezbindowski, D. R., 1981, Burial diagenesis, Edwards Formation, Lower Cretaceous, South-Central Texas: The University of Texas at Austin, Ph.D. dissertation, 235 p.

Proctor, C. V., Jr., Brown, T. E., Waechter, N. B., Aronow, Saul, Pieper, M. K., and Barnes, V. E., 1974, Seguin sheet: The University of Texas at Austin, Bureau of Economic Geology, Geologic Atlas of Texas, scale 1:250,000.

Quick, R. A., 1985, A hydrogeological and hydrochemical investigation of the Edwards aquifer in the San Marcos area, Hays County, Texas: University of Arkansas, Master's thesis, 183 p.

Raney, J. A., and Collins, E. W., 1991, Geologic map of the Devils Backbone 7.5-minute quadrangle, Texas: The University of Texas at Austin, Bureau of Economic Geology, open-file map prepared for U.S. Geological Survey under cooperative agreement, scale 1:24,000.

Razack, M., and Huntley, David, 1991, Assessing transmissivity from specific capacity in a large and heterogeneous alluvial aquifer: Ground Water, v. 29, no. 6, p. 856–861.

Reaser, D. F., and Collins, E. W., 1988, Style of faults and associated fractures in Austin Chalk, northern extension of the Balcones Fault Zone, Central Texas: Gulf Coast Association of Geological Societies Transactions, v. 38, p. 267–276.

Rose, P. R., 1972, Edwards Group, surface and subsurface, Central Texas: The University of Texas at Austin, Bureau of Economic Geology Report of Investigations No. 74, 198 p.

Rothermel, S. R., 1984, Hydrogeological and hydrochemical investigation of springs in Hays and Comal Counties, Texas: University of Arkansas, Master's thesis, 347 p.

Schultz, A. L., 1992, Using geophysical logs in the Edwards aquifer to estimate water quality along the freshwater/saline-water interface (Uvalde to San Antonio, Texas): Edwards Underground Water District Report 92-03, 47 p.

_____ 1993, Defining the Edwards aquifer freshwater/saline-water interface with geophysical logs and measured data (San Antonio to Kyle, Texas): San Antonio, Texas, Edwards Underground Water District Report 93-06, 81 p.

_____ 1994, Review and update of the position of the Edwards aquifer freshwater/saline-water interface from Uvalde to Kyle, Texas: Edwards Underground Water District draft report.

Sieh, T. H., 1975, Edwards (Balcones Fault Zone) aquifer test well drilling investigation: Texas Water Development Board unpublished file report, 127 p.

Slade, R. M., Jr., Ruiz, Linda, and Slagle, Diana, 1985, Simulation of the flow system of Barton Springs and associated Edwards aquifer in the Austin area, Texas: U.S. Geological Survey Water-Resources Investigations Report 85-4299, 49 p.

Small, T. A., 1984, Identification and tabulation of geological contacts in the Edwards aquifer, San Antonio, Texas: U.S. Geological Survey, Open-File Report OF 84-0075, 68 p.

Smith, C. I., 1964, Physical stratigraphy and facies analysis, Lower Cretaceous limestones, Edwards Plateau, West Texas: Houston, Texas, Shell Development Company, EPR Special Report 45, 138 p.

Snow, D. T., 1969, Anisotropic permeability of fractured media: Water Resources Research, v. 5, p. 1273–1289.

Stein, W. G., 1993, Hydrogeologic map and characteristics of the recharge zone of the Edwards aquifer, Bexar County, Texas: The University of Texas at San Antonio, Master's thesis, 83 p.

Taylor, R. W., and Fleming, A. H., 1988, Characterizing jointed systems by azimuthal resistivity surveys: Ground Water, v. 26, no. 4, p. 464–474.

Theis, C. V., 1963, Estimating the transmissivity of a water-table aquifer from the specific capacity of a well: U.S. Geological Survey Water Supply Paper 1536-I, p. 332–336.

Theis, C. V., Brown, R. H., and Myers, R. R., 1963, Estimating the transmissibility of aquifers from the specific capacity of wells: methods of determining permeability, transmissivity, and drawdown: U.S. Geological Survey Water Supply Papers, 1536-I.

Thorkildsen, D., and McElhaney, P. D., 1992, Model refinement and applications for the Edwards (Balcones Fault Zone) aquifer in the San Antonio region, Texas: Austin, Texas, Texas Water Development Board, Report No. 340, 33 p.

USDA Soil Conservation Service, 1993, Seco Creek water quality demonstration project: annual project report, fiscal year 1993, variously paginated.

Veni, George, 1987, Fracture permeability: implications on cave and sinkhole development and their environmental assessments, *in* Beck, B. F., Wilson, W. L., eds., Karst hydrogeology: engineering and environmental applications: proceedings of the Second Multidisciplinary Conference on Sinkholes and the Environmental Impacts of Karst: Boston, A. A. Balkema, p. 101–105.

_____ 1988, The caves of Bexar County: The University of Texas at Austin, Texas Memorial Museum Speleological Monograph 2, 2d ed., 300 p.

Villaescusa, E., and Brown, E. T., 1990, Characterizing joint spatial correlation using geostatistical methods, *in* Barton, Nick, and Stephansson, Ove, eds., Rock joints, proceedings of the International Symposium on Rock Joints, Loen, Norway: Brookfield, Vermont, A. A. Balkema, p. 115–122.

Waechter, N. B., Lozo, F. E., Jr., and Barnes, V. E., 1977, Del Rio sheet: The University of Texas at Austin, Bureau of Economic Geology, Geologic Atlas of Texas, scale 1:250,000.

Walton, W. C., 1970, Ground-water resource evaluation: New York, McGraw-Hill, 664 p.

Wanakule, Nisai, and Anaya, Roberto, 1993, A lumped parameter model for the Edwards aquifer: Texas A&M University, Texas Water Resources Institute, Technical Report No. 163, 84 p.

Wanakule, Nisai, Mays, L. W., and Lasdon, L. S., 1986, Optimal management of large-scale aquifers: methodology and applications: Water Resources Research, v. 22, no. 4, p. 447–465.

Ward, J. C., 1964, Turbulent flow in porous media: Journal of the Hydraulics Division, American Society of Civil Engineers, September, p. 1–12.

Waugh, J. R., 1993, South Medina County observation well project: Edwards Underground Water District Report 93-11.

Wermund, E. G., Cepeda, J. C., and Luttrell, P. E., 1978, Regional distribution of fractures in the southern Edwards Plateau and their relationship to tectonics and caves: The University of Texas at Austin, Bureau of Economic Geology Geological Circular 78-2, 14 p.

Woodruff, C. M., and Abbott, P. L., 1986, Stream piracy and evolution of the Edwards aquifer along the Balcones Escarpment, Central Texas, *in* Abbot, P. L., and Woodruff, C. M., Jr., eds., The Balcones Escarpment, Central Texas: Geological Society of America Annual Meeting, p. 77–100.

BUREAU OF ECONOMIC GEOLOGY
THE UNIVERSITY OF TEXAS AT AUSTIN
NOEL TYLER, DIRECTOR

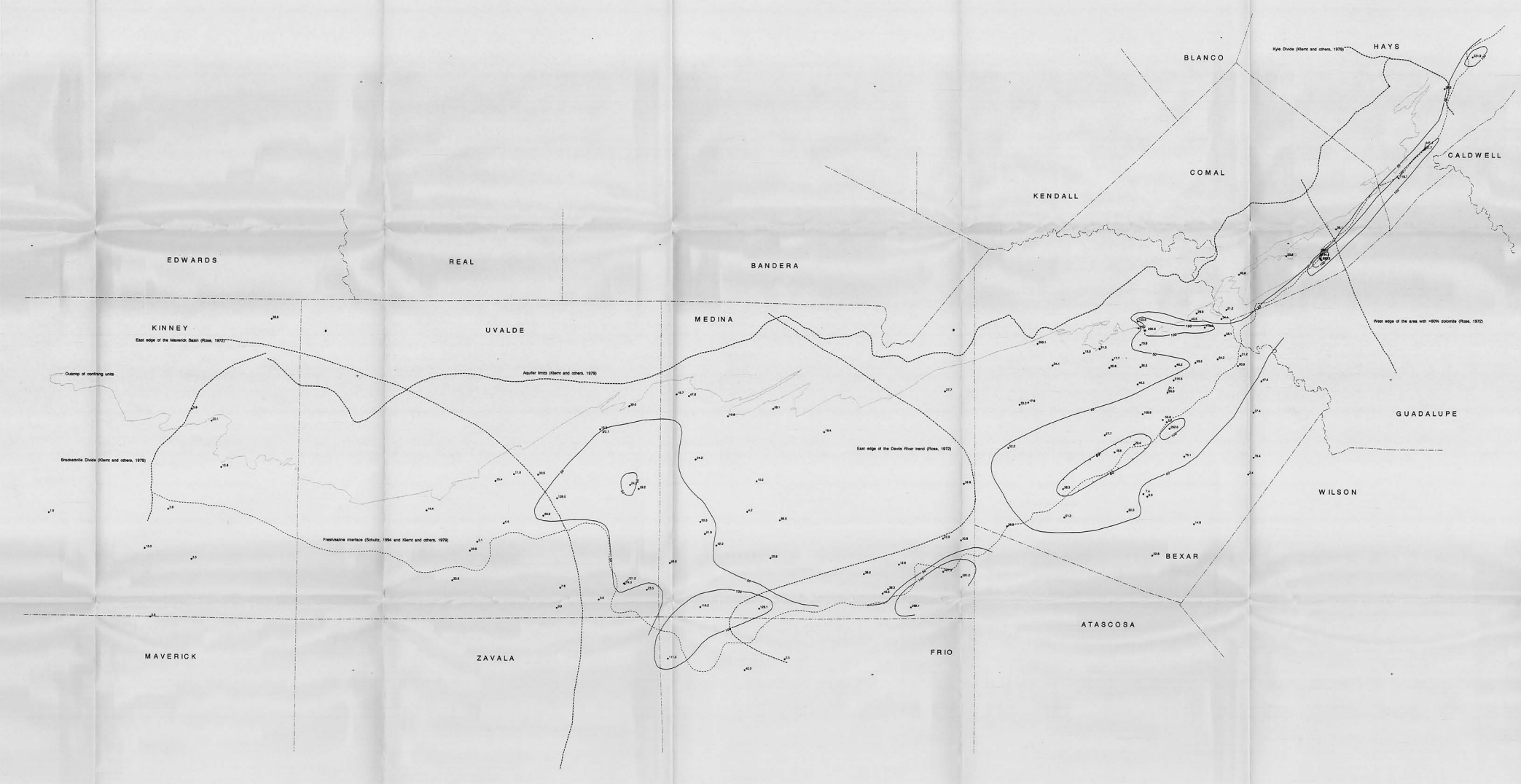

N

0 10 mi
0 15 km

1:250,000

Permeability (millidarcy)

PLATE 6. MATRIX PERMEABILITY FROM WIRELINE LOGS

1995

by Susan D. Hovorka, Robert E. Mace, Edward W. Collins
Alan R. Dutton, Principal Investigator

Prepared for
Edwards Underground Water District
under Contract No. 93-17-FO

GA9702fg

BUREAU OF ECONOMIC GEOLOGY
THE UNIVERSITY OF TEXAS AT AUSTIN
NOEL TYLER, DIRECTOR

PLATE 2. AQUIFER TEST LOCATIONS

1995

by Susan D. Hovorka, Robert E. Mace, Edward W. Collins
Alan R. Dutton, Principal Investigator

Prepared for
Edwards Underground Water District
under Contract No. 93-17-FO

BUREAU OF ECONOMIC GEOLOGY
THE UNIVERSITY OF TEXAS AT AUSTIN
NOEL TYLER, DIRECTOR

Transmissivity values (ft^2/day)

TESTS WITH DRAWDOWN	ZERO-DRAWDOWN TESTS
10,000,000 to 100,000,000	10,000,000 to 100,000,000
1,000,000 to 10,000,000	1,000,000 to 10,000,000
100,000 to 1,000,000	100,000 to 1,000,000
10,000 to 100,000	10,000 to 100,000
1,000 to 10,000	1,000 to 10,000
100 to 1,000	100 to 1,000
10 to 100	10 to 100
1 to 10	1 to 10
0.1 to 1	0.1 to 1

0 10 mi
0 15 km

1:250,000

N

PLATE 5. TRANSMISSIVITY FROM AQUIFER TESTS

1995

by Susan D. Hovorka, Robert E. Mace, Edward W. Collins
Alan R. Dutton, Principal Investigator

Prepared for
Edwards Underground Water District
under Contract No. 93-17-FO

GHa7197g

BUREAU OF ECONOMIC GEOLOGY
THE UNIVERSITY OF TEXAS AT AUSTIN
NOEL TYLER, DIRECTOR

PLATE 4. ISOPACHS OF
THE EDWARDS GROUP

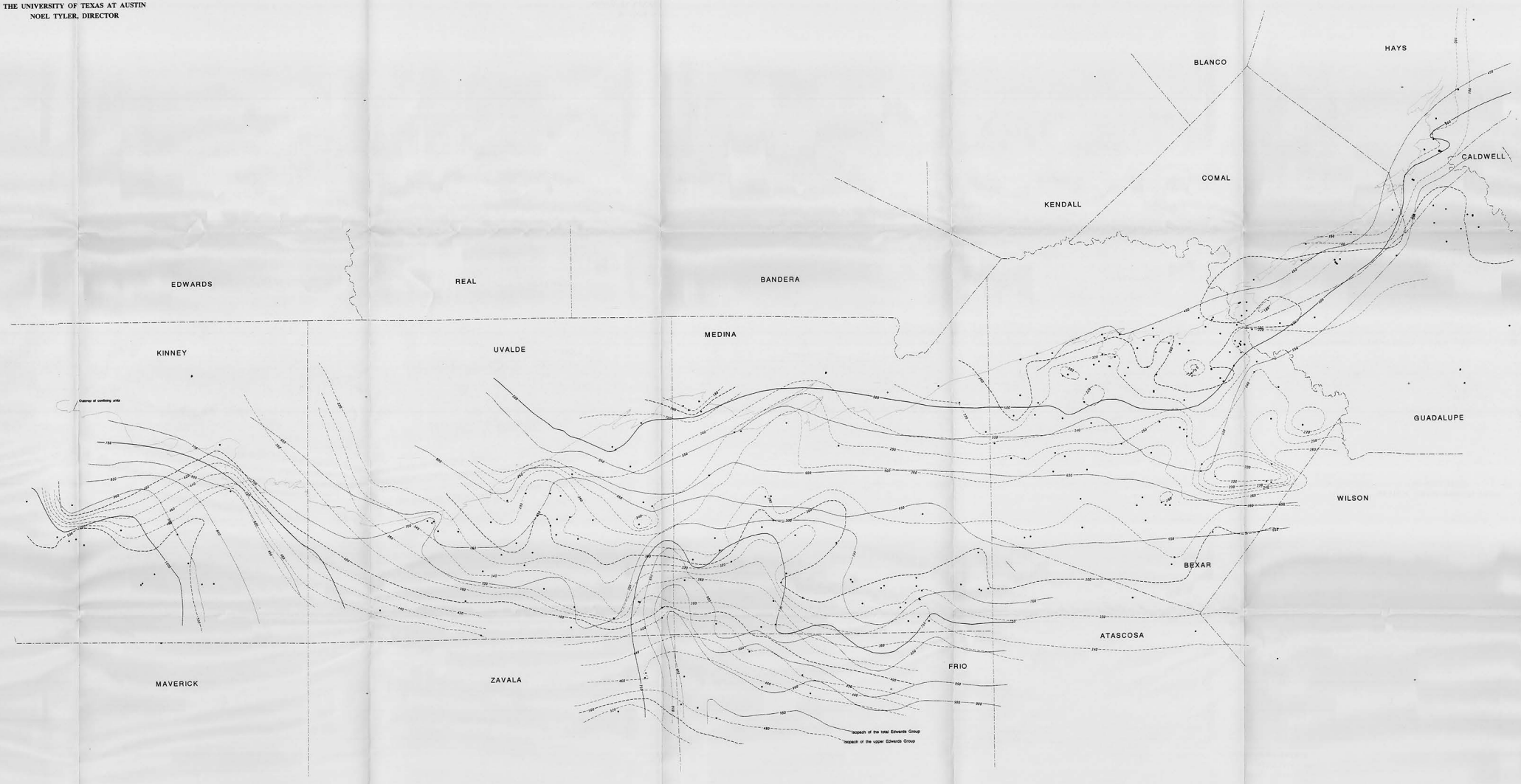

0 10 mi
0 15 km

1:250,000
Contour interval variable

N

PLATE 4. ISOPACHS OF THE EDWARDS GROUP

1995

by Susan D. Hovorka, Robert E. Mace, Edward W. Collins
Alan R. Dutton, Principal Investigator

Prepared for
Edwards Underground Water District
under Contract No. 93-17-FO

GA#7824g

BUREAU OF ECONOMIC GEOLOGY
THE UNIVERSITY OF TEXAS AT AUSTIN
NOEL TYLER, DIRECTOR

PLATE 3. STRUCTURE OF THE EDWARDS AQUIFER

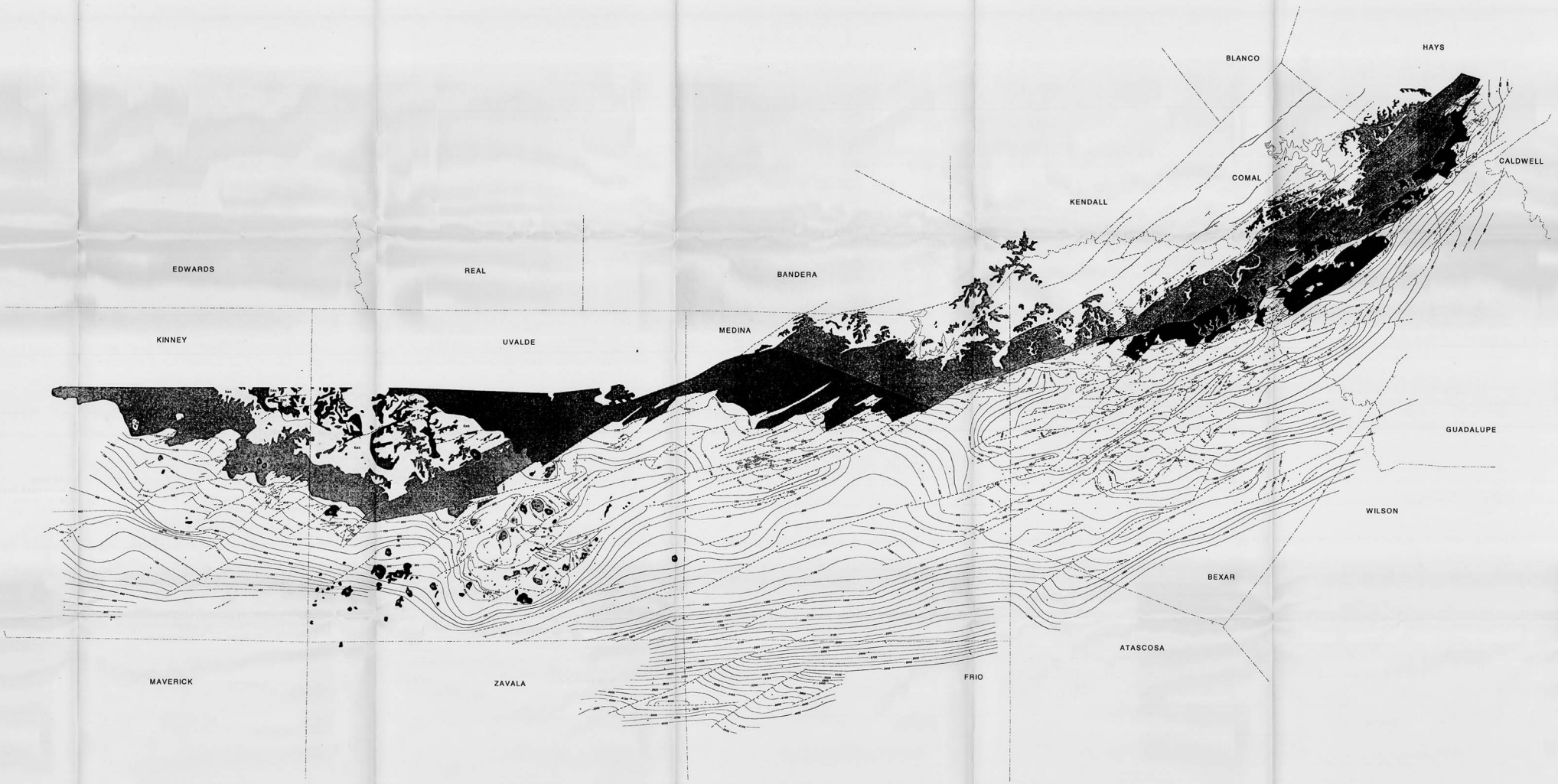

PLATE 3. STRUCTURE OF THE EDWARDS AQUIFER

1995

Geology by E. W. Collins

Cartography by Parice A. Porter

Geology of the Edwards Group outcrop belt was compiled from a variety of sources. Outcrop belt geology from the western edge of the map to longitude 99 00' is modified from Brown and others (1974) and Weeckler and others (1977). Outcrop belt geology at the western part of Bexar County is modified from Arnow (1959), Brown and others (1974), Waddell (1977), and Stein (1993). Outcrop belt geology between longitudes 99 30' and 98 00' is modified from open-file quadrangle maps by E. W. Collins. Outcrop belt geology west of longitude 98 00' is modified from Proctor and others (1974) and Grimshaw (1976).

Subsurface structure at the base of the Del Rio Formation (approximate top of the Edwards aquifer) is interpreted from about 1,000 data points and utilization of knowledge of the outcropping geologic units and thicknesses of strata overlying Edwards Group. Subsurface data base was collected by S. D. Hovorka. Erika Beghtol digitized the data.

0 10 mi
0 15 km

1:250,000
Contour interval 100 ft

N

Kcs Cretaceous igneous rocks at surface

Edwards Group strata in outcrop belt

Salmon Peak Formation
Devils River Limestone
Person Formation
Kainer Formation
McKnight Formation
West Nueces Formation

Normal fault, dashed where inferred. Bar on downthrown side

Structure data point

-100- Elevation of the base of the Del Rio Formation (approximate top of the Edwards aquifer)

Gis7525g

BUREAU OF ECONOMIC GEOLOGY
THE UNIVERSITY OF TEXAS AT AUSTIN
NOEL TYLER, DIRECTOR

PLATE 2. AQUIFER TEST LOCATIONS

1995

by Susan D. Hovorka, Robert E. Mace, Edward W. Collins
Alan R. Dutton, Principal Investigator

Prepared for
Edwards Underground Water District
under Contract No. 93-17-FO

BUREAU OF ECONOMIC GEOLOGY
THE UNIVERSITY OF TEXAS AT AUSTIN
NOEL TYLER, DIRECTOR

PLATE 1. STRATIGRAPHIC WELLS AND OUTCROPS

1995

by Susan D. Hovorka, Robert E. Mace, Edward W. Collins
Alan R. Dutton, Principal Investigator

Prepared for
Edwards Underground Water District
under Contract No. 93-17-FO

GMAT5274j

Note: Large-format versions of the plates for this report are available in a companion document.